

Experimental and mathematical investigation into the heat-transfer processes within the heat exchangers of an α type Stirling engine

Bartłomiej Rutczyk

Supervisor: prof. dr hab. inż. Ireneusz Szczygieł

PhD Thesis



**Politechnika
Śląska**

Wydział Inżynierii Środowiska i Energetyki, Katedra Techniki Ciepłej
Politechnika Śląska
Gliwice
2023

Preface

Abstract

Mathematical modelling of Stirling engines has been a widely researched topic over the course of the last few decades. Amongst different approaches, many zero-dimensional models based on solving differential mass and energy balances have been proposed by different authors. As some of these models necessitate the use of heat transfer coefficients characterizing the convective processes in the heat exchangers, the method by which those are calculated demands close attention. The aim of this work is to investigate this matter. This was done by validating different heat transfer models within the framework of a zero-dimensional model created by the author. The work presents a comprehensive review of heat transfer correlations adequate for Stirling Engine calculations. Experimental results are obtained from a rig based on a Genoastirling ML3000 engine. These results are compared with model results utilizing different heat transfer models, narrowing the selection to the heat transfer correlations of Anannd and Pinfold (1980), Toda (1994) and Kanzaka and Iwabuchi (1992). For the best performing models further refinement to the equations is proposed and evaluated showing an improved quality of model prediction in terms of indicated power.

The presented dissertation is organized into six Chapters, expanding on content which was in part already published by the author in several publications in the course of performing PhD studies. **Chapter I** outlines the problem in question and the state of the art. The description of the state of the art in regards to heat transfer correlations has been published in the article by Bartłomiej Rutczyk and Ireneusz Szczygieł: "Development of internal heat transfer correlations for the cylinders of reciprocating machines." *Energy* 230 (2021): 120795. **Chapter II** concerns Stirling engine modelling, the outline of the author's model described within it (or rather the first version of thereof), in Section 2.1 has been published in the article by Bartłomiej Rutczyk, Ireneusz Szczygieł, and Zbigniew Buliński: "A zero-dimensional, real gas model of an α Stirling engine." *Energy Conversion and Management* 199 (2019):

111995 and expanded upon in the paper by Bartłomiej Rutczyk, Ireneusz Szczygieł, and Adam Kabaj: "Evaluation of an α type stirling engine regenerator using a new differential model." *Energy* 209 (2020): 118369. Some of the data used in Section 2.2 has also been published before, in the following articles: Stanek, Wojciech, et al. "Thermo-ecological assessment of Stirling engine with regenerator fed with cryogenic exergy of liquid natural gas (LNG)." *Energy* 185 (2019): 1045-1053 and Buliński, Zbigniew, et al. "A Computational Fluid Dynamics analysis of the influence of the regenerator on the performance of the cold Stirling engine at different working conditions." *Energy Conversion and Management* 195 (2019): 125-138. **Chapter III** deals with the construction of the experimental stand. The work described within it has not been published as of the time of thesis publication, it has been however partially presented during the 2022 Symposium on Heat and Mass Transfer. **Chapters IV and V** describe the validation of the aforementioned model and the work concerning the fine-tuning of the selected heat transfer correlations. Likewise, this has been shown during the 2022 Symposium on Heat and Mass Transfer, and not published as of yet. **Chapter VI** are the overall conclusions from the work.

Contents

1	Introduction	7
1.1	Work premise	7
1.2	The Stirling Engine - a brief history and overview	9
1.3	Approaches to Stirling engine modelling and heat transfer considerations	13
1.3.1	Use of non-dimensional numbers for engine modelling	15
1.3.2	Overview of Stirling engine mathematical models	15
2	Stirling engine modelling	20
2.1	The zero-dimensional, real gas model	20
2.1.1	The development of the zero-dimensional real gas model	20
2.1.2	Kinematics of the piston movement	21
2.1.3	Mass and energy balance	22
2.1.4	Pressure losses	25
2.1.5	Leakage losses	26
2.1.6	Heat losses through cylinder walls	27
2.1.7	Evaluation of heat transfer coefficients	27
2.1.8	The model solution procedure	48
2.1.9	The simplified regenerator model	54
2.1.10	Heat transfer inside the regenerator	58
2.1.11	Regenerator differential model	58
2.1.12	Parametric study of the regenerator	61
2.2	Model validation and tests, pre-experimental stage	65
2.2.1	CFD comparison	65
2.2.2	Regenerator differential model validation	68
2.2.3	Cleanergy C9C engine data	71
3	Experimental setup	76
3.1	The Genoastirling ML3000 engine	76
3.1.1	Crankshaft and kinematics	78

3.1.2	The cylinders and pistons	80
3.1.3	Heat exchange surfaces	82
3.1.4	Engine dimensions	87
3.2	Auxiliary equipment	87
3.3	Measurement system	88
3.3.1	Volume and shaft angle measurement	88
3.3.2	Pressure measurement	89
3.3.3	Data acquisition and processing	90
4	Measurements and model validation	92
4.1	Sensitivity of the ML3000 engine model to heat transfer coefficients .	92
4.2	Model validation methodology	94
4.3	Evaluation of heat transfer correlation validity	96
4.3.1	Investigation of model discrepancies	101
5	Measurement based model tuning	104
5.1	Fine-tuning of correlations	104
5.1.1	Selection of correction method	104
5.1.2	The adjustment process	105
5.1.3	Adjustment results	108
5.2	Influence of correlation selection on local, instantaneous heat transfer	111
5.2.1	Comparison of pressure-angle signals for selected measurements	111
5.2.2	Investigation of possible further adjustment	130
6	Summary and conclusions	134
	References136List of Figures145List of Tables150	

Nomenclature

Roman letters

m	mass, kg
n	rotational speed, rpm
H, h	enthalpy, specific enthalpy kg
U, u	internal energy, specific int.en. , J, Jkg ⁻¹
V	volume, m ³
Q	heat exchanged, J
L	work, J
T	temperature, K
p	pressure, Pa
w	velocity, ms ⁻¹
Er	error (of internal energies), J
V	volume, m ³
L	work, J
T	temperature, K
t	time, s
$t^{(c)}$	temperature, deg C
S	entropy, $\frac{J}{K}$
Cp	isobaric heat capacity, $\frac{J}{kgK}$
r	radius, m
s	piston position, -
\dot{q}, \dot{Q}	heat flow, $\frac{W}{m^2}$, W
k	thermal conductivity, $\frac{W}{mK}$
a, b, C, m, n	arbitrary constants, -
B	temperature amplitude, K

Non-dimensional numbers

Nu	Nusselt number
Pr	Prandtl number
Re	Reynolds number
Pe	Peclet number
St	Stanton number
A_o	dimensionless oscillation
L	compressibility number

Greek Letters

α	heat transfer coefficient, $\frac{W}{m^2K}$
φ	angle, deg
κ	specific heat ration, -
μ	dynamic viscosity, Pa · s
ν	kinematic viscosity, $\frac{m^2}{s}$
ρ	density, $\frac{kg}{m^3}$ 5
ϵ	pressure ratio, -
ω	angular velocity, rad/s
ϵ	fraction or ratio, per subscript and description -

Subscripts

<i>p</i>	piston
<i>i</i>	internal
<i>cl</i>	clearance
<i>r</i>	regenerator
<i>w</i>	wall
<i>o</i>	initial
<i>m</i>	averaged across stroke
<i>v</i>	volume
<i>avg</i>	area to volume
<i>avg</i>	average
<i>g</i>	gas
<i>cyl</i>	cylinder
<i>max</i>	maximum
<i>sc</i>	from Schmidt model
<i>c</i>	compressor/cold cylinder
<i>h</i>	expander/hot cylinder
<i>ω</i>	rotational/angular

Chapter 1

Introduction

1.1 Work premise

Stirling engines have been known and built since their invention date, widely accepted as 1816 by Robert Stirling [56, 58]. Within this time, starting as simple "hot air-engines" and undergoing a renaissance first in the postwar era by the work of Phillips and later during the energy crisis in the 1970's which both lead to a better scientific understanding of their workings [58, 50, 80]. However the question of internal heat transfer in these machines and its mathematical description still remains open. Very few heat transfer correlations describing the conditions in reciprocating cylinder-piston systems exist in general, and even fewer for Stirling engines in particular [63]. On the other hand, heat transfer correlations serve as a vital component of zero and one dimensional models of Stirling engines, which are in common use by both engineers and researchers [79, 50]. The main thesis behind this work, is that:

- **Stirling engine modelling can be successfully performed with the use of simple models, provided that the heat transfer correlations within them are adequate.**

Conversely, it is posed that it is possible to arrive at a correlation aptly predicting the heat transfer coefficients in the Stirling engine working spaces using an approach coupling both a Stirling engine model and experimental measurements. Such a correlation would be directly coupled with the used model, providing the user with a semi-empirical engine parameter estimation method, trading the general applicability of 0D models for higher prediction accuracy.

The motivation for performing this work can be illustrated with a chart created using the data and methods outlined within, showing the results of an analysis of model sensitivity to the heat transfer coefficient values. Using the zero-dimensional

real gas Stirling engine model, as explained in Chapter 2, to simulate the Genoa ML3000 engine described in detail in Chapter 3, one can perform simulations for one of the measurement points of the engine. In this example the point entails a buffer pressure of 5.44 bar, and a rotational speed of 501.40 rpm. Figure 1.1 shows the relationship between the predicted engine power and the heat transfer coefficient value within the range of 0 to $1000 \frac{\text{W}}{\text{m}^2\text{K}}$.

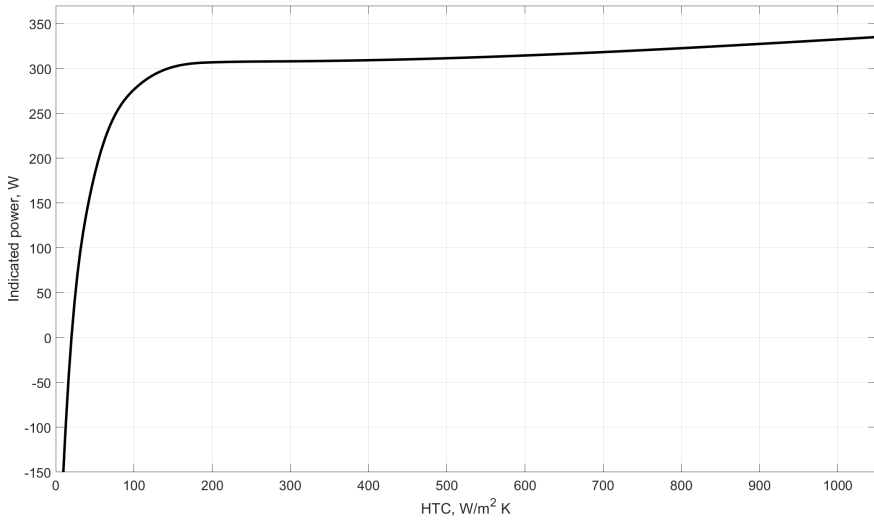


Figure 1.1: An illustration of engine power dependence on internal heat transfer coefficients for the Genoa ML3000 Stirling Engine

It can be seen, that the indicated power prediction strongly depends on the value of the HTC for the $0 - 200 \frac{\text{W}}{\text{m}^2\text{K}}$ range. Afterwards, the variation is not as strong, however still present as an almost linear function. The high sensitivity to the heat transfer coefficients in the lower range leads to the formulation of a secondary thesis, that is:

- **Stirling engine power density can in some cases be highly improved by moderately intensifying the internal heat transfer**

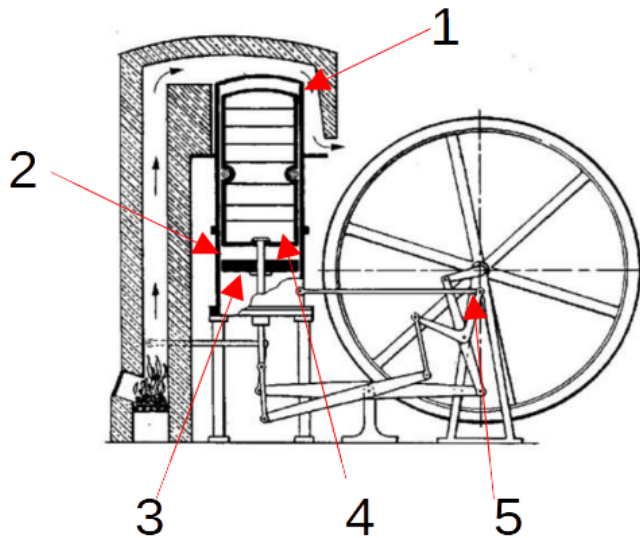


Figure 1.2: Stirling engine original 1816 patent drawing [95] with marks; 1 - heater, 2 - cooler, 3 - working piston, 4 - displacer, 5 - crank mechanism

1.2 The Stirling Engine - a brief history and overview

The purpose of this Section is to serve as a glossary of terms, as descriptions of Stirling engines are plentiful in thermodynamic and mechanical literature. In Poland, a general overview of their designs was published by Żmudzki in 1993 [95]. Despite never reaching widespread use, Stirling engines have since the very beginning been a fruitful object of scientific study. A mathematical description of the Stirling engine was attempted by William Thomson (Lord Kelvin) in 1847 [47]. In 1871, Gustav Schmidt of the Prague German Polytechnic Institute proposed an "isothermal" model of the engine cycle, in an attempt to describe the behaviour of a Lehman type machine. This model finds use to this day, as it provides a closed form solution for the power output at set boundary conditions [65].

The engines of the era were simple, unpressurised machines built for light work and their main market advantage was the possibility of working unattended or with minimum attention. Applications included water pumping, driving fans, and likely small workshop and craft machinery. The patent drawing of the original engine is

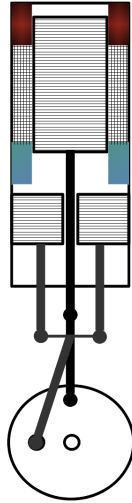


Figure 1.3: The β type Stirling engine

shown in Fig.1.2.

The Stirling engine is primarily divided into three configurations, α , β and γ . Free-piston engines and thermoacoustic engines could also be classified as separate configurations [95] or lumped into the known categories. β and γ rely on a displacer piston for moving the gas within a closed space, so it can be cooled or heated, the α configuration relies on the movement of two working pistons to facilitate the transport of gas between hot and cold spaces.

The β configuration is identical in principle to Robert Stirling's original engine. It can be built either to a design such as in Fig. 1.3, where the displacer moves the fluid through separate exchangers (see the Philips engine [50]), or in a fashion similar to the historical engines, where the cylinder has heat transfer areas mounted directly on its body. The cooling area, due to tribological and material constraints, is usually built closer to the working piston [95], which has the thermodynamical disadvantage of providing cooling during the expansion stroke.

The γ engine, is similar to the β (see Fig.1.4)), however the working piston is separated in its own cylinder. As can be seen from the drawings, the use of either of those engine configurations necessitates a large clearance space. In the β configuration, the clearance spaces can be minimized in some drive mechanisms, such as the rhombic drive or Ross yoke [50], which allow the working piston to effectively

"venture" into the cold space following the displacer.

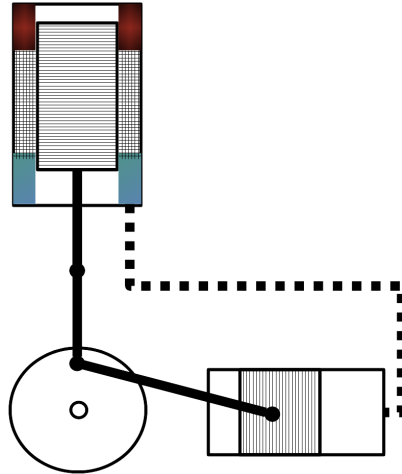


Figure 1.4: The γ type Stirling engine

The α machine (see Fig.1.5) allows avoiding large clearance spaces. As the α configuration also results in a more compact engine, it was chosen as the main subject of this work. An additional advantage of the alpha configuration lays in the ability to separate the hot and cold spaces so as to minimize conduction loss through the solid material.

Most early engines would be in modern terms classified as beta and in some cases gamma types. Examples include the machines of Lehman (1867), Ericsson (1833) or Robinson (1881). Most of these early engines did not have regenerators. The first alpha type engine, that is the same type as the subject of this work, without a displacer but with separate compression and expansion pistons was manufactured by Rider in 1875, which is also interesting due to the presence of a regenerator made from a bank of flat plates, and the elongation of cylinders and pistons to increase the heat surface area.

The sliding surface of the hot cylinder was cooled, which decreases thermal efficiency but prevents negative tribological effects from high temperature, which is another common feature of modern Stirling engines.

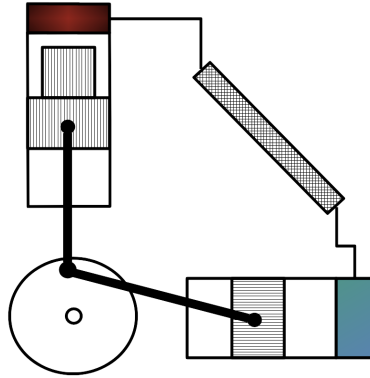


Figure 1.5: The α type Stirling engine

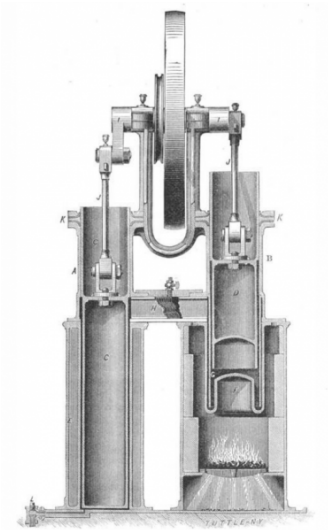


Figure 1.6: A Rider engine in cross-section [90]



Figure 1.7: A Rider engine found by the author in the collection of the National Agricultural museum in Szreniawa.

1.3 Approaches to Stirling engine modelling and heat transfer considerations

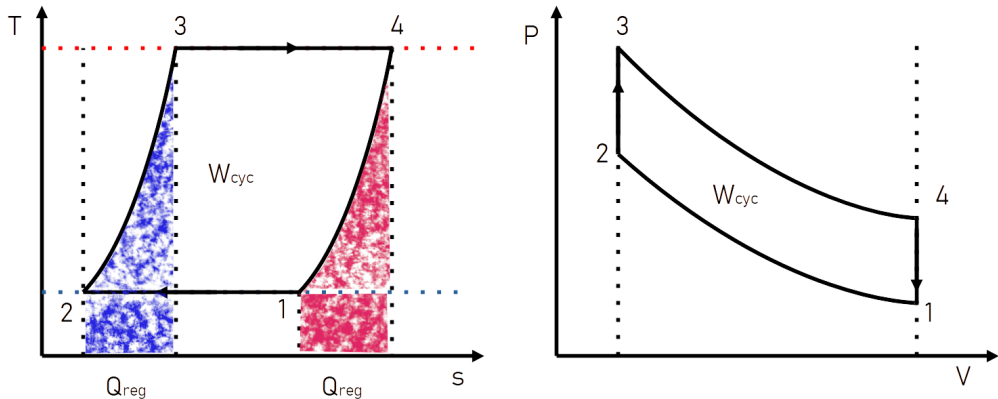


Figure 1.8: A $T - s$ and $p - V$ diagram for the ideal Stirling cycle

A general overview of the engine working cycle is often given in literature by the "Stirling Cycle", as shown in Fig.1.8:

1. 1-2 isothermal heat removal and compression,
2. 2-3 isochoric heat addition,
3. 3-4 isothermal heat addition and expansion,
4. 4-1 isochoric heat removal.

Ideally, these phases would occur as follows; 1 - with the expansion (hot) piston fixed in the upper position, with the bulk of the gas in the cold space, with the compression (cold) piston moving up, 2 - with the working pistons travelling in parallel displacing the gas from the cold to the hot space, 3 - with the compression piston fixed in the upper position and the expansion piston moving down due to expansion of the gas, 4 - with the pistons moving in parallel displacing the gas from the hot back to the cold space. Ideally, during the processes 2 and 4 regeneration should occur, that is the gas should impart its heat onto a regenerator (in the case of the patent drawing we can imagine the displacer walls serving this purpose) and vice versa, such that the gas entering the cold space reaches the cold space temperature

and likewise in the other direction. On the $T - s$ diagram, the heat of regeneration is denoted by Q_{reg} . It can be seen from the diagram that if perfect regeneration is achieved, the cycle will be equivalent to an ideal Carnot cycle and so will be the thermal efficiency.

$$\eta_T = 1 - \left(\frac{T_c}{T_h}\right) \quad (1.1)$$

It can be shown, that this efficiency will drop if the regenerator is imperfect. Żmudzki [95], shows that:

$$\eta_T = \frac{(\kappa - 1)\left(1 - \frac{T_c}{T_h}\right)\ln\varepsilon_{com}}{(\kappa - 1)\ln\varepsilon_{com} + \left(1 - \frac{T_c}{T_h}\right)(1 - \varepsilon_r)} \quad (1.2)$$

Where κ is the isentropic exponent, ε_{com} is the compression ration ($\frac{V_2}{V_1}$) and ε_r is the regenerator efficiency (as defined by Żmudzki)

$$\varepsilon_r = \frac{T_{r-v} - T_c}{T_h - T_c} \quad (1.3)$$

It can be seen, that equation (1.2) is only reduced to the Carnot efficiency with a regenerator that is 100% effective. Otherwise, it will be lower and also negatively impacted by low compression ratios or a high isentropic exponent. The awareness of those trends is imperative when designing an engine for efficiency.

Though this thermodynamic cycle serves as a decent illustration and cannot be discounted as the thermodynamic upper bound, as all thermodynamic reference cycles it doesn't describe the behaviour of a real machine accurately. For example Organ [6, 56] questions its use as the processes 2 and 4 are never in practice isochoric, due to the system kinematics. Neither is it possible to achieve perfect regeneration, due to the second law of thermodynamics. An issue is also in the achievement of isothermal expansion and compression. As both are dependent on heat transfer from the cylinder (or heat exchanger) walls to the fluid, it is immediately visible that isothermality would only be achieved if the piston movement occurred infinitely slowly or if the heat transfer coefficients were infinitely high (and likewise the thermal diffusivity of the bulk gas). It can be therefore reasoned, that even in a kinematically perfect engine, with perfect regeneration processes 1 and 3 would be polytropic, with the polytropic exponent dependant on the heat transfer coefficients, and likely varying throughout the process.

Empirical evidence also shows [56], that high compression ratios, contrary to implications of equation 1.2 do not necessarily lead to higher efficiencies. Work on low temperature difference engines shows, that high compression ratios are only feasible with high temperature differences, otherwise, the engine will not produce

positive work [66]. This effect is not possible to describe in terms of the classical Stirling cycle. Due to those limitations, the employment of more detailed models is therefore necessary.

1.3.1 Use of non-dimensional numbers for engine modelling

Non-dimensional formulas are useful for preliminary calculation but do not provide the user with much information. A common example is the use of the Beale number. It is defined as [50]:

$$\text{Be} = \frac{N}{p_m V_{sw} n_s}, \quad (1.4)$$

where N is the engine power in Watts, p_m the mean effective pressure in Pa, V_{sw} the swept volume and n_s the engine rotational frequency in s^{-1} . The value of the Be number was estimated by Beale as constant, around 0.15 for the engines he was working with [83]. Noting the fact that it was derived based on data acquired from engine working between similar temperature bounds, West in 1981 proposed to expand the formula by inclusion of temperatures, creating the West number.

The West number is similar to the Beale number in its definition:

$$\text{We} = \frac{N}{p_m V_{sw} n_s} \frac{T_h - T_c}{T_h + T_c}, \quad (1.5)$$

where T_h and T_c are the hot and cold sink temperatures respectively. West numbers are assumed to be of a value between 0.25 and 0.35 [56].

The assumed values of those numbers can be used to estimate engine power by solving the equations for engine power, with a set of design conditions for the pressure, volume and temperatures of the heat source and sink. Calculations using first order models can only be used for general assessment when starting the design process [50].

1.3.2 Overview of Stirling engine mathematical models

Stirling engine models tackle these issues in various ways. The Schmidt Isothermal model, (see Fig. 1.9) takes into account the issues connected with kinematics, by the inclusion of motion equations, however the heat transfer problem can only be taken into account by raising and lowering the constant temperatures in expansion and compression volumes above and below the wall temperatures so that the temperature gradient corresponds to the heat transfer coefficient [56, 79].

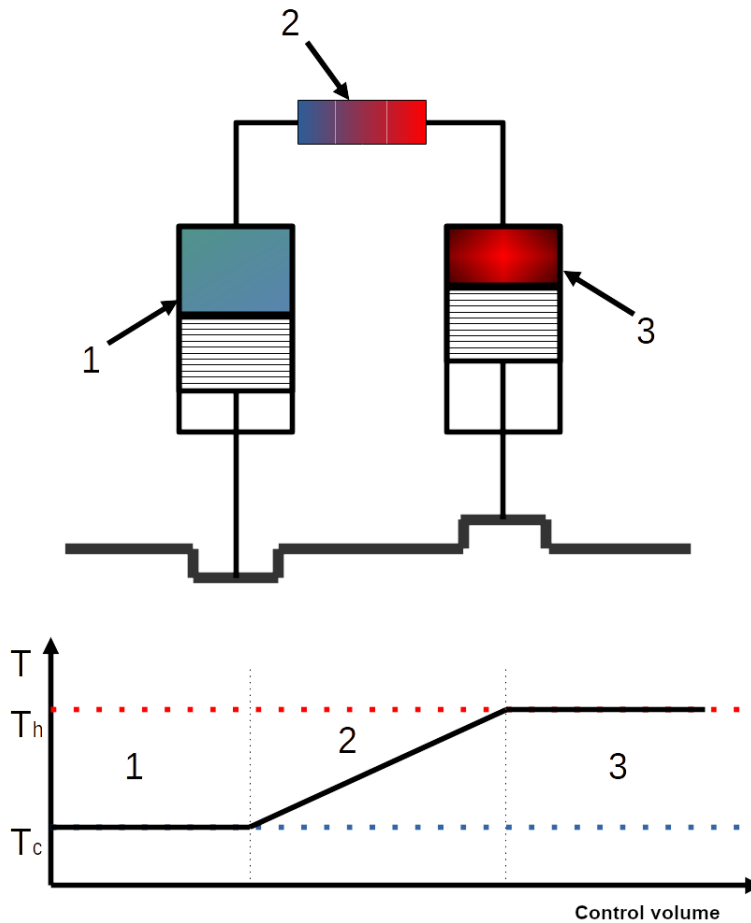


Figure 1.9: Schematic and temperature distribution in the control volumes of the Schmidt isothermal model. 1 - compressor/cooler, 2 - regenerator, 3 - expander/heater. T_c - cooler temperature, T_h - heater temperature

The class of adiabatic models is built on the idea of the isothermal models by adding additional control volumes for the heater and cooler heat exchangers. The most basic adiabatic model assumes that the gasses exiting the heat exchangers have a constant temperature (see Fig. 1.10).

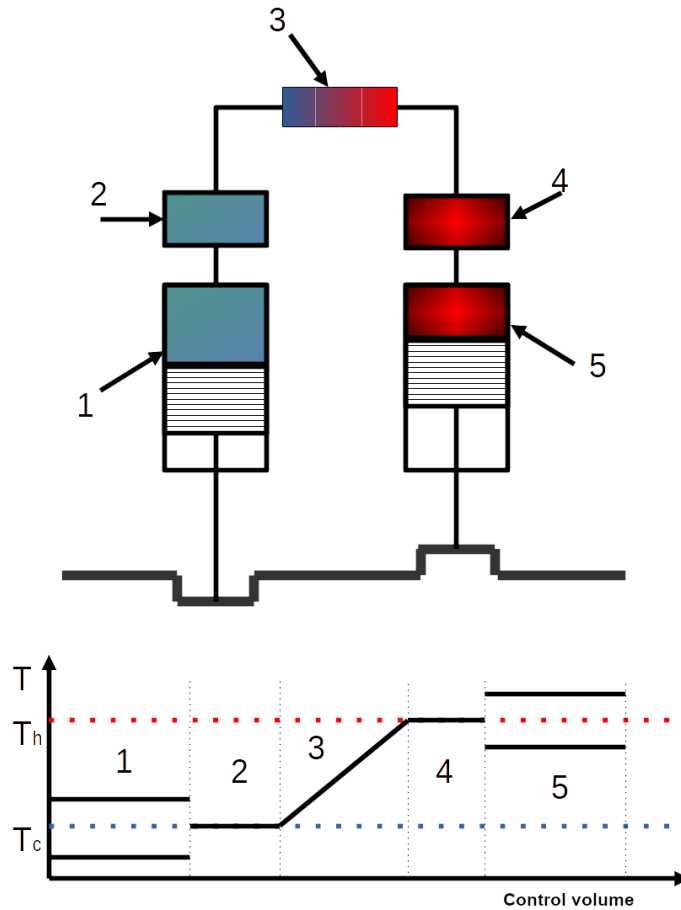


Figure 1.10: Schematic and temperature distribution in the control volumes of the adiabatic model. 1 - compressor, 2 - cooler, 3 - regenerator, 4 - heater, 5 - expander. T_c - cooler temperature, T_h - heater temperature

Urieli's "SIMPLE" (Fig. 1.11) model incorporates internal heat transfer and temperature variations in the heater and cooler spaces, though it uses correlations for developed flow, citing the lack of other options [79]. A similar method was applied by Finkelstein, who uses the NTU method for heat transfer analysis, though sources don't state how the values of the NTU were calculated [50].

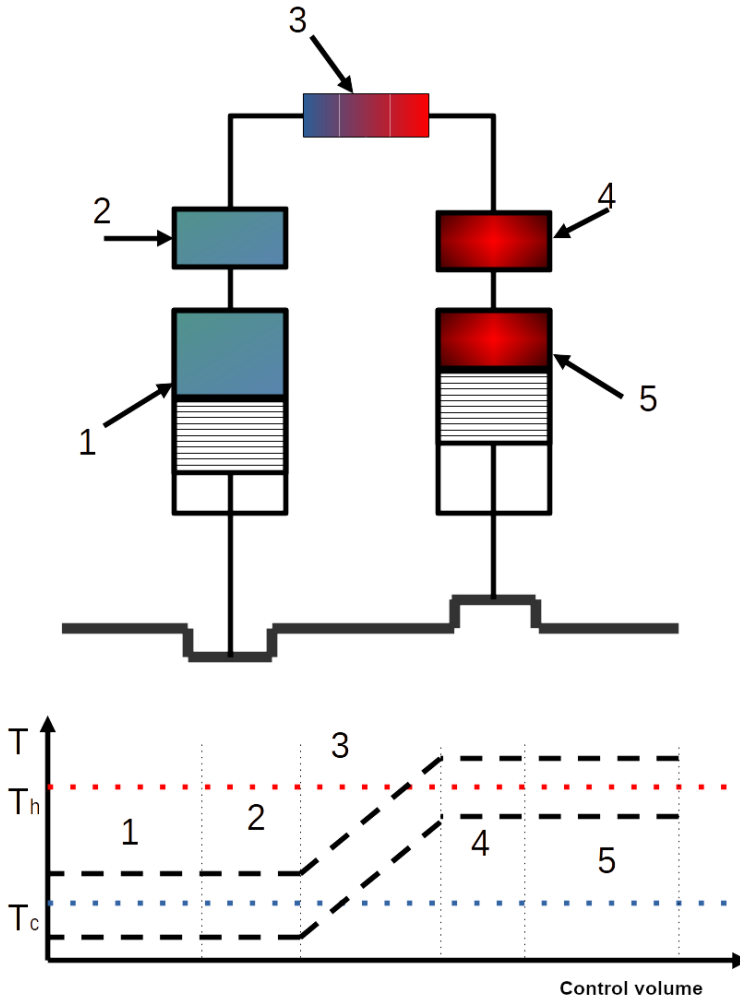


Figure 1.11: Schematic and temperature distribution in the control volumes of the "SIMPLE" model. 1 - compressor, 2 - cooler, 3 - regenerator, 4 - heater, 5 - expander. T_c - cooler temperature, T_h - heater temperature

A different class of models are the "polytropic" models (Fig. 1.12), which join the heat exchangers together with the cylinders, while making provisions for variable temperatures, heat transfer rates and heat exchange areas. A model like this was proposed by Szczygieł et al [16] in 2017 and validated by comparison with data obtained from CFD simulations. In that particular work, constant values of heat transfer coefficients were used and the gas was assumed ideal.

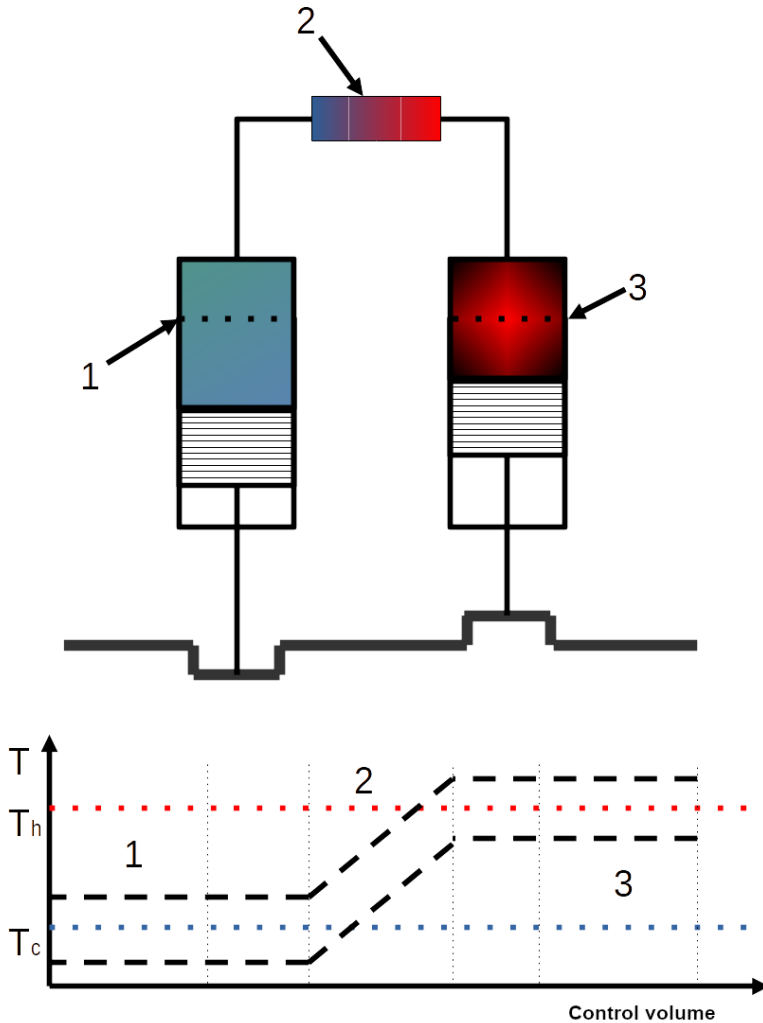


Figure 1.12: Schematic and temperature distribution in the control volumes of the polytropic model. 1 - compressor/cooler, 2 - regenerator, 3 - expander/heater. T_c - cooler temperature, T_h - heater temperature

Other models, such as the model of Wang [82] use correlations used by other authors in the modelling of cryocooler of the pulse tube variety [32, 81], which is ultimately taken from Kay's textbook on compact heat exchangers [33]. Aksoy et al use fixed values of heat transfer coefficients [5] and test the model output for these assumptions.

Chapter 2

Stirling engine modelling

As outlined in the previous Chapter, there are several approaches to constructing Stirling engine mathematical models. They have however certain shortcomings. Isothermal and adiabatic models, due to assuming temperature values in control volumes don't allow for calculation of heat transfer coefficients inside the model. More elaborate adiabatic models such as the "SIMPLE" model however do allow this. Another shortcoming is the customary assumption of the ideal gas model. This can lead to error in high pressure engines [54]. Due to the aforementioned considerations, it was decided to construct a model based on assumptions similar to the model of Szczygieł et al [16], which showed good agreement with CFD data for a low pressure engine, but to use a real gas model (CoolPROP libraries) for the fluid properties.

2.1 The zero-dimensional, real gas model

2.1.1 The development of the zero-dimensional real gas model

In order to ascertain engine behaviour and characteristics, a model had been developed accounting for the thermodynamic processes occurring inside the engine. This was done by formulating energy and mass balance equations for the three separate chambers of the engine, eg. the heater/expander, regenerator and cooler/compressor. What is taken into account, is energy exchange by the means of mechanical work and heat transfer into the gas medium from the heater, regenerator and cooler. In order to simplify the model and shorten the computational time, following assumptions were made:

- the pressure inside the engine is uniform, pressure losses are neglected,
- the walls of heater and cooler are of constant temperature,

- the regenerator changes its temperature in a uniform manner,
- outside of the cooler area heat losses are neglected,
- no leakages of the medium are considered,

Furthermore, there are certain assumptions made when convective heat transfer is analysed, these being taken from their respective heat transfer models. The equations of balance take form of differential equations, expressed as a function of crank angle. Real gas has been used as the working fluid due to the discrepancies of ideal gas calculations at high pressures. The gas parameters are calculated using CoolProp libraries.

2.1.2 Kinematics of the piston movement

First, the relationship between crank angle, angular velocity and the surface area and volume need to be discussed. The angular velocity is derived from the given rotational speed (which is an input for the model) as:

$$\omega = \frac{2\pi n}{60}. \quad (2.1)$$

The piston position is described by equation is [2]:

$$x(\varphi) = r(1 - \cos\varphi) + \frac{r/l}{4}(1 - \cos 2\varphi). \quad (2.2)$$

The derivative of the piston position in respect to time constitutes the piston velocity:

$$w(\varphi)_v = \omega(-r\sin\varphi - \frac{r^2\sin\varphi\cos\varphi}{\sqrt{l^2 - r^2\sin^2\varphi}}), \quad (2.3)$$

where l is the connecting rod length, r the radius of the crank, and φ the crank angle. It has to be noted, that those equations are only valid for a conventional crank mechanism. The cylinder volume for any cylinder can be expressed as:

$$V_v = V_{cl} + A_v x_v(\varphi_v), \quad (2.4)$$

where V_{cl} is the clearance volume of the cylinder, this can be assumed as a fraction of the total swept cylinder volume, and denoted as ε_{cl} . The fraction can be also expressed as:

$$V_v = A_v x_v(\varphi_v) + 2\varepsilon_{cl} A_v r. \quad (2.5)$$

The piston velocity multiplied by piston area gives the derivative of cylinder volume over crank angle:

$$\frac{dV_v}{d\varphi} = \frac{dx_v}{d\varphi} A_v = \frac{dx_v}{d\tau} \frac{d\tau}{d\varphi} A_v = w_v \frac{d\tau}{d\varphi} A_v = \frac{w_v A_v}{\omega}, \quad (2.6)$$

where τ is time – in case of numerical integration, this is equivalent to the time period of a step in the model. Equations of motion and volume are solved separately for the compressor and expander volumes, one of which being advanced by the angle γ . The volume of the regenerator remains constant and is one of the input arguments of the model.

The adiabatic model of Urieli [79] separates the heat exchange surfaces from the cylinders. This is valid only for some engines, and can be questioned due to the open connections existing between the exchangers and cylinders in most designs [75]. Therefore, the approach of Szczygieł et al. [72] is considered more valid – that is the cylinders are not separated from the heat exchange volumes as far as balance equations are concerned. The assumption of that model, that the cylinder wall is the only heat exchange surface is however not used in this work, and a more general approach is taken, where the area is expressed as:

$$A_v = \varepsilon_{av} x_v(\varphi) O_v + A_d, \quad (2.7)$$

where A_d is any additional area, such as the cylinder head, additional exchangers or other solutions discussed further. This is assumed to be constant. O_v is the cylinder perimeter. The number ε_{av} is defined as the cylinder surface development coefficient and can equal anything from 0 for an engine with no heat transfer through the cylinder walls, 1 for a conventional design, and any higher positive value if the surface is developed, elongated, etc.

2.1.3 Mass and energy balance

To use the first law of thermodynamics, a system needs to be defined. It is proposed, that for different equations used in the model, the boundaries be set as:

1. the expansion cylinders,
2. the compression cylinders,
3. the gas space of the regenerator,
4. the solid mass of the regenerator,
5. the engine as a whole sans the regenerator solid mass.

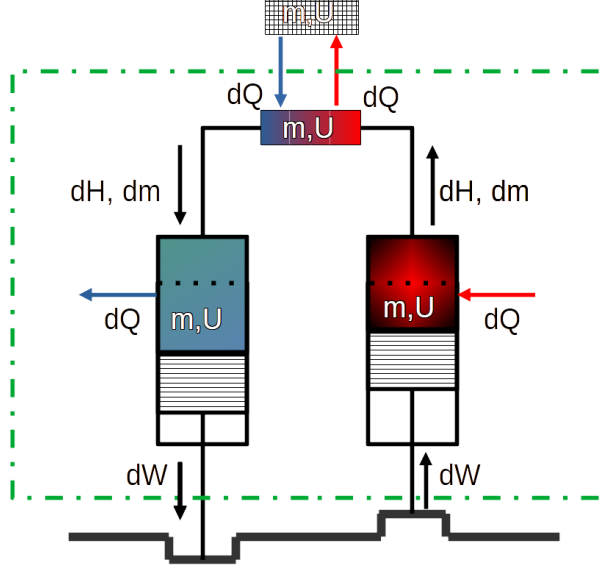


Figure 2.1: System boundaries of the model

The control volume is illustrated in Fig. 2.1

The energy balance, according to Ocheduszko [54], can be written in a general, differential form for a cylinder-piston apparatus:

$$dU = dH + dQ + dL = d(mh) + dQ + pdV, \quad (2.8)$$

which can be expressed with respect to the crank angle:

$$\frac{d(mu)}{d\varphi} = \frac{dmh}{d\varphi} + \frac{dQ}{d\varphi} + p(\varphi) \frac{dV}{d\varphi}. \quad (2.9)$$

This equation is true for all the control volumes. It can be noted, that for the both the solid (metal filament) and gas regenerator masses, where the volume is constant, $dV/d\varphi = 0$ and the work expression is omitted. Furthermore, for the solid mass, there is no inflow or outflow of fluid, therefore $dm/d\varphi = 0$. It can also be seen, that as no leakage is assumed, setting the boundary outside the engine eliminates the terms related to the exchange of mass, eg. $dm/d\varphi$ (though the internal energies of each gas spaces being different needs to be taken into account). Those considerations, lead to formulating the form of the energy conservation equation for each volume.

For the expansion cylinder, seen on the left in Fig.2.1, energy leaves the boundary as work, enters as the heat flux and as the enthalpy into the cylinder from the regenerator. Therefore:

$$\frac{d(m_h u_h)}{d\varphi_h} = \frac{dm_{r-h} h_{r-h}}{d\varphi_h} + \frac{dQ_h}{d\varphi_h} + p(\varphi_h) \frac{dV_h}{d\varphi_h} \quad (2.10)$$

The convention assumed for this volume, is the flow of mass into, and the flow of heat into this volume will have a positive sign. It can be noted, that the pressure, as a global parameter of the whole engine is referred to as a function of the angle of the expander crank, and will be referred to that way in this work. The pressure is the function of at least two independent gas properties, and the evaluation method will be shown further. The expression referring to heat flow can be understood as the amount of energy passed from the walls to the gas in the cylinder during a change of the crank angle by $d\varphi$. If so, it can be evaluated as:

$$\frac{dQ_h}{d\varphi_h} = A_h(\varphi_h) \alpha_h(\varphi_h) [T_{wh} - T_h] \cdot \frac{d\tau}{d\varphi_h} = \frac{A_h(\varphi_h) \alpha_h(\varphi_h) [T_{wh} - T_h]}{\omega} \quad (2.11)$$

The area A_h is to be evaluated from equation (2.7.) The convective heat transfer coefficient α is itself a function of the gas parameters at the particular angle. Its evaluation is a matter of current research and the applicability of models is discussed further. The temperature of the wall is proposed to be assumed constant and part of the input data. It is known [54], that fluctuations in the wall temperature will occur in piston-cylinder devices due to cyclically varying boundary conditions. However as the work of Martage et.al [49], shows the variations in temperature to be in the range of 1K. The compression cylinder, seen on the right of Fig.2.1, is a subject to the same mass and energy transfer mechanisms. A different approach is however taken in the regard to the signs, that is, the outflow of mass to the regenerator is considered positive, the heat flow out of the volume is considered negative. Therefore:

$$\frac{d(m_c u_c)}{d\varphi_c} = \frac{-dm_{c-r} h_{c-r}}{d\varphi_c} + \frac{dQ_c}{d\varphi_c} + p(\varphi_c) \frac{dV_c}{d\varphi_c}, \quad (2.12)$$

and:

$$\frac{dQ_c}{d\varphi_c} = A_c(\varphi_c) \alpha_c(\varphi_c) [T_{wc} - T_c] \cdot \frac{d\tau}{d\varphi_c} = \frac{A_c(\varphi_c) \alpha_c(\varphi_c) [T_{wc} - T_c]}{\omega} \quad (2.13)$$

Also, notably $\varphi_c = \varphi_h - \gamma$, where the phase offset γ is equal to 90 degrees (conventionally) or a different value.

Inside the regenerator, energy is only exchanged through heat transfer through the walls, the area being constant, and the volume being constant [79], no mechanical work occurs. Therefore, the equation of energy balance for the gas in regenerator can be written as:

$$\frac{d(m_r u_r)}{d\varphi_c} = \frac{dm_{c-r} h_{c-r}}{d\varphi_c} + \frac{dQ_r}{d\varphi_c} - \frac{dm_{r-h} h_{r-h}}{d\varphi_c} \quad (2.14)$$

While the derivative of heat exchanged over crank angle is:

$$\frac{dQ_r}{d\varphi} = \frac{A_r \alpha_r(\varphi_c) [T_{avg-r} - T_{mr}]}{\omega} \quad (2.15)$$

As this heat is being exchanged between the gas and the solid mass, the energy balance equation for the solid mass follows as:

$$m_{mr} C p_{mr} \frac{dT_{mr}}{d\varphi_c} = -\frac{dQ_r}{d\varphi_c}, \quad (2.16)$$

where m_{mr} is the solid mass of the regenerator matrix and $C p_{mr}$ its specific heat. The mass balances for each control volume can be summed as (using the angle of the cold cylinder crank as the variable):

$$dm_{c-r} - dm_{r-e} = dm_r \quad (2.17)$$

$$m_c(\varphi_c) + m_e(\varphi_c) + m_r(\varphi_c) = m_{tot} = const, \quad (2.18)$$

as the mass of the gas remains constant in the system as a whole. This is based on the no-leakage assumption.

The presented model has been published in a 2019 paper [64]. In further work the model was improved. The improvements entailed the inclusion of several separate loss mechanisms. This includes:

1. pressure losses,
2. finite time losses,
3. leakage to the buffer space,
4. heat loss through cylinder walls,

2.1.4 Pressure losses

In the case of pressure losses the approach taken is similar to the Schmidt model based models of the Philips company [50]. Losses are calculated separately after the calculation is finished, based on the state data and velocities in each volume for each time step, then integrated, and the pumping loss is subtracted from the

work produced in each time step. The pressure difference was calculated using a formula applied by Wang [82] and by Petrescu [59], which takes the form of a simple correlation related to piston speed (in m/s) and outputs the pressure loss in Pa:

$$\Delta p = \pm(0.97 + 0.045w_p) \cdot 10^5 \text{ Pa.} \quad (2.19)$$

The finite time loss was evaluated by a formula used by the same authors, which has the form

$$\Delta p = \pm \frac{aw_p}{c} \text{ Pa,} \quad (2.20)$$

where $a = \sqrt{3\kappa}$, and c is the "average molecular speed" calculated as $c = \sqrt{3R_{fluid}T_{fluid,v}}$ evaluated for each time step in each volume.

2.1.5 Leakage losses

Leakage losses were added due to the fact that the ML3000 engine (used for validation) has no piston rings or seals of any kind and rather relies on a good quality of part fit between the piston and cylinder. The leakage loss was therefore expected to be significant. The calculation method for the mass flows was based on the work of Wang [82], however with a key difference. Wang considers the leakage term only in regards to the energy balance, which is likely justifiable in their case due to a small volume of leak. In this work, the mass balances are considered as well. The mass flow between the buffer and the cylinder space is evaluated as:

$$\dot{m}_{vb} = \pi D_p \frac{p_v + p_b}{4R_v T_v} \left(w_p g - \frac{g^3(p_v - p_b)}{6\mu_v L_p} \right), \quad (2.21)$$

where the index vb denotes "from volume to buffer" and L_p is the piston length. The formula might introduce error due to not accounting for piston grooves, however this effect was neglected. As the model uses the engine crank angle for its integration steps, this formula is adjusted to provide a mass leak per angle difference:

$$\frac{dm_{vb}}{d\varphi} = \dot{m}_{vb} \cdot \frac{d\tau}{d\varphi}, \quad (2.22)$$

and the enthalpy transport due to leakage is calculated as:

$$\frac{dm_{vb}h_{vb}}{d\varphi} = \dot{m}_{vb} \cdot h_{vb} \frac{d\tau}{d\varphi}, \quad (2.23)$$

where h_{vb} is the gas specific enthalpy evaluated for the instantaneous cylinder or buffer temperature and pressure depending on the direction of flow. Importantly, the buffer pressure p_b is assumed to be equal to the mean cycle pressure, and the temperature to the cold space temperature. The buffer is treated as an infinite

reservoir due to its large volume. The values of energy and mass transport per angle difference are added to the mass and energy balances of the volumes.

2.1.6 Heat losses through cylinder walls

Heat losses through cylinder walls are evaluated by the same methodology as heat transfer through heat exchangers, that is equations (2.11) and (2.13). It has to be noted however, that the heat transfer area is variable (unlike for the fixed exchanger surfaces). It also needs to be noted that the wall temperature is assumed as T_c for both cylinder. This is due to the fact that in the Genostirling engine, the surfaces of the expansion cylinders are cooled for tribological reasons.

2.1.7 Evaluation of heat transfer coefficients

Nusselt's correlations

The first, in the historical sense, correlation for estimating the heat transfer in a piston-cylinder system is due to Nusselt [52], published in 1923. This is a global correlation, describing the heat transfer coefficient averaged across the stroke period. It was formulated as follows:

$$\alpha_m = 1.16 \left[1 + 1.24 \cdot w_p p^{\frac{2}{3}} T_i^{\frac{1}{3}} + 0.421 \frac{\left(\frac{T_i}{100}\right)^4 - \left(\frac{T_w}{100}\right)^4}{T_i - T_w} \right], \quad (2.24)$$

where T_i is the internal gas temperature in K, p is the mean effective pressure in Pa, w_p is the piston speed and T_w is the wall temperature in K.

The correlation is given in a dimensional form. The work it originates in is concerned with internal combustion engines. The second part of the equation is the radiant heat transfer term, while the first is the convective one. The formula was based on experiments simulating the conditions in internal combustion engines using cylindrical bombs and separate experiments with forced convection on plane surfaces [52].

A correlation for instantaneous heat transfer coefficient by the same author, from 1928 [53] has been determined for piston machines in general, and can be stated as follows:

$$\alpha(t) = 0.0278(1 + 0.38w_p)p(t)^{\frac{2}{3}} \cdot T_i(t)^{\frac{1}{3}}, \quad (2.25)$$

This formula lacks the radiant term, likely due to the lack of combustion being considered, though similarities between the two are clear. The formulae of Nusselt can be considered to be of historical rather than practical significance today.

Although Nusselts formulas were created to provide an average heat transfer coefficient, they have also been utilized to provide instantaneous values [13], hence, they are shown as a function of time.

The Nusselt correlation from equation 2.24 has been expanded upon by Brillig [94], who proposed a different values of some of the constants. This is shown below:

$$\alpha(t) = 1.16 \left[3.5 + 0.185 \cdot w_p p^{\frac{2}{3}} T^{\frac{1}{3}} + 0.421 \frac{\left(\frac{T_i}{100}\right)^4 - \left(\frac{T_w}{100}\right)^4}{T_i - T_w} \right]. \quad (2.26)$$

Eichelberg's correlation

The correlation of Eichelberg, from 1939 [20] is based on experiments carried out on an actual internal combustion engine. The correlation was to predict instantaneous heat transfer rates. The experiments were carried out on a naturally aspirated, two stroke engine and later four stroke engine (both Diesel Engines) [13]. The formula is as follows:

$$\alpha(t) = 7.67(w_p)^{1/3}(pT_i)^{1/2}, \quad (2.27)$$

where T_i is the internal gas temperature in K, p the pressure in Pa, w_p the piston speed in m/s.

This direct measurement reportedly was based on harmonic analysis of temperature fluctuations in a probe normal to the cylinder surface. According to Annand [74] this formula is contradictory to later formulas and experimental work. It is necessary to note that the value of $\alpha(t)$ tends to zero when the piston speed reaches zero, that is, in the dead centres. This is obviously erroneous, though as it will be shown later, many other correlations show such behaviour. This, amongst other problems was the subject to a correction by Pflaum [60] in 1961 who modified the velocity term.

The work from 1960 by Oguri [55], experimentally confirmed the formula for a spark ignition engine (114.3x140 mm bore and stroke), though only for the expansion stroke.

Heinen [28] made an experimental investigation of heat transfer in the combustion chamber of an internal combustion engine and found that the Eichelberg formula can give good agreement if instantaneous gas velocity is substituted for the piston velocity. Otherwise, it was concluded that the heat transfer coefficient was underestimated.

Elser's correlation

Oguri [55] has also pointed to the works of Karl Elser [21]. The correlation is based on the following assumptions: heat transfer occurs mainly in a small boundary

layer close to the cylinder walls, the advective flow of particles occurs mainly perpendicular to the walls and thirdly, pressure fluctuations have no effect on the heat transfer phenomenon. Also, the formulas are derived for an ideal gas. It is important to note, that the experimental work by Elser had been done in a cylinder without combustion. The correlation derived in this work is as follows:

$$\text{Nu} = 6.5\sqrt{\text{Pe}'} \left(1 + 0.5\frac{\Delta s}{C_p} \right), \quad (2.28)$$

where Pe' is the Peclet number, here defined with the mean piston speed w_m :

$$\text{Pe}' = \frac{w_m L}{a}, \quad (2.29)$$

and the change of entropy over the specific heat $\frac{\Delta s}{C_p}$ can be calculated as:

$$\frac{\Delta s}{C_p} = \ln \left(\frac{T_i}{T_0} \right) - \frac{\kappa - 1}{\kappa} \ln \left(\frac{p}{p_0} \right), \quad (2.30)$$

where κ is the specific heat ratio, T_i means gas temperature, p_i is gas pressure and the index "0" refers to a reference value.

An ideal gas is assumed in the cylinder. The index 0 denotes the beginning of the stroke. Annand [74], pointed out that this ratio, although non-dimensional, had been derived by both thermodynamic and algebraic errors in the original derivation of the formulae by Elsner.

Despite this, the formula was partially validated and expanded upon by Oguri[55], to be written as:

$$\text{Nu} = 1.75\sqrt{\text{Pe}'} \left(1 + 0.5\frac{\Delta s}{C_p} \right) [2 + \cos(\phi - 20^\circ)], \quad (2.31)$$

where the crank angle ϕ is zero at the top dead center. Oguri's experiments have been carried out on two Diesel engines, of the bores and strokes of 380x460 and 390x520 mm.

Woschni's correlation

The Woschni correlation was created in 1967 as an empirical correlation for calculating the convective heat transfer coefficients in internal combustion engines. It was developed experimentally, using a motored and modified four stroke engine, with a custom camshaft (dimensions were not provided) [87]. The author had pioneered the use of computer aided engine modeling techniques, and the computer programs developed in this research were used as an aid in the creation of the heat transfer correlations [87, 86]. The correlation was validated using a Diesel engine, with

165x155 mm bore and stroke and a 14.7 compression ratio where a 10% uncertainty was shown [70]. In the original work, the author discusses two methods for the measurement of heat transfer inside an engine cylinder. One being the use of a spherical bomb to model the phenomena occurring during the combustion phase, the other being use of an un-fired engine treated essentially as a heat exchanger. The camshaft of the used engine had been modified in a manner that it would intake and exhaust gas once per cycle to investigate the parameters during the scavenging period, and with a normal camshaft to evaluate the heat transfer during the compression and exhaust. Additional experiments with a fired engine were also conducted and their results were compared to the results obtained from the spherical bombs to analyse the influence of combustion.

The correlation can be written in a non-dimensional form:

$$\text{Nu} = 0.035\text{Re}^{0.8}, \quad (2.32)$$

where:

$$\text{Re} = \frac{w_g D_v}{\nu}. \quad (2.33)$$

The gas velocity w_g is given as $w_g = 6.618w_p(\varphi_v)$ for the scavenging period and $w_g = 2.28 \cdot w_p(\varphi_v)$ for compression, where φ_v means the crank angle and D_v is the piston diameter. For combustion and expansion, the following formula is given for velocity:

$$w_{c+ex} = 2.28 \cdot w_p(\varphi_v) + 3.24 \cdot 10^{-3} \cdot \frac{V_s T_1}{p_1 V_1} (p - p_0), \quad (2.34)$$

where the second term is empirically derived and has to do with the intensity of combustion. p_1 and T_1 represent the known state of working gas related to the instantaneous cylinder volume V_1 at beginning of combustion, while p_0 means pressure in cylinder without the combustion process.

The Woschni correlation is one of the most widely used for internal combustion engine modeling, and is often applied to other reciprocating machines. Rutczyk et al [64] proposed using it for Stirling engines, Tuhovcak [78] proposed its use for compressors.

Annand's correlations

Annand was one of the first to provide a general overview of previous work on heat transfer in internal combustion engine cylinders [74] and to also re-analyse some of the available correlations using his own data. Another paper, concerning heat transfer in a cylinder head was published in 1970 [8]. His opinion of the previous correlations was highly critical, noting not only a lack of accuracy when such

experimental comparisons were made, but also the dimensional incorrectness of some of the formulae.

Annand makes extensive use of data obtained by other researchers, mainly of Overbye et al from 1961 [57], though the data of Elser [21] was also used for comparison. Other sets of analyzed experimental data are notably the local heat flux measurements of Pischinger and Pflaum [62, 60]. Experimental methods of using *heat collectors* placed in the clearance spaces of motored engines as employed by Moss and Ku are also discussed [51, 38].

After the extensive statistical analysis of the available data, Annand gave a formula for the overall heat transfer, which can be brought to a non-dimensional form for convection only as:

$$\text{Nu} = a\text{Re}^b, \quad (2.35)$$

where a, b are constants, which were defined in the paper from 1963 [74] as:

$$a = 0.35 - 0.8, \text{ depending on the intensity of motion of the charge;}$$

$$b = 0, 7.$$

Different values were provided by other authors [26]:

$$a = 0.2, b = 0.8 \text{ for port injection and;}$$

$$a = 1.1, b = 0.7 \text{ for direct injection.}$$

The equations can also be written as to include the radiant term, for example, as written in SI units by Ziong et al [94]:

$$\alpha(t) = 0.26 \cdot k \left(\frac{\rho^{0.7} w_p^{0.7}}{\mu^{0.7} D^{0.3}} \right) + c_{Ann}(T_i^4 - T_w^4), \quad (2.36)$$

where c_{Ann} is a constant equal to $2.1 \cdot 10^{-13} \frac{\text{W}}{\text{m}^2\text{K}^5}$, which is derived from Annands work [74]. Other variables are piston speed w_p , μ is the kinematic viscosity of the gas, ρ its density, k is the gas thermal conductivity and the temperatures T_i and T_w are of the gas and wall respectively. This can be also shown in a non-dimensional form:

$$\text{Nu} = 0.26\text{Re}^{0.7} + \frac{c_{Ann}D}{k}(T_i^4 - T_w^4), \quad (2.37)$$

where D is the cylinder bore, which is the characteristic dimension for the non-dimensional numbers. Note, that due to the dimension of the constant c_{Ann} this expression is non-dimensional.

Annand and Pinfeld have published another work in 1980, where measurements were made on an unfired cylinder of a diesel engine fed with pressurized air using a quartz pressure transducer and film thermocouple. The engine had a bore and stroke of 122 and 140 mm respectively. The inlet pressure was varied between 1.02 and 1.66 bar, the rotational speed between 1000 and 1600 rpm and temperature between 295 and 374 K. The pressure ratios varied between 16.6 and 20.4. The given correlation was:

$$\text{Nu} = 0.3\text{Re}^{0.7} + \left(1 + 0.27 \frac{D}{V\Delta T} \frac{dT}{dt}\right), \quad (2.38)$$

where V is the cylinder volume.

The influence of temperature fluctuations is of special interest as it can be considered a step towards a complex formulation of the problem, as proposed later by Kornhauser and Smith [36], which is discussed later in this work.

Adair's correlation

The Adair correlation was created in 1972 by Adair et al, for the use in reciprocating compressors [3]. The authors claim an accuracy of 20%, and the correlation was created based on an experimental investigation. The correlation was presented as:

$$\text{Nu} = 0.053 \text{Re}^{0.8} \text{Pr}^{0.6}. \quad (2.39)$$

The author claims, that the measurements were made on a three cylinder, reciprocating compressor (with air as the working fluid) running at constant rotational speed, though the exact dimensions nor parameters were not disclosed. Measurements were carried out using fast response thermocouples where the ones used to calculate heat flux were located in the cylinder head.

The gas velocity is calculated differently as in most other correlations. Adair made the attempt to estimate the swirl component of the gas velocity [3] working of the research of Shipinski [69] and proposed the formulas to be as follows:

$$w = \begin{cases} 2\omega[1.04 + \cos(2\varphi)], & \text{for } \frac{3}{2}\pi < \varphi < \frac{1}{2}\pi. \\ \omega[1.04 + \cos(2\varphi)], & \text{for } \frac{1}{2}\pi < \varphi < \frac{3}{2}\pi. \end{cases} \quad (2.40)$$

The Reynolds number and the characteristic diameter are defined differently also. According to the authors, this is to better model the swish and swirl of the gas [3]. The characteristic diameter is defined as:

$$D_v = \frac{6V_v(\varphi)}{A_v(\varphi)}, \quad (2.41)$$

where A_v , V_v are the cylinder area and volume as a function of the crank angle. This expression varies across the stroke. The Reynolds number is defined as:

$$\text{Re} = \frac{D_v(\varphi) \cdot \frac{D_v(\varphi)w_v}{2}}{\nu}, \quad (2.42)$$

where ν is the gas kinematic viscosity.

Note, that the quantity shown in (2.40) has a dimension of 1/s, which allows for the Reynolds number to be non-dimensional. This expression also varies across the stroke. Those variations have a clear effect on the variation of the heat transfer coefficient itself.

LeFeuvre's correlation

The approach of LeFeuvre (1969) proposed a conventional $\text{Nu} = a\text{Re}^n\text{Pr}^m$ form for the correlation, however with the Reynolds number related to the swirl of the gases rather than piston velocity [42]. The correlation can be written as:

$$\text{Nu} = 0.047 \text{Re}^{0.8} \text{Pr}^{0.33}, \quad (2.43)$$

and:

$$\text{Re} = \frac{r^2 \omega_{sw}}{\nu}, \quad (2.44)$$

where ω_{sw} is the angular velocity of the swirl and r the cylinder radius while ν is the kinematic viscosity.

The measurements are understood to have been done on an engine mentioned in LeFeuvre's work [42], which was 114.3 x 114.3 mm bore x stroke and operated between 100 and 2500 rpm. The author has claimed that the swirl velocity can be assumed constant and that it is the result of swirl created by gas flow to the engine. Reynolds number values are said to be in the range of $1 \cdot 10^5$ to $6 \cdot 10^5$. The measurements were carried out using thermocouples mounted in several positions on the head and sleeve of the cylinder used to determine the heat fluxes. The authors in both of the works [42] outline that the thermocouples used were of a special design suited for transient measurements as designed by Bendersky [12]. The data was then compared to existing correlations. The surface temperatures have been represented by a Fourier series in accordance to a method outlined by Carlsaw [18] and Overbye [57].

Hohenberg's correlation

Hohenberg [29] in 1979 had carried out measurements on Diesel engines. The range of speeds is not precisely given, though it can be deduced from charts they

were in the range between 700 and 2300 rpm. The tested engines had the following bore and stroke dimensions: 128 x 142, 125 x 150, 125 x 130 and 97 x 128 mm. The author had measured cylinder pressure and surface temperatures. The correlation proposed by the author has the form:

$$\alpha(\tau) = 130 \cdot T_i^{-0.4} (p_i \cdot 10^5)^{0.8} V_i^{-0.06} (w_m + 1.4)^{0.8}, \quad (2.45)$$

where T_i is the gas temperature, V_i the gas volume and w_m the mean piston speed. The values of the constants have been validated for all the engines. The correlation, though simple and conventional in form, deserves special attention due to the extensive experimental work carried out in its development. Three methods were used. First the surface temperature method of Eichelberg [20], where the variations of surface temperature of the cylinder wall are measured, and the heat equation is solved. Due to practical problems of this method, Hohenberg proposed to use it only to determine the variations of heat transfer by the variations in temperature. The author has presented his own design of a thermocouple suited for the purpose, built of NiCr and Ni wires coated with gold and insulated with cement. The author has also outlined that the probes could be used to obtain information about the gas flow. Second was the use of a heat flux probe, as proposed by Kind [34], however a major innovation was the use of air instead of ceramics as the insulating material in the probe. One surface of the probe was inserted into the combustion chamber, while the other cooled, ensuring a one dimensional flow of heat. The probe had a form of a cylinder. The third method employed was based on the comparisons of theoretical pressure variations to measured pressure variations. From the comparisons between the pressures it was then possible to determine the heat flow by thermodynamic methods. To simplify those calculations, Hohenberg introduced a thermodynamic loss angle. For an externally driven engine, maximum pressure would be reached at the top dead center, however in practice due to heat loss and gas blow-by this maximum is reached earlier. The author has separated this phase shift into two variables. The heat loss angle:

$$\phi_h = \frac{\Delta Q}{p_{max} \frac{Cp}{R} K_1}, \quad (2.46)$$

and the blow-by loss angle:

$$\phi_b = \frac{1.924 \sqrt{T_i} A_b}{n_m K_1}, \quad (2.47)$$

where:

$$K_1 = \frac{dV}{d\phi}, \quad (2.48)$$

and p_{max} is the maximum pressure, Cp is specific heat, A_b the blow-by area and n_m is assumed to be the rotational speed of the engine.

Disconzi's correlation

Disconzi et al in 2012 have shown interesting work in concerned in the modelling of heat transfer in reciprocating compressors for refrigeration [19]. Their correlation had been created based on CFD simulation results, with consideration paid to previous work, mainly by Adair [3], Annand [74], Fagotti [23] and others. They have shown a set of correlations, separate for the distinct phases of the compressors cycle, that is compression, discharge, expansion and intake. Discharge and intake have separately defined Reynolds numbers. All Reynolds numbers include the mean piston speed as a characteristic parameter, the mentioned two incorporate also the instantaneous velocity of the gas being exchanged. This is shown below:

- compression

$$\text{Nu} = 0.08\text{Re}^{0.8}\text{Pr}^{0.6}, \quad (2.49)$$

where:

$$\text{Re} = \frac{\rho(\tau)Dw_p}{\mu(\tau)}, \quad (2.50)$$

- discharge

$$\text{Nu} = 0.08\text{Re}^{0.8}\text{Pr}^{0.6}, \quad (2.51)$$

where:

$$\text{Re} = \frac{\rho(\tau)D(w_p + w_p^{0.8}w_c(\tau)^{0.2})}{\mu(t)}, \quad (2.52)$$

- expansion

$$\text{Nu} = 0.12\text{Re}^{0.8}\text{Pr}^{0.6}, \quad (2.53)$$

where:

$$\text{Re} = \frac{\rho(\tau)Dw_p}{\mu(\tau)}, \quad (2.54)$$

- intake

$$\text{Nu} = 0.08\text{Re}^{0.9}\text{Pr}^{0.6}, \quad (2.55)$$

where:

$$\text{Re} = \frac{\rho(\tau)D(w_p + 2w_p^{-0.4}w_c(\tau)^{1.4})}{\mu(t)}, \quad (2.56)$$

The quantity $w_c(\tau)$ is defined as:

$$w_c(t) = |\dot{m}|A_p\rho(\tau), \quad (2.57)$$

where $|\dot{m}|$ is the mean mass flow, ρ the fluid density and A_p the piston area.

It has to be noted, that as this is a result of a numerical study, experimental validation is necessary.

Aigner's correlation

Aigner's correlation (1972) has been constructed based on both numerical simulations and experimental measurements of an actual machine - a compressor. The following machines were considered:

- air compressor, of a 220 mm bore, 90 mm stroke, a rotational speed of 980 to 990 rpm and pressure ratios of 1/2 and 1/5 (Burckhardt 2K90-1A)
- compressor, of a 673 mm bore, 140 mm stroke 1182 rpm and a pressure ratio of 2.2/6.4, with nitrogen as a working fluid (Ariel JGD 26.5).

The main difference however had been the number of valves - two and eight respectively [4]. Aigner proposed the use of the Stanton number as his main parameter:

$$\text{St} = \frac{\alpha_c}{\rho w_p C_p}, \quad (2.58)$$

where α_c is the convective heat transfer coefficient, w_p is the piston speed, ρ is the fluid density.

The Stanton number was then adjusted by the authors to fit the numerically calculated heat fluxes from the available data. It was found, that a mean Stanton number value of 0.032 can provide good agreement. It is assumed that the correlation could be utilized in conjunction with a good model for calculating the Stanton number itself in piston cylinder machines.

Lawton's correlation

Lawton in 1987 [40], had provided a non-stationary correlation of engine heat transfer. This was both experimental and analytical work. The experiment consisted of applying a pressure sensor and surface thermocouple to a cylinder of a Perkins 98.4x127 mm bore and stroke, naturally aspirated Diesel engine. The engine was motored (driven externally), with the thermocouple residing inside the injector port, and a numerical scheme was employed for calculating the temperature distribution. The author proposed a non-stationary correlation of heat transfer due to his review of

previous work, such as that of Eichelberg [20] and Whitehouse [84] which suggested limitations of the quasi-stationary correlations.

Lawton observed heat fluxes of an opposite sign to the difference between bulk gas temperature and wall temperature, that is despite the bulk gas being hotter than the wall heat would flow from the wall to the gas. He explained this phenomenon by proposing that there exists a boundary layer near the cylinder surface, the temperature of which follows, but lags behind the bulk gas temperature which changes across the stroke. This assumption is proven by extensive theoretical analysis [40], which itself however assumes a one-dimensional condition within the cylinder.

The author has validated the equation proposed by Annand [8], however has introduced a correction related to a compressibility number, defined as:

$$L = \frac{\kappa - 1}{V(t)} \frac{dV(t)}{dt} \sqrt{\frac{D^3}{aw_{avg}}}, \quad (2.59)$$

where κ is the specific heat ratio, a is the thermal diffusivity and w_{avg} the mean piston speed and postulated an error term which should be added to the original formula:

$$\text{Nu} = 0.28\text{Re}^{0.7} - \frac{2.75LT_w}{T_i - T_w}. \quad (2.60)$$

According to the author, a radiant term can also be added to the overall heat flux. The Reynolds number is defined the same way as in the work of Annand - that is an energy mean velocity suggested by Knight [35].

Kornhauser and Smith correlation

The correlation of Kornhauser and Smith published in 1994 showed a very different approach to most other correlations - that is not based on the assumptions of Newton's law of cooling [36, 37]. As the authors state, the law is only an engineering approximation, not valid when the processes of compression or expansion occur, due to the fact that work is imparted or extracted from the bulk of gas, while heat transfer phenomena occur in the boundary layer. Therefore, a phase lag exists between the bulk gas temperature and the wall temperature. The authors propose to take this into account by the use of a complex Nusselt number, as complex analysis is often applied to wave phenomena. This is largely based on the theoretical work of Pfreim [61] from 1943, who investigated similar phenomena in relation to pressure fluctuations near a flat wall (though with engine cylinders in mind) and also investigated by Lee [41]. This demands a complex formulation of heat flux as:

$$\dot{q}_c = \frac{k}{D_h} (\text{Nu}_r + i\text{Nu}_i) [\Re(T_i - T_w) + i\Im(T_i - T_w)]. \quad (2.61)$$

For sinusoidal temperature fluctuations in the cylinder and a constant wall temperature, this can be written as [36]:

$$\dot{q}_c = \frac{k}{D_h} \left[\text{Nu}_r(T_i - T_w) + \frac{\text{Nu}_i}{\omega} \frac{dT_i}{dt} \right], \quad (2.62)$$

where Nu_r and Nu_i stand for the real and imaginary part of the Nusselt number.

The authors used a gas spring built on top of a compressor to carry out their measurements and derived the temperature based on pressure. Fins have also been applied internally. The experimental rigs main parameters were: bore to stroke - 0.67, 0.42, 1.23, compression (volume ratio) - 2, 4, 8, number of external cylinder fins - 0, 1, 3, 7, working gas - helium, hydrogen, nitrogen, argon. They have related the heat transfer to the oscillation Peclet number defined as:

$$\text{Pe}_\omega = \frac{\omega D_v^2}{4a}, \quad (2.63)$$

where a is the thermal diffusivity, D_v the piston diameter and ω the crank angular velocity. They found that for high Peclet numbers (above 100):

$$\text{Nu}_r = \text{Nu}_i = 0.56\text{Pe}_\omega^{0.69}. \quad (2.64)$$

That is, that the real and imaginary parts are effectively equal. They also claim that the Annand-Pifold correlation [9] was reasonably accurate in the setup. They proposed the rewriting of that correlation for a complex Nusselt number Nu_c as:

$$\text{Nu}_c = 0.3\text{Re}^{0.7} + \left(0.25 \frac{D}{L} \text{Re}^{0.7} \right) \cdot i. \quad (2.65)$$

Lekic and Kok correlation

The complex Nusselt number correlation of Kornhauser and Smith [36] was studied extensively by Lekic and Kok [43, 45, 44] between 2008 and 2011. They endeavored to either validate the Kornhauser Smith correlation or to improve on it. At first, CFD simulations were carried out [44, 43] and later an experimental rig was used [45], consisting of a gas spring with extremely precise tolerances fitted on the base of a Stirling cryo-cooler. The bore and stroke were 50 x 52 mm. This was equipped with pressure transducers, static and dynamic and several thermocouples; two miniature gas thermocouples one in the center of the gas space, one on the wall, three thermocouples on the piston, and a custom heat flux sensor based on several thermocouples. For the heat flux measurement eroding type thermocouples were used to accommodate for the the fast temperature oscillations, similar to ones described in literature [17, 24]. Helium was used as the working fluid. The rotational speeds investigated are 2, 10, 100, 500, 1000, and 1500 rpm.

The authors propose the following correlation for the real (Nu_r) and imaginary (Nu_i) part of the Nusselt number as:

$$\text{Nu}_r = 1.33\text{Pe}_\omega^{0.56} + 5.36, \quad (2.66)$$

$$\text{Nu}_i = 2.04\text{Pe}_\omega^{0.46} - 1.46, \quad (2.67)$$

where Pe_ω is defined the same as for the Kornhauser Smith correlation, Nu_r and Nu_i stand for the real and imaginary part of the Nusslet number.

Toda's correlation

The Toda correlation of heat transfer was developed experimentally, by measuring heat transfer on cylinder walls of the expansion cylinder of an α Stirling engine heated by a separate, electric heating element [77]. As such, it is not intended for the compression cylinder. The correlations are given in both dimensional and non-dimensional forms, the former being an approximation of the latter. Different equations are given for the expansion stroke and compression strokes. For heating and expansion strokes:

$$\alpha_e = 0.042D_v^{-0.42}w_p^{0.58}p^{0.58}T_i^{-0.19}, \quad (2.68)$$

$$\text{Nu} = 0.70\text{Re}^{0.58}. \quad (2.69)$$

For cooling and compression strokes:

$$\alpha_c = 0.042D_v^{-0.47}w_p^{0.53}p^{0.53}T_i^{-0.11}, \quad (2.70)$$

$$\text{Nu} = 0.63\text{Re}^{0.53}. \quad (2.71)$$

The Reynolds number is defined the same as for the Woschni correlation, but the characteristic velocity w_v is simply the instantaneous velocity of the piston without introducing any corrections for internal movement of gas [77].

Liu's correlation

Liu and others have made an experimental investigation into compressor heat transfer in 1984. The experiment had been carried out on an R12 refrigeration compressor, 100 mm x 70 mm bore and stroke of a rotational speed of 1440 rpm, with two cylinders. Wall temperature, pressure fluctuation, gas suction temperature and oil temperature were taken into consideration [46]. Though the correlation derived by the authors has a conventional form of $\text{Nu} = a\text{Re}^b\text{Pr}^c$, the work is of special

interest as apparently measurements were made of temperature distributions inside the cylinder wall. The wall effect has been known to be substantial in reciprocating machines since the early research on steam engines in the 19th century, though very little attention is paid to it in modern work. They proposed a formula for the temperature given in degrees Celsius of the wall at different points along the stroke:

$$t_w^{(c)} = 24.32 + 0.7191t_s^{(c)} + 5.64\varepsilon - 17.936s^2 + 14.183s \text{ deg C}, \quad (2.72)$$

where $t_s^{(c)}$ is the suction temperature in °C, ε the pressure ratio and s is the ratio of the piston position to the bore (the formula is limited to the s/d of 1 or smaller).

Note that the formula does not take into account the temporal variation of the wall temperature. The authors propose a similar formula for the cylinder head:

$$t_{wc}^{(c)} = 13.64 + 0.1791t_s^{(c)} + 11.235\varepsilon \text{ deg C}. \quad (2.73)$$

They also derive empirical equations for the suction gas and oil temperature. The correlation itself is stated as:

$$\text{Nu} = 0.75 \text{Re}^{0.8} \text{Pr}^{0.6}, \quad (2.74)$$

where:

$$\text{Re} = \frac{D_h^2 \omega_g}{2\nu}, \quad (2.75)$$

D_h is the hydraulic diameter:

$$D_h = \frac{3ds}{2s + d}. \quad (2.76)$$

In the equation s and d are the stroke and bore, and the ω_g is the swirl velocity, defined as:

$$\omega_g = 2\omega(1.04 + 0.45 \cos(2\phi)), \text{ for } \frac{\pi}{2} < \phi < \frac{3\pi}{2}, \quad (2.77)$$

$$\omega_g = \omega(1.04 + 0.5 \cos(2\phi)), \text{ for } \frac{3\pi}{2} < \phi < \frac{\pi}{2}, \quad (2.78)$$

ω stands for the crankshaft angular velocity. Above formulas are similar to the formulation by Adair [3].

Fagotti's correlation

Fagotti and others have presented some work on heat transfer in reciprocating compressors in 1994 [23] which was followed by their own correlation for compressor heat transfer in 1998 [22]. Though they have found a fairly good agreement between the correlations of Adair and Annand with real measurements for reciprocating compressors, they decided to follow the work of Lawton [40] on internal combustion

engine heat transfer and of Kornhauser [36]. That is to say, to acknowledge the existence of a phase difference between the wall and gas temperature, negating Newton's law of cooling for reciprocating machine applications.

Their work validates the correlation using a finite-volume method simulation which and only then compares it with experimental results. This is largely due to the difficulty of making instantaneous in-cylinder measurements. The authors used a reciprocating, hermetic compressor working with R134A, though the fitting was done based on results from a valveless machine. The correlation obtained has the following form:

$$\text{Nu} = 0.28\text{Re}(t)^{0.65} + 0.25\text{L}(t)\frac{T_w}{T_i - T_w}, \quad (2.79)$$

where $\text{L}(t)$ is the compressibility number as defined by Lawton:

$$\text{L} = \frac{\kappa - 1}{V(\tau)} \frac{dV(\tau)}{d\tau} \sqrt{\frac{D^3}{aw_{avg}}}. \quad (2.80)$$

The authors state however that the correlation is only valid for their experimental machine, the parameters of which are not fully disclosed.

Kanzaka and Iwabuchi correlation

Oscillatory flow heat transfer correlations are considered to be out of the scope of this paper. However, as some of them were created in and for the process of investigating heat transfer in Stirling cycle machines (engines and refrigerators) which are piston machines the authors felt it was necessary to bring some of them to light in this review.

Chronologically, the first such correlation found is the correlation of Kanzaka and Iwabuchi [30, 30]. The authors have published two papers in 1992. The first one [30], detailed an experimental study based on a test rig consisting mainly of a tube connected between two reciprocating piston machines which induced periodically oscillating flow. This tube was electrically heated and fluid temperatures were measured inside the tubing. Wall temperatures were also measured. The tube was 10.5 mm in diameter with a wall thickness of 1.7 mm. The piston bore was either 20 or 30 mm, while the stroke was kept constant at 150 mm. The phase angle between the two driving cranks was chosen as either 90, 120 or 180 degrees. nitrogen and helium were used as the working fluids. According to their results, they presented a correlation:

$$\text{Nu} = 0.21\text{Re}_{sc}^{0.8}\text{Pr}^{0.4} \left(\frac{T_w}{T_i}\right)^{-0.5} C', \quad (2.81)$$

where:

$$C' = 0.923 + 0.75 \left(\frac{T_w}{1000} \right). \quad (2.82)$$

The Reynolds number Re_{sc} is evaluated using the gas velocity from calculations using the Schmidt isothermal Stirling engine model. This correlation was later validated using an actual Stirling engine in their second paper from 1992 [30].

Zhao and Cheng correlation

Zhao and Cheng in 1994 proposed a correlation that can be used for the design of Stirling engine heat exchangers [91]. This correlation was derived numerically, using a controlled volume approach, for a laminar, oscillatory flow through a pipe of constant temperature. The calculations were mostly done for air, with $Pr = 0.71$, with the ratio with length to diameter of the pipe $L/D = 40$. The correlation is based on four similarity parameters, this being $A_0 = x_{max}/D$, the dimensionless oscillation (x_{max} is the maximum fluid displacement), L/D - the length to diameter ratio, Pr being the Prandtl number and a kinetic Reynolds number $Re_\omega = \frac{\omega D^2}{\nu}$, where ω is the oscillatory frequency and ν the kinematic viscosity of the fluid. This nomenclature is often used in other oscillatory flow models based of the authors' work [91]. The correlations provided are for a time-space averaged Nusselt number, and are as follows:

$$Nu_{avg} = 0.00495A_0^{0.9}Re_\omega^{0.656}, \quad (2.83)$$

for $A_0 = 10$ to 35 , $Re_\omega = 10$ to 400 , $L/D = 40$,

$$Nu_{avg} = 0.00495A_0^{0.9}Re_\omega^{0.656} \cdot [43.74(D/L)^{1.18} + 0.06]. \quad (2.84)$$

for varying L/D , $A_0 = 20$ and $Re_\omega = 250$, $A_0 = 25$ and $Re_\omega = 180$, $A_0 = 35$ and $Re_\omega = 100$.

The authors have continued their work on the problem, publishing a paper detailing an experimental study [92]. The experimental apparatus consisted of a long pipe filled with air, connected to coolers on both ends, and to two sides of a reciprocating, double acting cylinder with a piston, driven mechanically through a scotch yoke mechanism by an electric motor with speed control (variable between 7 and 570 rpm). The tube was $L = 60.5$ cm in length, with an inside diameter of $D_i = 13.5$ mm, outside diameter of $D_{out} = 15.7$ mm and made of copper. This tube was uniformly heated by an electric heating element. It is important to note that x_{max} is noted by the authors as the air pump's stroke. The correlation (valid for very long tubing) presented based on the results of the experiment and parallel numerical investigation is:

$$\text{Nu}_{\text{avg}} = 0.02A_0^{0.85}\text{Re}_\omega^{0.58}. \quad (2.85)$$

Xiao's correlation

This correlation is proposed by Xiao et al [88] in 2014 for Stirling engine heaters, where the correlation can be written:

$$\text{Nu} = 0.0162A_o^{0.85}\text{Re}_\omega^{0.43}. \quad (2.86)$$

The nomenclature used in the correlation is similar to the correlation of Zhao et al [91]. The parameters are defined as A_o being the dimensionless displacement, and Re_ω being the kinetic Reynolds number.

$$A_o = \frac{x_{\text{max}}}{d_i}, \quad (2.87)$$

where x_{max} is the maximum displacement and d_i is the heater tube diameter. The number ω is the angular frequency.

$$\text{Re}_\omega = \frac{\omega d_i^2}{\nu}. \quad (2.88)$$

The correlation was developed using an experimental Stirling engine, fitted with a heater of 36, u-shaped tubes, 6 mm in diameter and 298 mm in length. The piston had a diameter of 110 mm.

This correlation differs significantly from the previous ones, in the fact that it was developed for oscillating flow in small diameter tubing. It was experimentally investigated in a Stirling engine and compared with other oscillating flow and developed flow models by Kuosa [39].

Organ's correlation

Organ in his 2013 book [56] proposed an entirely different approach to Stirling engine heat transfer calculations rooted in the dimensionless (0-order) modeling of Stirling engine behavior as proposed by Beale. He proposes the use of a parameter XQ_E , which is non-dimensional and defined as:

$$XQ_E = \frac{Q_v}{\omega p_o V_{sw}} \cdot \frac{N_T}{L_x/d}, \quad (2.89)$$

where N_T is defined as the ratio of expander and compressor temperatures:

$$N_T = \frac{T_e}{T_i}, \quad (2.90)$$

while ω is the crank angular velocity, Q_v is the engine heat consumption, p_o a reference engine pressure, V_{sw} the swept volume of the engine, L_x the heat exchanger length, d its diameter. This parameter XQ_E is referred to as the thermal load.

Using measured Stirling engine data from several researchers [27, 58, 73, 48] the author derives a fitted equation relating the thermal load to a characteristic Reynolds number Re_ω . This Reynolds number is defined as:

$$Re_\omega = \frac{N_{sg} N_{ma}^2}{\delta_x f (T/T_i)} \cdot \frac{(L_x/V_{sw}^{1/3})^2}{L_x/d}, \quad (2.91)$$

where f is frequency in cycles per second, δ_x is dimensionless deadspace, N_{sg} is the *Stirling parameter*, defined as:

$$N_{sg} = \frac{p_o}{\mu\omega}, \quad (2.92)$$

and N_{ma} is the *characteristic Mach number*:

$$N_{ma} = \frac{\omega L_{ref}}{\sqrt{RT_i}}, \quad (2.93)$$

L_{ref} means reference length.

The derived correlation is given as:

$$XQ_E = \frac{4}{Re_\omega} + 1.9 \cdot 10^{-4}. \quad (2.94)$$

Though this is not a correlation for a heat transfer coefficient in the same sense as the others, this relation provides a way of estimating heat transfer in Stirling engine, multitube heat exchangers if the non-dimensional analysis as outlined by Organ [56] is utilized. As such it was decided to include it in this paper.

Formula summary

The analyzed formulas have been gathered together chronologically in the list below. Any variables or non-dimensional numbers if not defined classically are explained below the equation. Machines or processes on which the data was obtained and their dimensions are listed if available.

- Nusselt, 1923, measured on cylindrical bombs,

$$\alpha(t) = 1.16 \left[1 + 1.24 \cdot w_p p^{\frac{2}{3}} T^{\frac{1}{3}} + 0.421 \frac{\left(\frac{T_i}{100}\right)^4 - \left(\frac{T_w}{100}\right)^4}{T_i - T_w} \right], \quad (2.95)$$

where: w_p - piston speed.

- Nusselt, 1928, for general reciprocating machines,

$$\alpha(t) = 0.0278(1 + 0.38w_p)p(t)^{\frac{2}{3}} \cdot T(t)^{\frac{1}{3}}, \quad (2.96)$$

symbols as above.

- Brilling, 1931, diesel engine of unknown dimensions,

$$\alpha(t) = 1.16 \left[3.5 + 0.185 \cdot w_p p^{\frac{2}{3}} T^{\frac{1}{3}} + 0.421 \frac{\left(\frac{T_i}{100}\right)^4 - \left(\frac{T_w}{100}\right)^4}{T_i - T_w} \right], \quad (2.97)$$

symbols as above.

- Eichelberg, 1939, 2 and 4-stroke diesel engine, bore and stroke 114.3x140 mm,

$$\alpha(t) = 7.67(w_p)^{1/3}(pT_i)^{1/2}, \quad (2.98)$$

where: T_i - instantaneous temperature.

- Elser, 1954, 2 and 4-stroke diesel engine, bore and stroke 381x460, 460x521 mm, at 200 – 400 and 200 rpm

$$\text{Nu} = 6.5\sqrt{\text{Pe}'} \left(1 + 0.5 \frac{\Delta S}{C_p} \right), \quad (2.99)$$

where: $\text{Pe}' = \frac{w_m L}{a}, \frac{\Delta s}{C_p} = \ln\left(\frac{T}{T_0}\right) - \frac{\kappa-1}{\kappa} \ln\left(\frac{p}{p_0}\right)$.

- Oguri, 1960, diesel engine, bore and stroke 380x460, 490x520 mm,

$$\text{Nu} = 1.75\sqrt{\text{Pe}'} \left(1 + 0.5 \frac{\Delta S}{C_p} \right) [2 + \cos(\phi - 20^\circ)], \quad (2.100)$$

where: $\text{Pe}' = \frac{w_m L}{a}, \frac{\Delta s}{C_p} = \ln\left(\frac{T}{T_0}\right) - \frac{\kappa-1}{\kappa} \ln\left(\frac{p}{p_0}\right)$.

- Annand, 1963, IC engines, with use of data from Elser,

$$\text{Nu} = aRe^b, \quad (2.101)$$

where: $0.35 < a < 0.7, b = 0.7$ for Diesel, $a = 0.2, b = 0.8$ for port injection - spark ignition, $a = 1.1, b = 0.7$ for direct injection - spark ignition.

- Ziong, 1960, IC engines, for Annands data,

$$\text{Nu} = 0.26\text{Re}^{0.7} + \frac{c_{Ann}D}{k}(T_i^4 - T_w^4), \quad (2.102)$$

where: $c_{Ann} = 2.1 \cdot 10^{-13} \frac{\text{W}}{\text{m}^2\text{K}^5}$.

- Woschni, 1967, for diesel engines:

$$\text{Nu} = 0.035\text{Re}^{0.8}, \quad (2.103)$$

where: $\text{Re} = \frac{w_g D_v}{\nu}$, $w_g = 6.618w_v(\varphi_v)$ (intake, exhaust), $w_g = 2.28 \cdot w_v(\varphi_v)$ (expansion, compression) .

- Le Feuvre, 1969, diesel engine, bore and stroke 114.3x114.3 mm, at 100 – 2500 rpm,

$$\text{Nu} = 0,047\text{Re}^{0.8}\text{Pr}^{0.33}, \quad (2.104)$$

where: $\text{Re} = \frac{r^2 \omega_g}{\nu}$.

- Adair, 1972, for compressors:

$$\text{Nu} = 0.053\text{Re}^{0.8}\text{Pr}^{0.6}, \quad (2.105)$$

where: $\text{Re} = \frac{D_v(\varphi) \cdot \frac{D_v(\varphi) w_v}{2}}{\nu}$, $w = 2\omega[1.04 + \cos(2\varphi)]$ if $\pi < \varphi < \pi$, $w = \omega[1.04 + \cos(2\varphi)]$, if $\pi < \varphi < \pi$, $D_v = \frac{6V_v(\varphi)}{A_v(\varphi)}$.

- Aigner, 1972, air compressor, bore and stroke 220x90 mm, at 980 – 990 rpm, compression ratio $x = 2 - 4$

$$\text{St} = \frac{\alpha_c}{\rho w_p C p}, \quad (2.106)$$

where: $\text{St} = 0.032$.

- Hohenberg, 1979, diesel engine, bore and stroke 128x142, 97x128, 125x150, 125x130 mm, at 700 – 2300 rpm,

$$\alpha(t) = 130 \cdot T^{-0.4} (p_i \cdot 10^5)^{0.8} V_i^{-0.06} (w_m + 1.4)^{0.8}. \quad (2.107)$$

- Annand and Pinfeld, 1980, for diesel engines (unfired in experiment), bore and stroke 120x140 mm, at 1000 – 1600 rpm, compression ratio $x = 16.6 - 20$:

$$\text{Nu} = 0.3\text{Re}^{0.7} + \left(1 + 0.27 \frac{D}{V \Delta T} \frac{dT}{dt} \right), \quad (2.108)$$

where: $\text{Re} = \frac{w_g D}{\nu}$, with w_g obtained experimentally.

- Liu, 1984, for R12 fluid compressor, 100x70 mm, at 1440 rpm :

$$\text{Nu} = 0.75\text{Re}^{0.8}\text{Pr}^{0.6}, \quad (2.109)$$

where: $\omega_g = 2\omega(1.04 + 0.45\cos 2\phi)$, when $\frac{\pi}{2} < \phi < \frac{3\pi}{2}$ and $\omega_g = \omega(1.04 + 0.5\cos 2\phi)$ when $\frac{3\pi}{2} < \phi < \frac{\pi}{2}$, also $t_w = 24.32 + 0.7191t_s + 5.64\epsilon - 17.936s^2 + 14.183s$, $t_{wc} = 13.64 + 0.1791t_s + 11.235\epsilon$.

- Lawton, 1987, for Diesel Engines, bore and stroke 98.4x127 mm:

$$\text{Nu} = 0.28\text{Re}^{0.7} - \frac{2.75\text{L}T_w}{T_i - T_w}, \quad (2.110)$$

where: $\text{L}(t) = \frac{\kappa-1}{V(t)} \frac{dV(t)}{dt} \sqrt{\frac{D^3}{aw_{avg}}}$.

- Kanzaka and Iwabuchi, 1992, for Stirling Engines, 20x150 and 30x150 mm bore and stroke, tubular heat exchanger, internal tube diameter 10.5 mm:

$$\text{Nu} = 0.21\text{Re}_{\text{sc}}^{0.8}\text{Pr}^{0.4} \left(\frac{T_w}{T_i}\right)^{-0.5} C', \quad (2.111)$$

where: $C' = 0.923 + 0.75 \left(\frac{T_w}{1000}\right)$ and Re_{sc} with velocity from Schimdt model (velocity from own model substituted).

- Kornhauser and Smith, 1994, for gas springs using helium, hydrogen, nitrogen and argon. Bore to stroke ratios $B/S = 0.67, 0.42, 1.23$, compression ratios $x = 2, 4, 8$, designs with 0, 1, 3 and 7 fins :

$$\text{Nu}_r = \text{Nu}_i = 0.56\text{Pe}_\omega^{0.69}, \quad (2.112)$$

where: $\text{Pe}_\omega = \frac{\omega D_h^2}{4a}$, note that $\dot{q}_c = \frac{k}{D_h} (\text{Nu}_r + i\text{Nu}_i) [\Re(T_i - T_w) + i\Im(T_i - T_w)]$ or $\dot{q}_c = \frac{k}{D_h} \left[\text{Nu}_r (T_i - T_w) + \frac{\text{Nu}_i}{\omega} \frac{dT_i}{dt} \right]$.

- Toda, 1994, for Stirling Engines, 50x87.5 mm bore and stroke, at 400 – 800 rpm:

$$\text{Nu} = c\text{Re}^a, \quad (2.113)$$

where: $\text{Re} = \frac{w_g D}{\nu}$, $c = 0.7, a = 0.58^{\text{r}}$ for heating and expansion, $c = 0.63, a = 0.53$ for cooling and compression.

- Zhao and Cheng, 1994, for Stirling Engines tubular exchangers, tube internal diameter 13.5 mm, length 605 mm:

$$\text{Nu}_{\text{avg}} = 0.00495\text{A}_0^{0.9}\text{Re}_\omega^{0.656} \cdot [43.74(D/L)^{1.18} + 0.06], \quad (2.114)$$

where: $\text{A}_0 = x_{\text{max}}/D$, x_{max} is the fluid max displacement.

- Fagotti, 1998, for R134A compressor:

$$\text{Nu} = 0.28\text{Re}(t)^{0.65} + 0.25\text{L}(t) \frac{T_w}{T_i - T_w}, \quad (2.115)$$

where: $\text{L}(t) = \frac{\kappa-1}{V(t)} \frac{dV(t)}{dt} \sqrt{\frac{D^3}{aw_{avg}}}$.

- Lekic and Kok, 2011, for gas springs using helium, 50x52 mm bore and stroke, 2 – 1500 rpm:

$$\text{Nu}_r = 1.33\text{Pe}_\omega^{0.56} + 5.36, \quad \text{Nu}_i = 2.04\text{Pe}_\omega^{0.46} - 1.46, \quad (2.116)$$

where: $\text{Pe}_\omega = \frac{\omega D_h^2}{4a}$.

- Disconzi, 2012, for compressor, based on CFD results:

$$\text{Nu} = C\text{Re}^a\text{Pr}^b, \quad (2.117)$$

where the constants and Re depend on process; $C = 0.08, a = 0.8, b = 0.6$ and $\text{Re} = \frac{\rho(t)Dw_p}{\mu(t)}$ for compression, $C = 0.08, a = 0.8, b = 0.6$ and $\text{Re} = \frac{\rho(t)D(w_p+w_p^{0.8}w_c(t)^{0.2})}{\mu(t)}$ for discharge, $C = 0.12, a = 0.8, b = 0.6$ and $\text{Re} = \frac{\rho(t)Dw_p}{\mu(t)}$ for expansion, $C = 0.08, a = 0.9, b = 0.6$ and $\text{Re} = \frac{\rho(t)D(w_p+2w_p^{-0.4}w_c(t)^{1.4})}{\mu(t)}$ for intake.

- Organ, 2013, based on Philips and GPU-3 Stirling engine experimental data:

$$\text{XQ}_E = \frac{4}{\text{Re}_\omega} + 1.9 \cdot 10^{-4}, \quad (2.118)$$

where: $\text{N}_{\text{sg}} = \frac{p_o}{\mu\omega}$, $\text{N}_{\text{ma}} = \frac{\omega L_{ref}}{\sqrt{RT_i}}$, $\text{XQ}_E = \frac{Q_v}{\omega p_o V_{sw}} \cdot \frac{\text{N}_T}{L_x/d}$ and $\text{N}_T = \frac{T_e}{T_i}$.

- Xiao, 2014, for Stirling Engines tubular exchangers, tube internal diameter 6 mm, length 298 mm, engine bore 110 mm:

$$\text{Nu}_{\text{avg}} = 0.0162A_o^{0.85}\text{Re}_\omega^{0.43}, \quad (2.119)$$

where: $A_o = x_{max}/D$, x_{max} is the fluid max displacement.

2.1.8 The model solution procedure

The proposed method of solution of the mass and energy balance equations is quasi-static. As a real gas model is considered, the combination of analytic and numerical solutions such as used by Urieli [79] or Szczygiel et al [72, 71], cannot be utilised, as those are derived from the ideal gas equation of state. As for a real gas, each parameter of state including specific enthalpy and internal energy is a function of two independent parameters, when dividing the working cycle into steps, at least two parameters must be known for each volume for a given integration step and calculated for the next step.. Furthermore, unlike for the Schmidt model [79] no closed form solution can be provided. For this reason, a set of initial conditions

(guesses) has to be specified. Those conditions have to describe gas and regenerator mass properties for the engine, based on which heat transfer conditions are also specified. Temperature and pressure of the gas in the control volumes must have certain initial values. The model, as the model of Urieli [79] starts with guesses, and simulates successive, full engine cycles until convergence. The convergence criteria is the vector sum of differences between the internal energies of all control volumes in subsequent steps. The initial parameters considered in the model that is a subject of this work are:

- temperature of the compression cylinder gas,
- temperature of the expansion cylinder gas,
- temperature of the regenerator gas,
- temperature of the regenerator matrix,
- engine pressure,
- initial crank angle.

The error is calculated as (where k denominates the number of the cycle, v - the volume and i - the time step):

$$Er = \left[\sum_v (U_{v,k+1,i} - U_{v,k,i})^2 \right]^{\frac{1}{2}}. \quad (2.120)$$

For the pressure and temperatures in the volumes, the mass of the working fluid is assumed, as:

$$m_v = V_v(\varphi_v) \cdot \rho(p, u) \quad (2.121)$$

The volumes are known from the functions specifying the volume for crank position, and part of the input data, which includes:

- compressor diameter and stroke,
- expander diameter and stroke,
- clearance space in each volume,
- regenerator volume,
- inputs for the heat transfer area functions,
- regenerator mass and area,

- engine rotational speed,
- phase angle between pistons.

As the functions have been evaluated with respect to the crank angle in the previous Sections, the discretisation is also done with respect to this variable. Starting from the given starting position, for each step the angles change as:

$$\varphi_{c,i+1} = \varphi_{c,i} + \Delta\varphi \quad (2.122)$$

$$\varphi_{h,i+1} = \varphi_{h,i} + \Delta\varphi, \quad (2.123)$$

where:

$$\Delta\varphi = \frac{2\pi}{k_k}. \quad (2.124)$$

The number k_k is the number of steps for the full cycle of the engine. The internal energies for each step and volume are evaluated as:

$$U_{v,i+1} = m_i u_i + \Delta Q_v + \Delta L_v \pm \Delta m_{v-v,i} h_{v-v,i}, \quad (2.125)$$

which in turn allows to calculate the specific values:

$$u_{v,i+1} = \frac{U_{v,i+1}}{m_i + \Delta m_{v-v,i}}. \quad (2.126)$$

For clarity, heat and work transfer are calculated separately for each step and volume. The values are calculated using functions described in the previous subsection. Therefore, it can be written that the specific internal energies for the next step are:

$$u_{c,i+1} = \frac{m_{c,i} u_{c,i} + \Delta Q_{c,i} + \Delta L_{c,i} - \Delta m_{c-r,i} h_{c-r,i}}{m_{c,i} - \Delta m_{c-r,i}} \quad (2.127)$$

$$u_{h,i+1} = \frac{m_{h,i} u_{h,i} + \Delta Q_{h,i} + \Delta L_{h,i} + \Delta m_{r-h,i} h_{r-h,i}}{m_{h,i} + \Delta m_{r-h,i}} \quad (2.128)$$

$$u_{r,i+1} = \frac{m_{r,i} u_{r,i} + \Delta Q_{r,i} - \Delta m_{r-h,i} h_{r-h,i} + \Delta m_{c-r,i} h_{c-r,i}}{m_{h,i} - \Delta m_{r-h,i} + \Delta m_{c-r,i}} \quad (2.129)$$

The values of $\Delta Q_{c,i}$ and $\Delta Q_{h,i}$ are evaluated from equations:

$$\frac{\Delta Q_c}{\Delta\varphi_c} = \frac{A_c(\varphi_c) \alpha_c(\varphi_c) [T_{wc} - T_c]}{\omega}, \quad (2.130)$$

$$\frac{\Delta Q_h}{\Delta \varphi_h} = \frac{A_h(\varphi_h)\alpha_h(\varphi_h)[T_{wh} - T_h]}{\omega}. \quad (2.131)$$

It is here that the heat transfer correlations enter the solution. As per their individual descriptions, the parameters such as pressure, gas velocity, piston velocity and gas temperature in the volume need to be known. These are taken from the previous step. Formulas need to be selected for each engine individually based on its working parameters and constructions. The issue of their selection and veracity, as the main problem set for this work will be elaborated on in due course.

The values of the mass change are unknown. Those values are however not just the amount of mass exchanged between volumes in the given step, but also the difference between masses in a given volume between steps.

The pressure in the next step is still unknown. However the energy balances for all volumes can be added together:

$$m_{tot}u_{avg,i+1} = m_{tot}u_{avg,i} + \Delta Q_{h,i} + \Delta L_{h,i} + \Delta Q_{c,i} + \Delta L_{c,i} + \Delta Q_{r,i}, \quad (2.132)$$

and the expression:

$$u_{avg,i} = \frac{m_{r,i}u_{r,i} + m_{h,i}u_{h,i} + m_{c,i}u_{c,i}}{m_{tot}}, \quad (2.133)$$

is the average specific internal energy of the gas in the engine. This is the energy balance for a boundary comprising of all the engine gas spaces. This allows to disregard the transfer of mass. As the volume of the whole engine in the next step can be explicitly calculated as the sum of all volumes:

$$V_{tot,i+1} = V_{c,i+1} + V_{h,i+1} + V_r. \quad (2.134)$$

The pressure can be found as a function of internal energy and density:

$$p_{i+1} = f(u_{avg,i+1}, \rho_{avg,i+1}) = f\left(u_{avg,i+1}, \frac{m_{tot}}{V_{tot,i+1}}\right), \quad (2.135)$$

as the mass of trapped gas is constant. This approach cannot be carried out to find the temperatures, as those differ across volumes. Therefore the energy balance equations still must be solved for each volume. To find the amount of mass exchanged, it can be written:

$$m_{v,i+1} = m_{v,i} \pm \Delta m_{v-v}, \quad (2.136)$$

$$\Delta m_{v-v,i} = m_{v,i} - V_{v,i+1}\rho(p_{i+1}, u_{v,i+1}), \quad (2.137)$$

where the values of u , are given by the energy balance equations for the step. Note that the energy balance equations include the Δm_{v-v} values. For a real gas, where are computed using functions from libraries this doesn't allow for a closed form solution. The system of equations is therefore solved numerically. The values of enthalpy of gas flowing through control volumes depends on the regenerator model, and can be derived as:

$$\Delta m_{c-r,i} > 0 \rightarrow h_{c-r,i} = f(p_i, T_{c,i}), \quad (2.138)$$

$$\Delta m_{c-r,i} < 0 \rightarrow h_{c-r,i} = f(p_i, T_{rC,i}), \quad (2.139)$$

$$\Delta m_{r-h,i} < 0 \rightarrow h_{r-h,i} = f(p_i, T_{h,i}), \quad (2.140)$$

$$\Delta m_{r-h,i} > 0 \rightarrow h_{r-h,i} = f(p_i, T_{rH,i}), \quad (2.141)$$

where temperature T_{rH} and T_{rC} are the temperatures of gas flowing from the hot and cold end of the regenerator respectively, calculated from the regenerator model. After solving the equations, the mass and internal energy in the volumes is known, allowing to calculate the temperatures for the next step as:

$$T_{v,i+1} = f(p_{i+1}, \rho_{v,i+1}) \quad (2.142)$$

A flowchart for the algorithm is presented in a simplified form in Fig.2.2.

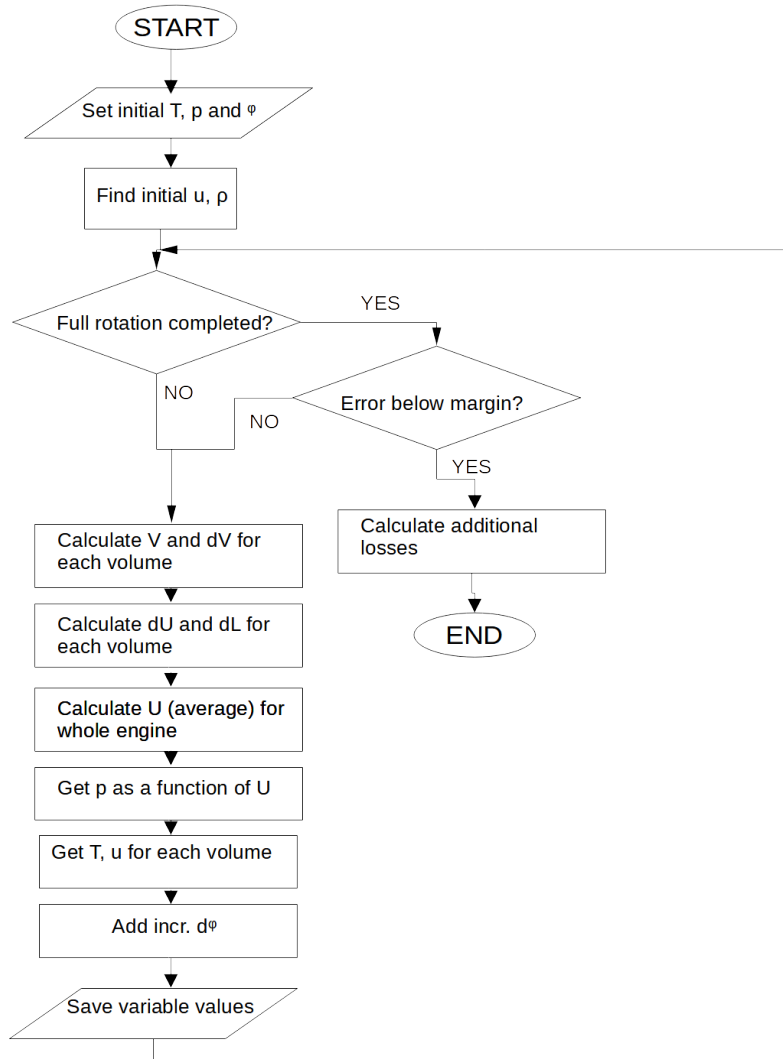


Figure 2.2: A simplified flowchart for the algorithm used with the real gas model

One of the biggest issues for performing model computations was convergence time due to regenerator solid mass temperature. As the heat capacity of this solid mass is high compared to the overall heat capacities of the gasses, it will take a large

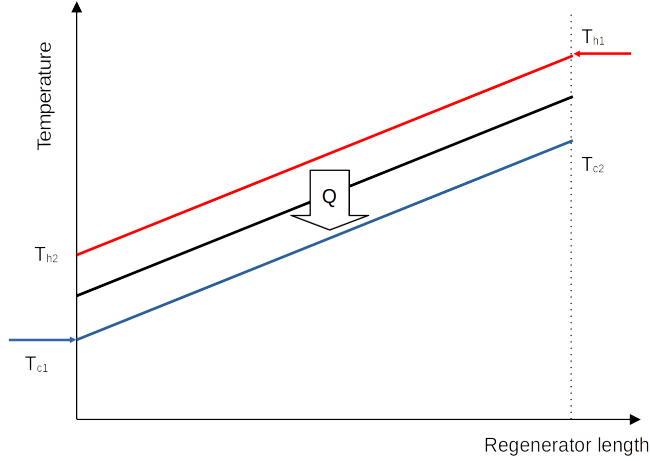


Figure 2.3: Simple regenerator model [79]

number of rotations for it to stabilize. Likewise is the case in the model. Mean cycle pressure was also a problem, due to the algorithm allowing only for stating the initial pressure (at initial crank angle) and buffer pressure. Despite the implementation of leakage losses, reaching equality between the mean cycle pressure and buffer space pressure (assumed constant) take a long time. For this reason, if the convergence of pressure and regenerator solid mass temperature is not reached after a certain number of cycles, these parameters are adjusted using the Levenberg-Marquardt algorithm.

2.1.9 The simplified regenerator model

The Urieli model [79], assumes that the temperature distribution in the regenerator is linear, with the bounds on each end being the cooler and heater temperatures. The regenerator effectiveness is then noted as:

$$\varepsilon_r = \frac{T_{h1} - T_{h2}}{T_{h1} - T_{c2}}. \quad (2.143)$$

The symbols being the same as on the figure 2.3, the indices h signifying flow from the hot to the cold side, and k , the opposite direction.

This regenerator model is utilized in this work, but with certain changes, that is, the temperatures of the gas flowing from inlet and outlet of the regenerator are assumed as the cycle weighted average of the temperature of the gas in the compressor and expander volumes, where the weight factor is the mass change dm . Note, the equation (2.144) is based on an assumption of a constant specific heat capacity, for simplification.

$$T_{avg-v} = \frac{\oint T dm_{v-r}}{\oint dm_{v-r}}. \quad (2.144)$$

Another departure from the Urieli model, is the introduction of mean averaged gas temperature. As the distribution of temperature is assumed linear both the in gas, and the solid mass domains, it follows, that for each step the amount of heat flowing from the gas to the solid mass and vice versa, is a function of their average temperatures. This allows to introduce the regenerator mass and area into the model. An efficiency parameter is therefore used to find the ΔT as a function of the mass averaged inlet and outlet temperature, and the mean regenerator gas temperature as:

$$T_{r-c} = T_{avg-r} - \varepsilon_r(T_{avg-r} - T_{avg-c}), \quad (2.145)$$

$$T_{r-h} = T_{avg-r} + \varepsilon_r(T_{avg-h} - T_{avg-r}). \quad (2.146)$$

As can be seen, for a regenerator having a 100% efficiency the temperature reaches the averaged value of the respective cylinder, and for a 0% effective one, the regenerator loses its "counterflow" characteristic.

The regenerator is evaluated using the Hausen method. The Hausen method is based on the use of two parameters, the reduced length Λ and the reduced period Π [76, 85]. Derivative methods also utilize those parameters. They are defined as:

$$\Lambda = \frac{2\alpha_r(\tau_1 + \tau_2)A_r}{m_g C p_g}, \quad (2.147)$$

$$\Pi = \frac{2\alpha_r(\tau_1 + \tau_2)A_r}{m_{mr} C_{mr}}, \quad (2.148)$$

where α_r is the overall heat transfer coefficient for the regenerator. The regenerator can be classified as either symmetrical or asymmetrical, based on the Λ being the same or not for the hot and cold blast, therefore it can be classified as balanced or unbalanced based on whether the heat capacity of each blast is equal. An evaluation of the mass flows in the Stirling engine shows that the Stirling engine regenerator is both asymmetrical and unbalanced. This is visible in the mass flows from the cylinders to the regenerator are shown as a function of the crank angle in Fig.2.4. These

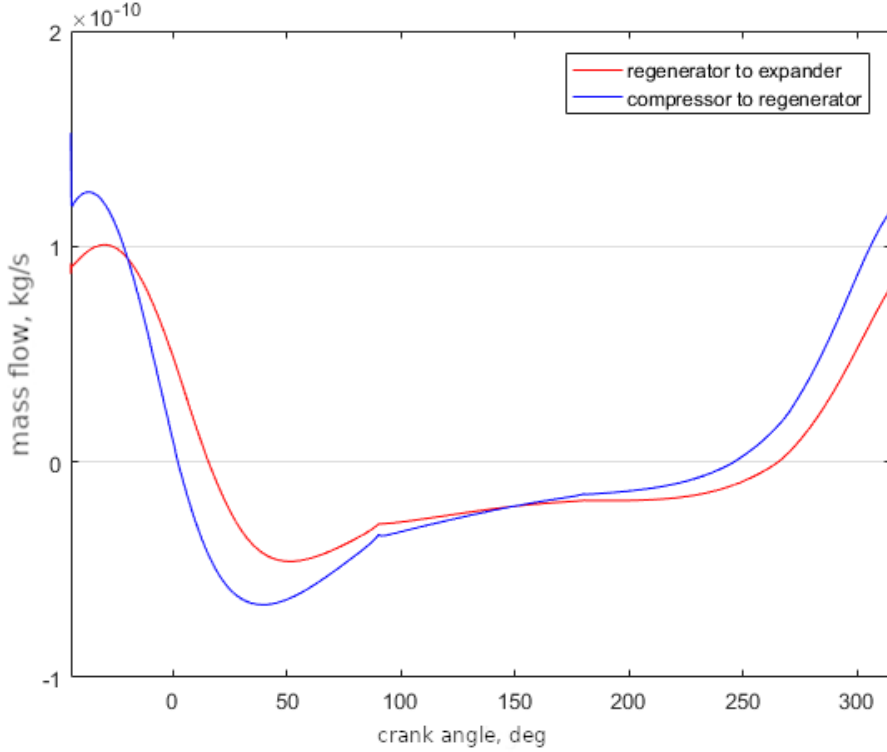


Figure 2.4: Mass flows between the cylinder and the regenerator as a function of crank angle

have been obtained as a result of a differential Stirling engine model calculations described by the authors in [64, 14].

The Λ - Π method can be used for an asymmetrical, unbalanced regenerator if both parameters are noted separately for the hot and cold blasts, and mean parameters are calculated as:

$$\Pi_m = \frac{2}{\frac{1}{\Pi_h} + \frac{1}{\Pi_c}} \quad (2.149)$$

$$\Lambda_m = \frac{2\Pi_m}{\frac{1}{\Pi_h\Lambda_h} + \frac{1}{\Pi_c\Lambda_c}} \quad (2.150)$$

A value of ε_r can then be obtained by several methods outlined by Shah and Sekulic [68]. For the analyzed engine (described in Section 3.1) for an example case, it has been found that the values of the coefficients were respectively $\Lambda_m = 17.785$ and $\Pi_m = 0.0178$. As many authors propose [76, 68], when the value of Π is low in

relation to Λ , the regenerator effectiveness can be calculated from the asymptotic expression multiplied by an empirical expression [76]:

$$\varepsilon_r = \frac{\text{NTU}_o}{1 + \text{NTU}_o} \left(1 - \frac{1}{9C_r^{*1.93}} \right), \quad (2.151)$$

which comes from the well known $\varepsilon - \text{NTU}$ method. As the two methods are interchangeable:

$$\text{NTU}_o = \frac{\Lambda_m}{2} \quad (2.152)$$

$$C_r^* = \frac{\Lambda_c}{\Pi_c} \quad (2.153)$$

If the value of Π is higher, the effectiveness can be calculated by a method proposed by Baclic [10] or interpolated from tables available from sources such as [76]. Low values of the reduced period can be reasonably expected when taking into account the high frequencies of thermodynamic processes occurring in Stirling machines. Furthermore, it should also be noted that when Π approaches 0, C_r^* approaches infinity, which in turn reduces the formula for regenerator effectiveness to:

$$\varepsilon_r = \frac{\text{NTU}_o}{1 + \text{NTU}_o} \quad (2.154)$$

This is also the same as the equation proposed by Urieli [79] for estimating regenerator effectiveness.

It has to be noted, that this method approximates the value of effectiveness for an equivalent balanced and symmetrical regenerator, and further corrections have to be applied to the value. The corrected value can be shown as:

$$\varepsilon_{r-corr} = \frac{1 - \exp\left(\frac{\phi\varepsilon_r}{1-\varepsilon_r}\right)}{1 - \left(\frac{\Lambda_h\Pi_c}{\Pi_h\Lambda_h}\right) \exp\left(\frac{\phi\varepsilon_r}{1-\varepsilon_r}\right)}, \quad (2.155)$$

where:

$$\phi = \frac{\left(\frac{\Lambda_h}{\Pi_h}\right)^2 - \left(\frac{\Lambda_c}{\Pi_c}\right)^2}{2\left(\frac{\Lambda_h\Lambda_c}{\Pi_h\Pi_c}\right)}. \quad (2.156)$$

2.1.10 Heat transfer inside the regenerator

To implement the Hausen method, the values of α_r need to be calculated. The regenerator of the analysed engine, and of many other Stirling machines is composed of a matrix of thin, solid wire bundled up in the gas space so as that it forms a porous matrix. Experimental research on the processes in this kind of regenerator has been carried out by Gedeon and Wood [25], and the correlations elaborated by them have been used in this work. Those correlations take into account the porosity of the material, ε_{por} , which is defined as the ratio of the gas volume to the solid volume of the matrix.

$$\text{Nu} = (1 + 0.99[\text{RePr}]^{0.66}) \varepsilon_{por}^{1.79} \quad (2.157)$$

$$\text{Re} = \frac{w_r D_r \varepsilon_{por}}{(1 - \varepsilon_{por}) \nu} \quad (2.158)$$

$$w_r = \frac{w_g}{\varepsilon_{por}} \quad (2.159)$$

$$\text{Nu} = \frac{\alpha_r D_r \varepsilon_{por}}{(1 - \varepsilon_{por}) \lambda_r} \quad (2.160)$$

The characteristic diameter used in the numbers is the hydraulic diameter of the regenerator. The internal geometry of the regenerator chamber and the porosity being known, allows to, calculate the heat transfer area, the gas volume and the solid matrix volume for any given diameter if wire. This is because:

$$\varepsilon_{por} = \frac{V_r}{V_{rv}}, \quad (2.161)$$

where the subscript rv indicates the overall volume and r the gas volume. Also, the heat transfer area can be expressed as:

$$A_r = \frac{4V_{rv}(1 - \varepsilon_{por})}{D_{wire}}, \quad (2.162)$$

which can be derived from the assumption that the wire is a small diameter cylinder.

2.1.11 Regenerator differential model

The regenerator model described in the previous Section is highly simplified. For the purposes of more detailed analysis, a second regenerator model has also been created to use in conjunction with the Stirling engine model. This model is used for calculations in specified cases in later Chapters, otherwise, the simpler model is utilized.

For this model of the regenerator, the assumptions are the same as for the previous, simplified model, with the difference that:

- the wire mesh is treated by lumped analysis,
- the problem is one-dimensional (any temperature and other parameter variations across lines perpendicular to the regenerator axis are neglected).

The first assumption can be justified due to the mesh being made from thin wire of a cumulatively large length. The common condition for lumped system analysis is:

$$\text{Bi} = \frac{\alpha_r D_{\text{wire}}}{2k_{\text{wire}}} \leq 0.1 \quad (2.163)$$

For wiring in the considered diameter range (below 0.1 mm), made of steel, this assumption is justified.

The modelling of the working fluid as a real gas was necessitated by the fact that such an assumption has been made for the engine model used in conjunction with the presented regenerator calculations [64]. Using real gas parameters also has the benefit of providing necessary parameters for convective heat transfer calculations. Axial conduction is neglected due to the wire dimensions. A one dimensional approach is selected for simplification.

The modus operandi of the model is the division of the regenerator space into finite volumes of gas, and finite elements of the matrix for which equations of energy and mass balance are solved. This is similar to the Andersen model [7], and likewise, temperature of the matrix is allowed to fluctuate. The code in which this model was implemented solves it as an initial value problem: in the initial iteration, the distribution of temperatures within the regenerator matrix is assumed to be linear, and the temperatures of the gas in the cells are identical to the temperature of the solid matrix. When the flow "starts" the temperatures start to change. The problem is solved iteratively until the inequality between heat given out and taken in by the matrix across the cycle approaches equal value with set accuracy. A simplified representation of the model and a single cell in particular is shown in Fig.2.5.

Note, that the amounts of fluid dm entering and leaving the cell in a given time steps do not have to be equal - the mass can be accumulated to be discharged later. The energy and mass balance equations are solved for each volume and for each time step starting from the position of positive in-flow. The indexes i and j denote time step and volume respectably. The mass balance can be stated as:

$$m_{j,i+1} = m_{j,i} + \Delta m_{j,i} - \Delta m_{j+1,i}, \quad (2.164)$$

where $dm_{j+1,i}$ and $dm_{j,i}$ are the mass elements leaving and entering the volume during the time-step. Note that for the sake of making a clearer code, the indices

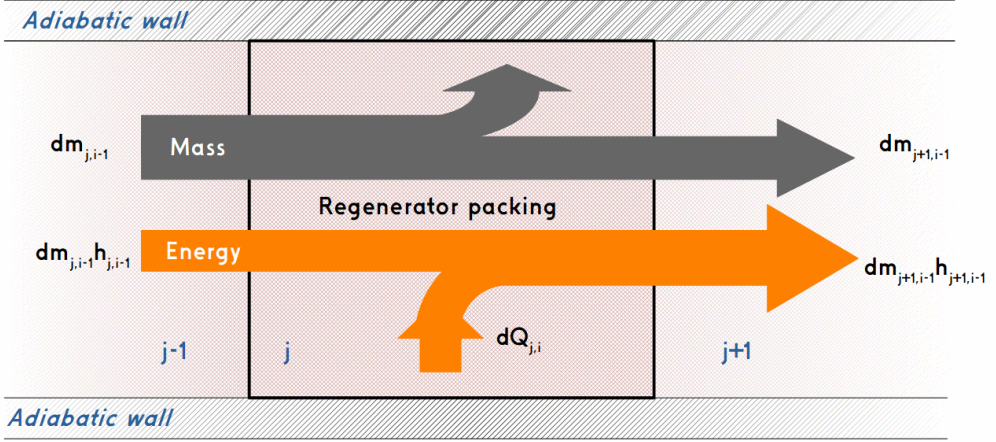


Figure 2.5: A schematic representation of the regenerator model

have been switched. The energy balance can be stated as:

$$m_{j,i+1} \cdot u_{j,i+1} = m_{j,i} \cdot u_{j,i} + \Delta m_{j,i} h_{f,j,i} - \Delta m_{j+1,i} h_{f,j+1,i} + \Delta Q_{j,i}, \quad (2.165)$$

and:

$$T_{mr,j,i+1} \cdot m_{mr} C_{mr} = T_{mr,j,i} \cdot m_{mr} C_{mr} - \Delta Q_{j,i} \quad (2.166)$$

Pressure losses are not included, neither are sonic flow effects, as even at high rotational speeds of the engine the gas flows with a low velocity [64]. The index f denotes flow of gas passing between the volumes. For gas flowing from the volume to the direction against the flow from the given volume, the specific enthalpy is evaluated for its parameters at i . For the gas flowing out of the given cell, this is also calculated for those parameters.

The solution for each time step and volume is reached by first calculating the amount of heat, dQ exchanged in the previous time steps as:

$$dQ_{j,i} = d\tau (T_{mr,j,i-1} - T_{j,i}) \cdot A_v \cdot \alpha_{j,i}, \quad (2.167)$$

and then solving the single unknown equation:

$$\begin{aligned} & V_j \rho(p_i, u_{j,i}) (u_{j,i} - h_{f,j+1,i-1}) = \\ & = \Delta Q_{j,i-1} + m_{j,i-1} (u_{j,i-1} - h_{f,j+1,i-1}) + \Delta m_{j,i-1} (h_{f,j,i-1} - h_{f,j+1,i+1}). \end{aligned} \quad (2.168)$$

Equation (2.168) is a restatement of equations of energy and mass balance for a given and adjacent volumes in the given and adjacent time steps re-arranged in a manner

which transforms it into a single-unknown equation. This equation can be solved in an iterative process for each control volume and time step using different algorithms - the Levenberg-Marquardt method was found to work best. This is namely due to the problem being non-linear for a real gas model.

The method of combining the regenerator model and the engine model [64] is as follows- an engine simulation is run, with the previous method implemented. Then, pressure, mass flows and flow temperatures are taken from this iteration and supplied to the regenerator model. The regenerator model gives as a result the regenerator effectiveness which is implemented back into the engine model under assumptions given below for the next iteration. The first iteration could also use an assumed regenerator efficiency without the use of simplified calculations, however this would entail the need for more iterations to reach convergence.

2.1.12 Parametric study of the regenerator

Unlike CFD models, the proposed scheme is well suited for performing parametric calculations and optimization due to its short computation time. Therefore a parametric study has been done, showing how the results vary with parameters interesting in Stirling Engine analysis, such as regenerator porosity, heat capacity and blast period. The results presented in this Section are also compared with the results for the Hausen derived model. The influence of pressure fluctuations and lack of time and mass symmetry between the blasts have been also analysed, though their influence on the regenerator performance was found negligible.

For the parametric calculations τ and m are the time and mass characterizing each blast. The inverse proportionality of the two is the consequence of the Stirling engine being a sealed system. Parameters were varied for a specific case, that is a regenerator with the base dimensions presented in table 2.1. Those differ from the case used in validation by the fact that the regenerator has the form of a tube instead of an annular gap.

Table 2.1: Regenerator base parameters

diameter	10	mm
length	80	mm
wire diameter	0.09	mm
cycle time	0.06	s
porosity	0.8	-
matrix sp. heat capacity	450	$\frac{\text{J}}{\text{kgK}}$

Using the presented methods, and the correlations for α_r , values of the regenerator effectiveness have been plotted as a function of porosity values. This is shown in Fig.2.6

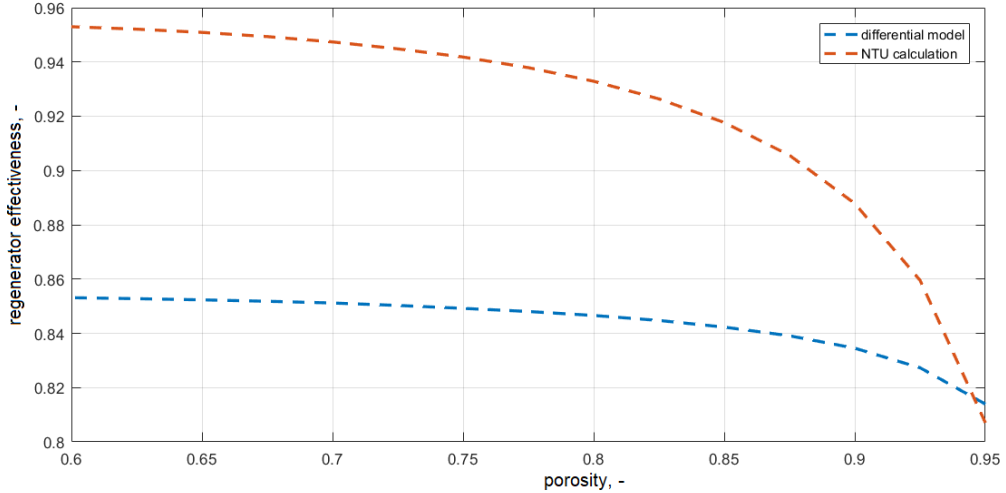


Figure 2.6: Regenerator effectiveness for an example engine as a function of porosity.

It should be noted, that while the regenerator effectiveness goes down with porosity, this has also a negative effect in reducing the flow area [50]. It can be seen, that the non-dimensional (NTU) method estimates somewhat smaller values of ϵ_r than the differential model, however a similar trend is clearly seen.

The specific heat capacity of the material has also been independently varied, for values between 100 and 900 $\frac{\text{J}}{\text{kgK}}$ (within the range for most metals). It must be noted, that the influence of this value on the regenerator effectiveness is negligible in the case of Stirling Engine regenerators, as the mass of the solid matrix is many times higher than the mass of the gas. Nonetheless, a slight downward trend is seen. The differential model again returns lower values of the effectiveness though the trend repeats in both models. Only if the calculations are carried out in a range of values of the heat capacity below those of known regenerator materials, a drop can be seen. This is shown in Fig.2.7.

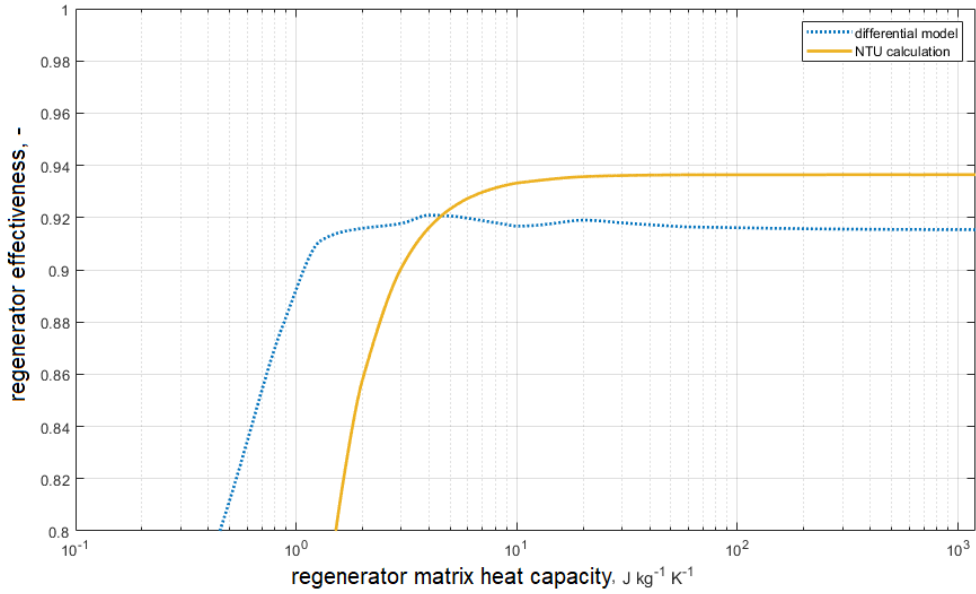


Figure 2.7: Regenerator effectiveness for an example engine as a function of matrix heat capacity.

When the cycle time (inversely proportional to the engine rotational speed) is varied, assuming the mass trapped inside the engine is constant, visible trends appear, that is the effectiveness raising with the time period duration

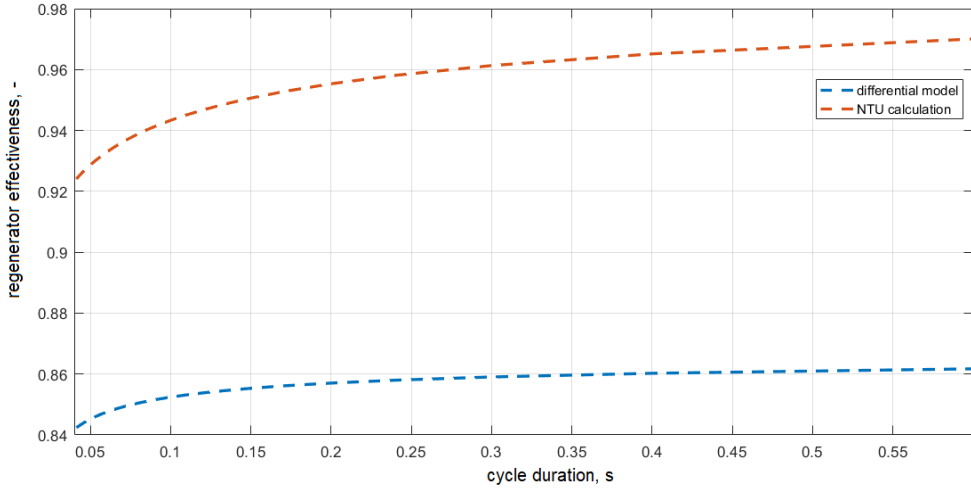


Figure 2.8: Regenerator effectiveness for an example engine as a function of the engine cycle duration.

Again, a similar difference in values is visible between the models.

The biggest difference between models is visible when unequal flows are assumed. For this, a parameter ψ is introduced, defined as the ratio of time of cold and hot blast (note that the overall mass flow is still the same in this case). It is defined as:

$$\psi = \frac{\tau_{hr}}{\tau_{rc}}, \quad (2.169)$$

where the indexes hr and rc refer to flows from heater to regenerator and from it to the cooler. If an analysis of the influence of this parameter on regenerator effectiveness is done for the analysed engine, a wide discrepancy is found between the models. This is shown in Fig.2.9

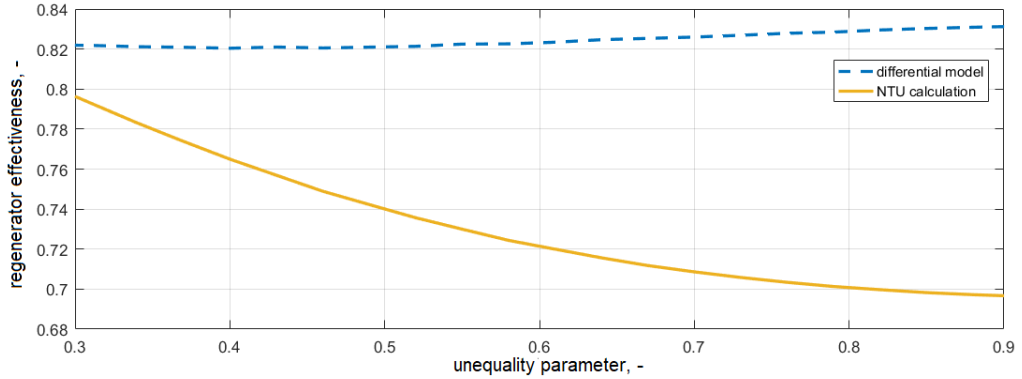


Figure 2.9: Influence of the inequality parameter ψ on regenerator effectiveness according to the differential and Hausen models.

2.2 Model validation and tests, pre-experimental stage

Before the experimental stand (described in Chapter 3) was constructed, a certain amount of validating exercises were performed connected with other ongoing research. This included comparing the model results against CFD results and experimental data obtained from other sources. The first comparisons were made with the results of a model created by Buliński et al [15], and though not being proper validation, they established that the authors model predicts similar trends and values as a CFD model, despite a far shorter computation time. Secondly, the regenerator model was validated against the data from the same CFD model, showing good agreement. Finally, the engine model was compared to measurement data obtained from the University of Zilina, during the authors internship with the Mechanical Faculty.

2.2.1 CFD comparison

The model evaluated in this work is of an α type engine, working in cryogenic conditions and follows the dimensions of an engine modeled with CFD techniques by Bulinski et al [16, 15, 14], dimensions of this unit are shown in table 2.2. A schematic drawing of the engine is shown in Fig.2.10.

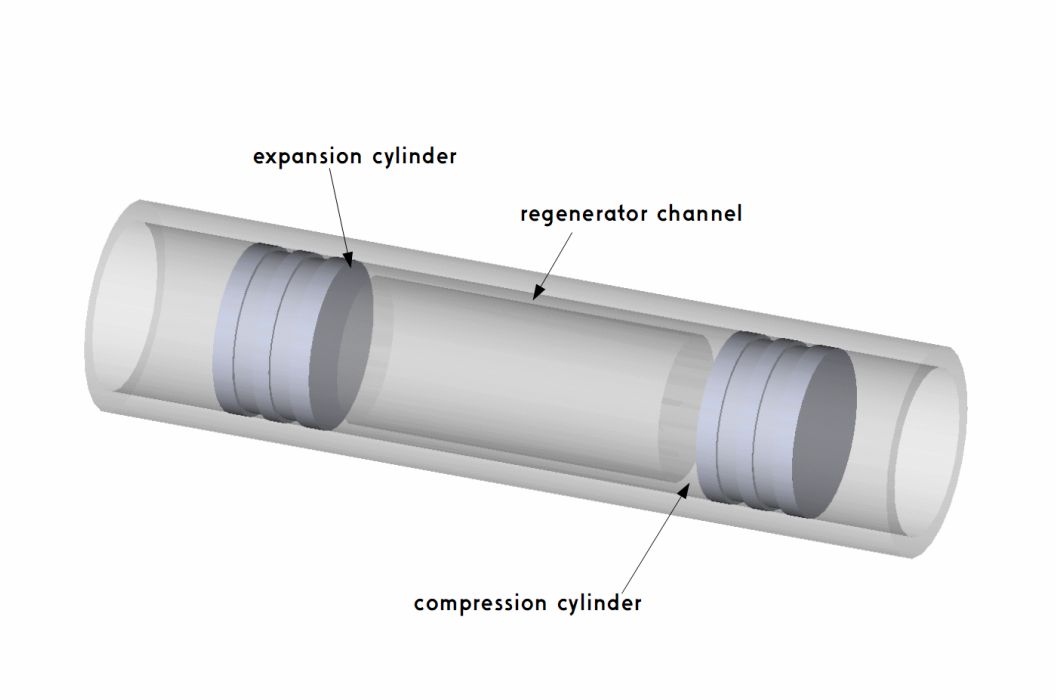


Figure 2.10: A schematic drawing of the evaluated engine

Table 2.2: Engine parameters

bore, D	0.04	m
stroke, s	0.02	m
clearance percentage ϵ_{cl}	10%	-
phase angle, ϕ	90	deg
regenerative channel length, L	0.08	m
regenerative channel height, h	0.005	m

The source temperatures were set as 113 K and 293 K for both the CFD and the 0D model. The nominal speed was 500 rpm. This pre-eliminary comparison allowed for the use of the 0D model as a tool for further analysis of LNG re-gasifier systems, for which Stirling engines were proposed.

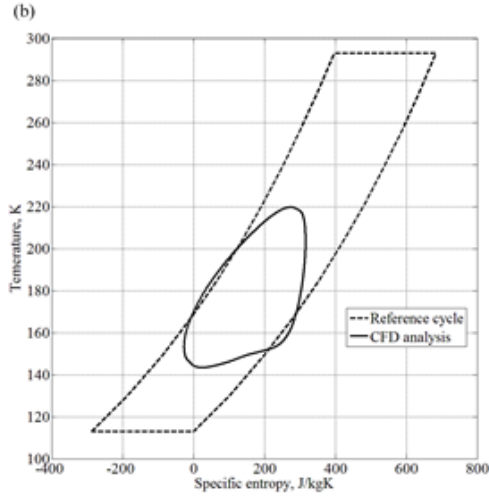


Figure 2.11: Stirling engine T-s diagram, as evaluated by CFD techniques by Bulinski et al [16].

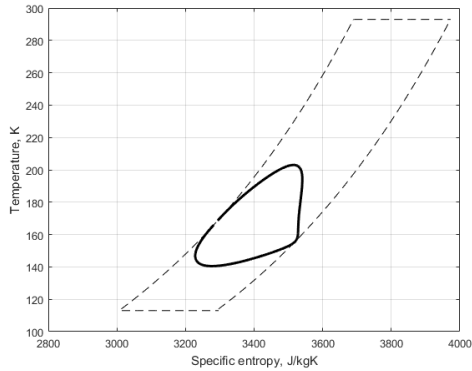


Figure 2.12: Stirling engine T-s diagram as evaluated with the 0D model.

Results can be compared on figures 2.11 and 2.12. As can be seen, the 0D model under predicts the power by a small amount. Importantly, the Woschni correlation was used for heat transfer evaluation, and a lumped model of the regenerator was used. Thermal efficiency characteristics were also comparable (see figure 2.13).

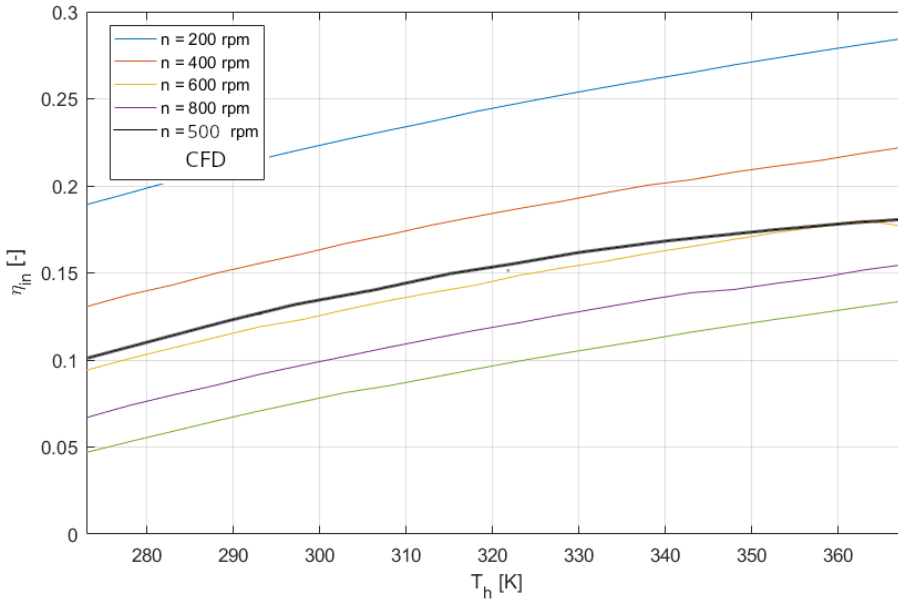


Figure 2.13: Cryogenic engine efficiency characteristics as plotted from the author’s model overlaid by cryogenic engine characteristics as plotted from the CFD model by Bulinski et al

This preliminary exercise, despite not fulfilling the criteria of proper model validation, was considered encouraging for further model development.

2.2.2 Regenerator differential model validation

This Section concerns the engine described in table 2.2.

For the engine, the efficiency is shown as a function of the regenerator effectiveness (Fig.2.14). The dependence of the engine efficiency on the effectiveness of the regenerator is clearly visible. The sensitivity of engine efficiency to the changes of regenerator effectiveness increases with its value. Thus, it is clear that around those values even small gains in regenerator performance are highly desirable.

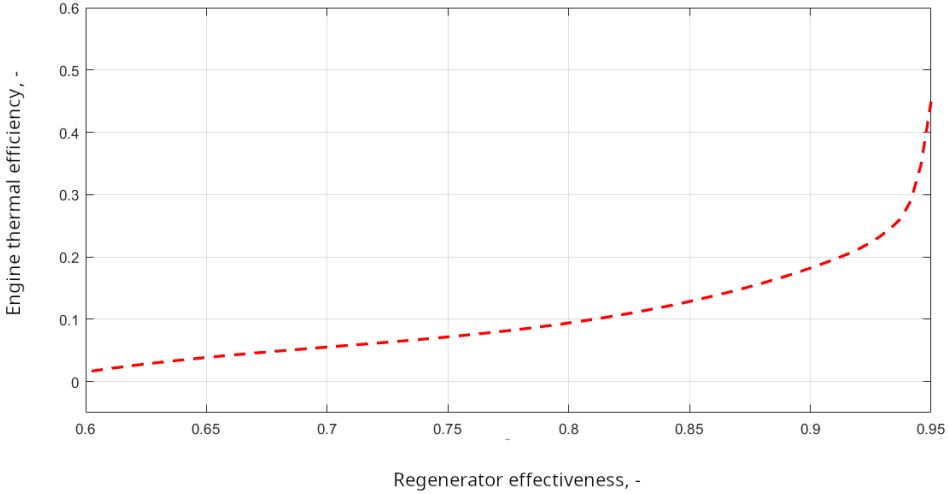


Figure 2.14: The evaluated engine's efficiency as a function of the regenerator effectiveness

A set of simulations of the regenerator have been carried out using the regenerator differential model in order to compare it with the CFD model as a form of validation. The boundary conditions were an example of asymmetrical and unbalanced regenerator flows. In regenerator theory, "balanced" and "symmetric" refers to the parameters of reduced period and reduced length being equal for the hot and cold blow. The parameters of mass flow \dot{m}_{c-r} , \dot{m}_{r-e} and temperatures T_{c-r} , T_{r-e} were taken from an engine simulation done in the zero-dimensional, real gas model. The regenerator was divided into 12 cells, and there were 4000 time steps per cycle. The crank rotational speed was 1000 rpm. A single cycle duration was therefore 0.06 s, and the regenerator dimensions were $D = 4$ cm, $h = 0.05$ mm, $L = 8$ cm, with the porosity set at 0.7, 0.8 and 0.9, the filament being steel wire 0.11 mm in diameter. The results were then compared with ones obtained for the same engine dimensions and conditions from the CFD model by Buliński et al [14]. The compared results were namely the temperatures of the gas when its direction of flow was to the outside of the regenerator. For the CFD model, this were averaged across the flow cross Section.

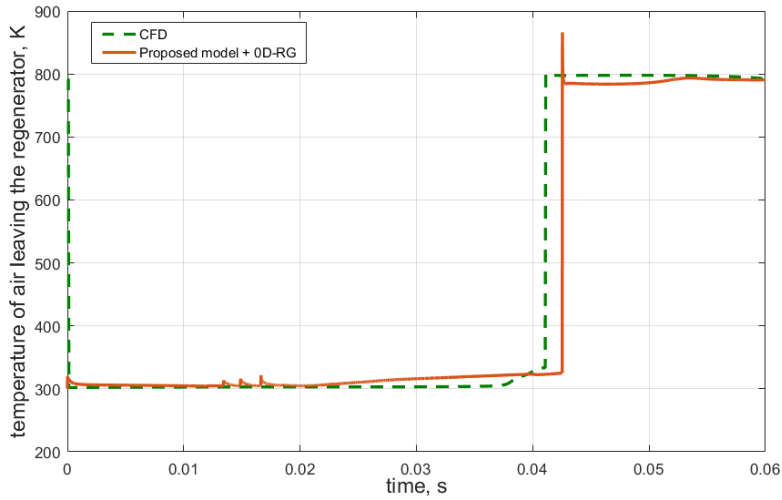


Figure 2.15: Temperatures of gas flowing outside of the regenerator across time for the proposed model and a CFD simulation, for the porosity of 0.7

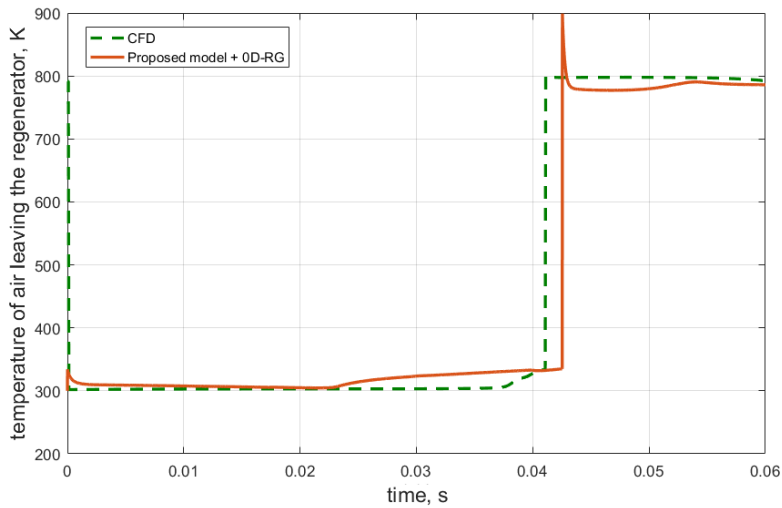


Figure 2.16: Temperatures of gas flowing outside of the regenerator across time for the proposed model and a CFD simulation, for the porosity of 0.8

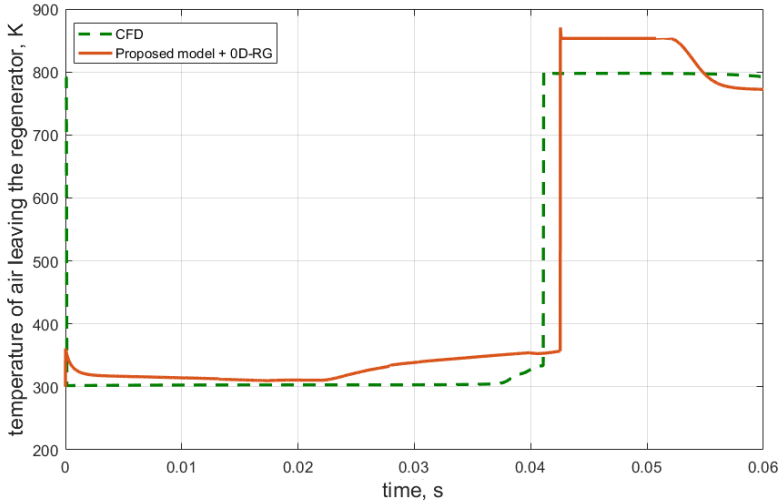


Figure 2.17: Temperatures of gas flowing outside of the regenerator across time for the proposed model and a CFD simulation, for the porosity of 0.9

The model shows good agreement with CFD calculations, as is seen by the temperature profiles on figures 2.15, 2.16 and 2.17. Due to the lack of experimental results, this is considered to serve as a form of validation. Certain differences are visible between the temperature profiles, namely a slight shift in phase between the hot and cold blast and the fact that the profiles for the proposed model are less flat. This is likely due to the mass flows being slightly different for the zero-dimensional engine model and CFD calculations.

2.2.3 Cleanergy C9C engine data

The C9C engine is a commercially available Stirling engine based cogeneration unit, producing useful heat and electrical power. The engine parameters are given in table 2.3.

Table 2.3: C9C engine parameters

	Value
Operating pressure P [bar]	25 - 150
Expansion piston stroke E [mm]	44
Compression piston stroke C [mm]	44
Expansion piston bore E [mm]	68
Compression piston bore C [mm]	68
Displacement [cm ³]	160
Maximum temperature [°C]	740
Engine speed [1 / min]	1500
Working gas volume [L]	0,6
Electrical power of cogeneration unit [kW]	2-9
Heat output of the cogeneration unit [kW]	8-25
Burner power - heater [kW]	18-40
Usable fuel	ZP, LPG, LFG

The machine is of an α type, and is of a semi-hermetic construction with an un-pressurized crankcase. The working fluid is helium, and the engine contains its own pressurized tank. An electronic control unit controls the power output by adjusting the pressure in the buffer space, which due to the un-pressurized crankcase is a separate container.

The cooling tubes were ascertained to have an inner diameter of 3 mm, and a length of 130 mm, with 14 of them in the bank. The heater tubes, which bend around the burner have an inner diameter of 5 mm, and overall length of 120 mm, with 24 of them in the bank. The regenerator design was not ascertained, due to it being impossible to disassemble and no data was found in literature. It was assumed to have a 95% porosity and treated as a lump model in calculations.

Measurement data was obtained thanks to the help of the Mechanical Engineering Faculty of the University of Zilina, Slovakia, where the engine resides. Data from modelling the engine with the use of the Adiabatic model of Urieli et al [79], has also been obtained and is presented for comparison.

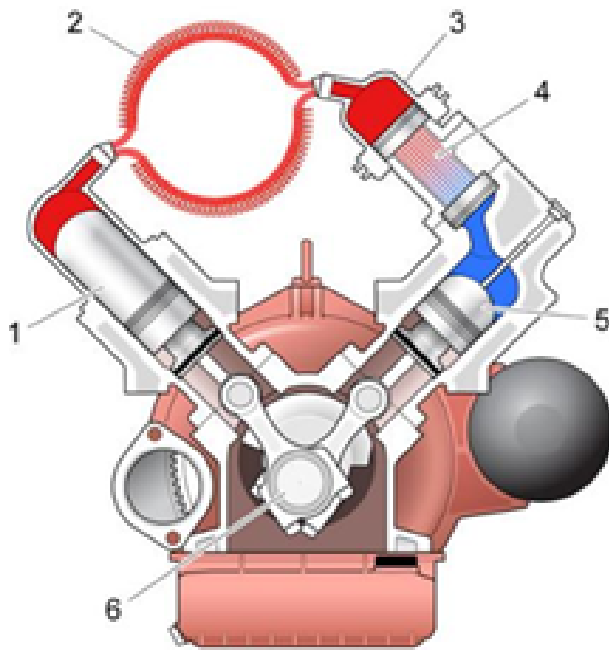


Figure 2.18: Cleanergy C9C, cross-section. 1 - hot piston, with cap, 2 - hot heat exchanger, 3 - regenerator, 4 - cooling tube bank, 5 - cold piston, 6 - crank mechanism

Table 2.4: C9C measurements, data obtained by the courtesy of "UNIZA"

Measurement	1	2	3	4	5	6	7	
Pressure	48,20	52,10	56,30	59,90	65,00	70,00	80,90	bar
Rotational speed	1504,80	1507,20	1507,20	1509,60	1512,00	1512,00	1514,40	rpm
Frequency	25,08	25,12	25,12	25,16	25,20	25,20	25,24	Hz
Temperature, coolant, in	28,60	32,60	33,60	33,90	35,20	35,40	39,30	°C
Temperature, colant out	46,70	50,30	49,10	48,70	50,70	50,20	55,20	°C
Burner temperature 1	764,50	776,30	784,90	785,60	790,70	792,30	804,40	°C
Burner temperature 2	770,30	783,70	719,90	792,80	796,30	799,30	810,90	°C
heat sink temperature	301,75	305,75	306,75	307,05	308,35	308,55	312,45	K
heat source temperature	1043,45	1056,85	993,05	1065,95	1069,45	1072,45	1084,05	K
Electrical power	2480,00	2730,00	2990,00	3240,00	3510,00	3820,00	4060,00	W
Heating power	7523,65	9074,00	9672,98	10118,57	10763,24	11003,29	11805,21	W
Adiabatic model el. Power	2646,47	2863,98	2893,72	3312,36	3596,68	3881,71	4485,17	W
Adiabatic model with losses	2786,52	3067,42	3359,55	3640,45	3943,82	4292,13	4561,80	W
Electrical efficiency	0,24	0,22	0,23	0,24	0,24	0,25	0,25	-
Electrical efficiency, adiabatic	0,66	0,66	0,66	0,66	0,66	0,66	0,66	-

Engine power and efficiency was calculated for the data shown in table ?? using the author's model, utilizing various heat transfer models. These included the models of Adair, Toda, Woschni, Xhao and Zhao, the last two were however discarded due to bad quality of fit. Engine power as a function of pressure for these and the measurements is shown in Fig.2.19, while the efficiency, including the electrical and mechanical loss in 2.20.

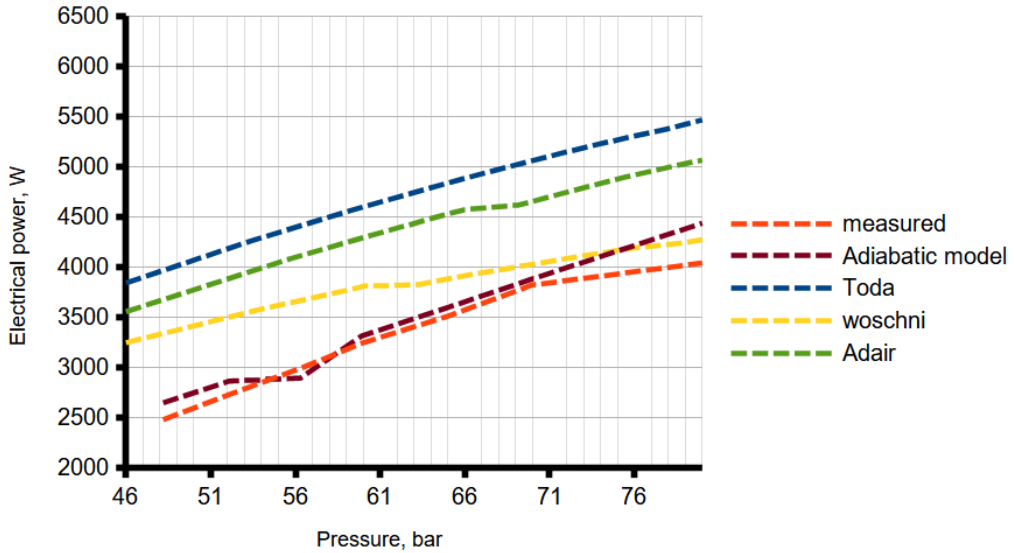


Figure 2.19: C9C engine power, different heat transfer models within the polytropic model, Adiabatic model and measurements included for comparison

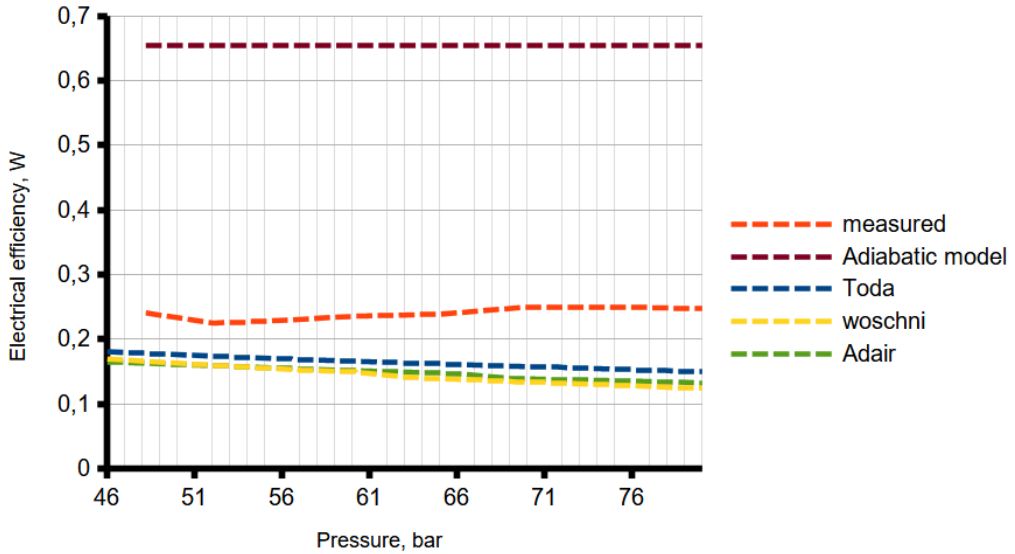


Figure 2.20: C9C engine electrical efficiency, different heat transfer models within the polytropic model, Adiabatic model and measurements included for comparison

Interestingly, the simple adiabatic model gives a very good quality of fit as far as power is concerned, however it overestimates the efficiency by a very large margin. The polytropic model fits reasonably well in regards to power, and far better than the adiabatic model in regards to efficiency. Likely, the selection of heat transfer correlations is one of the main issues here, as the adiabatic model foregoes this consideration completely. The hypothesis, that a far better quality of results could be achieved by varying the heat transfer correlations is investigated in later Chapter based on authors own measurements of the Genoastirling ML3000 engine.

Chapter 3

Experimental setup

In order to acquire data an experimental stand has been built. The stand consists of a Stirling Engine (Genoastirling ML3000), the necessary auxiliary equipment, such as a combustion chamber and cooling system. It was also equipped with measuring equipment for engine indication and temperature measurement. The engine in question was chosen due to its availability and its simple construction, which enables modifications and lends itself well to measurement.

3.1 The Genoastirling ML3000 engine

The Genoastirling ML3000 engine is an α type machine, or rather an double α engine, that is two power units within one chassis. A basic cross-Sectional image of the engine, courtesy of the manufacturer is shown in Fig.3.1.

The engine is property of the Department of Thermal Technology, acquired for research purposes in 2018 due to its availability, simple modular construction and pricing consideration. The construction of a functional lab-stand incorporating the engine has been one of the assumed deliverables of this work.

According to manufacturers data, the engine should have a power output of 3 kW, this has never been reached in practice. The data from the manufacturers specifications can be seen in table 3.1. The machine uses no lubrication, instead relying on roller bearings and friction resistant surfaces. The whole assembly together with the generator is hermetically sealed and pressurized.

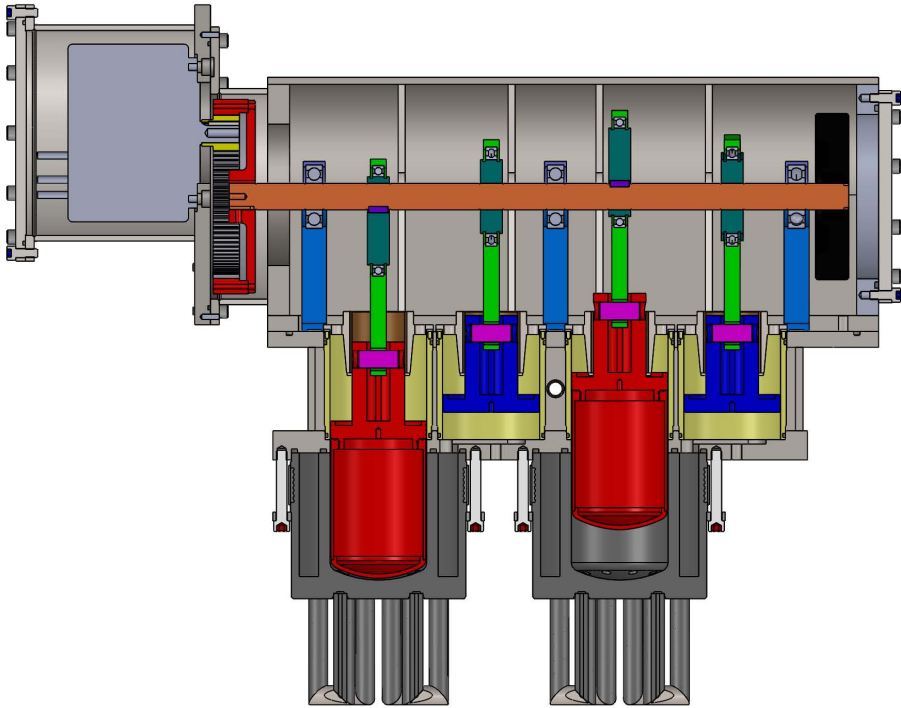


Figure 3.1: A cross-Section of the Genoastirling ML3000 engine

Table 3.1: Engine nominal parameters

Working fluid	nitrogen	-
Buffer pressure	<30	bar
Hot heat exchanger temperature	850-950	°C
Minimum hot side temperature	700	°C
Coolant temperature	30	°C
Rotational speed (nominal maximum)	600	rpm
Cooling system	water	
Coolant flow	4.5-6.5	l/min
Maximum electric power	3	kW
Weight	250	kg

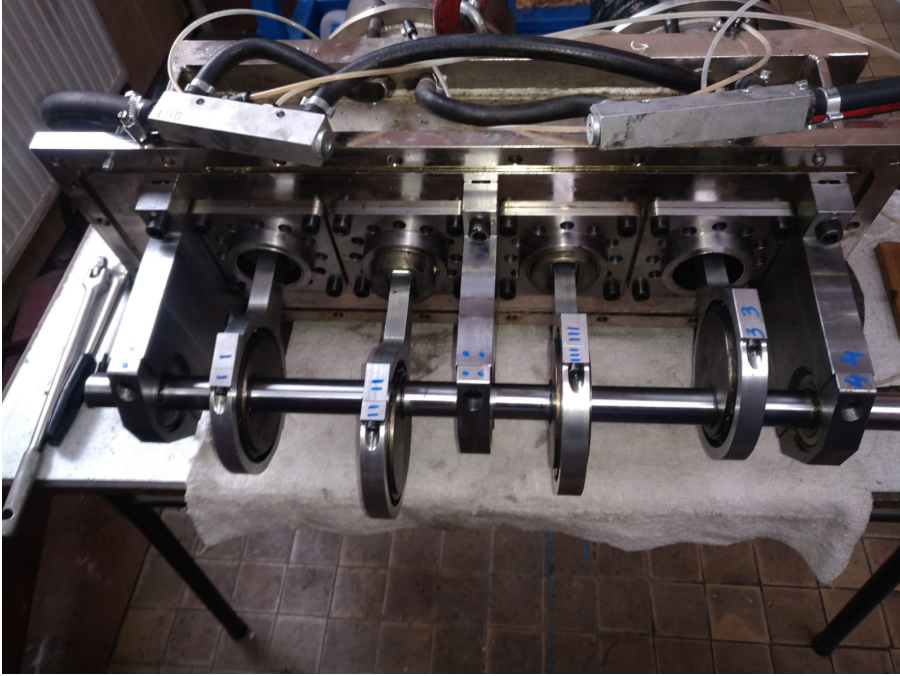


Figure 3.2: ML3000 engine crankshaft

In order to prepare data for use with the mathematical model developed in this work, a detailed survey of the engine has been carried out. This was made easier by the fact that the engine was in need of an overhaul (despite being new), as it has immediately in its working life developed a series of knocks. This were found to be a result of a badly selected axle key on the main gearwheel, and several minor issues.

3.1.1 Crankshaft and kinematics

The movement of the pistons is of utmost importance if one is to construct a mathematical engine model. The mechanical elements of the engine were therefore measured which allowed for a verification of the data from the manufacturer. The design of the crankshaft is fairly unconventional, as so far as it uses eccentrics instead of conventional cranks. Though this design would usually result in excessive friction, this is mitigated by the use of heavy duty roller bearings held with retaining rings. For this reason, the engine does not include any crankcase lubrication, instead, the crankshaft resides in a pressurized buffer space.

The dimensions of interest are the eccentricity (equivalent to the crank radius in a conventional design), as it determines the piston stroke, and the length of the

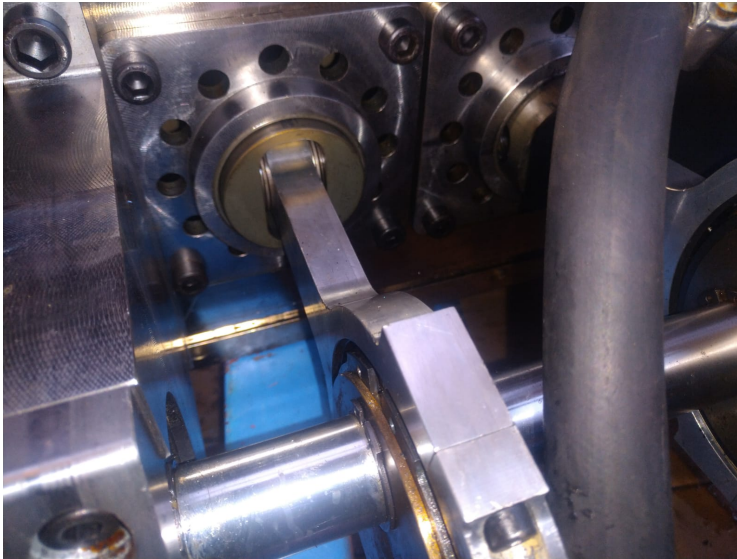


Figure 3.3: A view of the connecting rod

connecting rod as this accounts for the distortions of otherwise sinusoidal volume variations. The phase angle between cranks is also of interest.

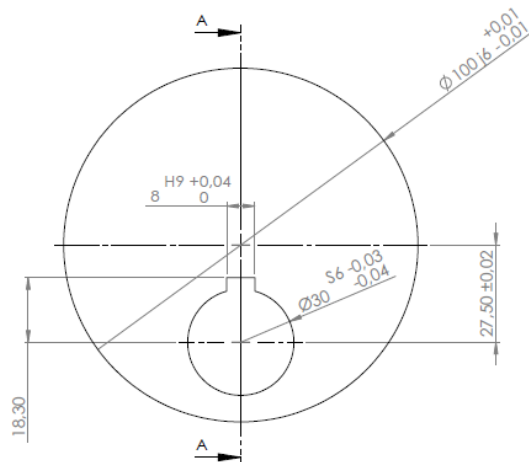


Figure 3.4: Drawing of the eccentric with major dimensions

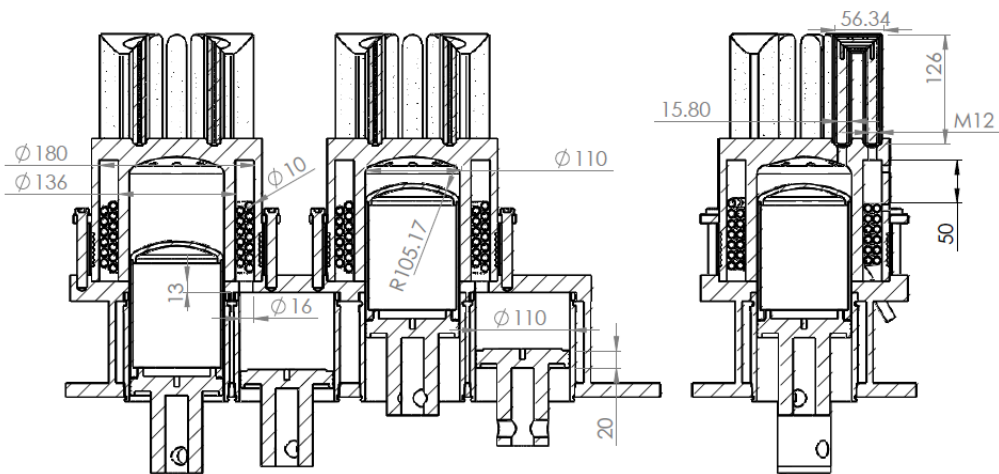


Figure 3.6: A crossSection of the engine working spaces

Cylinder liners are made of E355 steel, and the pistons are machined from AA7075 aluminum alloy, also known as Ergal, that is aluminum alloyed with zinc and traces of copper. The pistons are anodized and covered in a layer of molybdenum on the sliding surfaces. No piston rings are present, nor any kind of a seal, instead, the sealing is provided solely by the high quality of fit, and three cut groves in the piston throttling the flow. This allows the engine to work without lubrication, at the cost of significant blow-by losses. For this reason, blow-by loss cannot be ignored as is often the case when modelling Stirling engines.

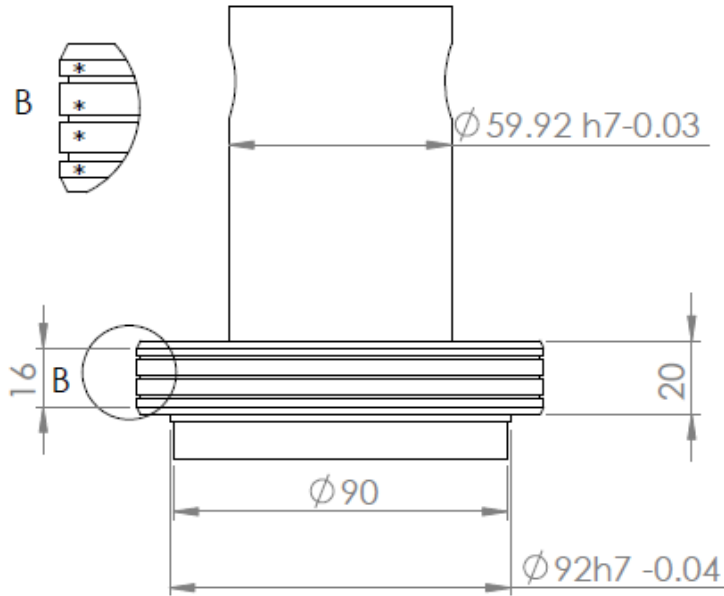


Figure 3.7: Side view of the piston. Sealing grooves visible in detail B.

The piston diameters are both 108 mm. The hot piston is extended by a hot cap, fitted with a Heylandt crown. The use of a hot cap is conventional in α type engines, as it prevents the sliding surface from being exposed to high working temperatures, which could have adverse tribological effects. It is important to mention, that the body into which the cylinder liners are inserted facilitates the flow of coolant, which cools the liners. This does not serve as the main cold heat exchanger, rather the reasoning behind it is mostly mechanical in nature. The liner of the hot cylinder being cooled leads to significant losses, which will have to be considered in the model.

3.1.3 Heat exchange surfaces

The working fluid has to be repeatedly heated and cooled within the engine in order to produce work. This is made possible by the three heat exchangers, the cooler, the regenerator and the heater. A certain amount of heat also flows through the cylinder liners, which is beneficial in the case of the compressor cylinder and thermodynamically adverse in the expander. The gas path of the engine might not be intuitive at first glance, which is why it is necessary to explain it in detail. If one imagines the part of the cycle when gas flows from the compressor to the expander, one can look to drawing 3.8; the gas flows from the compression A cylinder into the cooler through a small opening B, into an annular space C. The annular space is

part of the hot cylinder assembly D, containing all the three heat exchangers and the extension of the hot cylinder. The gas first encounters the cooling coils E, made from stainless steel. After flowing between the coils, it enters the regenerator F, made of a stainless steel mesh inserted into the annular space. From this annular space, the gas travels through the heater tubes G, made from heat resistant stainless steel alloy into the expansion cylinder H. The heater tubes are filled with insertions made from steel bolt stock, identified as M12, I. Likely those were installed as a way of minimizing the clearance volume.

The cooler tubes have a diameter of 8 mm, and they form a double coil for each power unit. They are shown in Fig.3.9. There are two winding diameters, one within the other, with the outer having a diameter of 168 mm. Overall, from measurement, the coil heat exchange area is 0.2388m^2 , while its volume is $5.07 \cdot 10^{-4}\text{m}^3$. The heater tubes are arranged into nine "u" shaped elements, 16 mm inner diameter, resulting in an overall surface area for heat transfer of 0.1244m^2 . The heater tubes are shown in Fig.3.10. The regenerator is made from a stainless steel wire mesh, inserted into the remaining annular space.

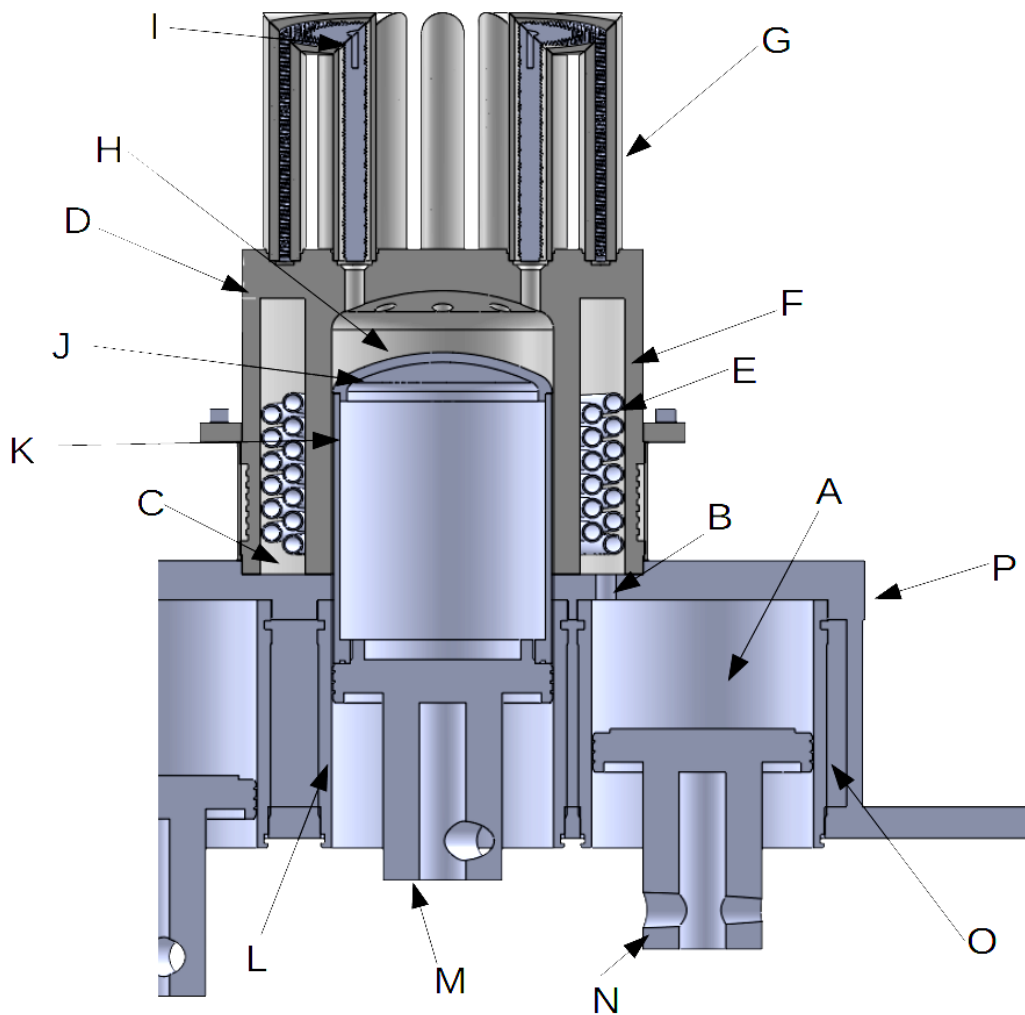


Figure 3.8: One of the cylinder pairs in crossSection. A - compression cylinder, B - gas opening, C - annular space, D - heat exchanger assembly, E - cooling coils, F - regenerator space, G - heater tubes, H - expansion cylinder, I - heater tube filaments, J - Heylandt crown, K - hot cap, L - expansion cylinder liner, M - expander piston, N - compressor piston, O - compression cylinder liner, P - engine body

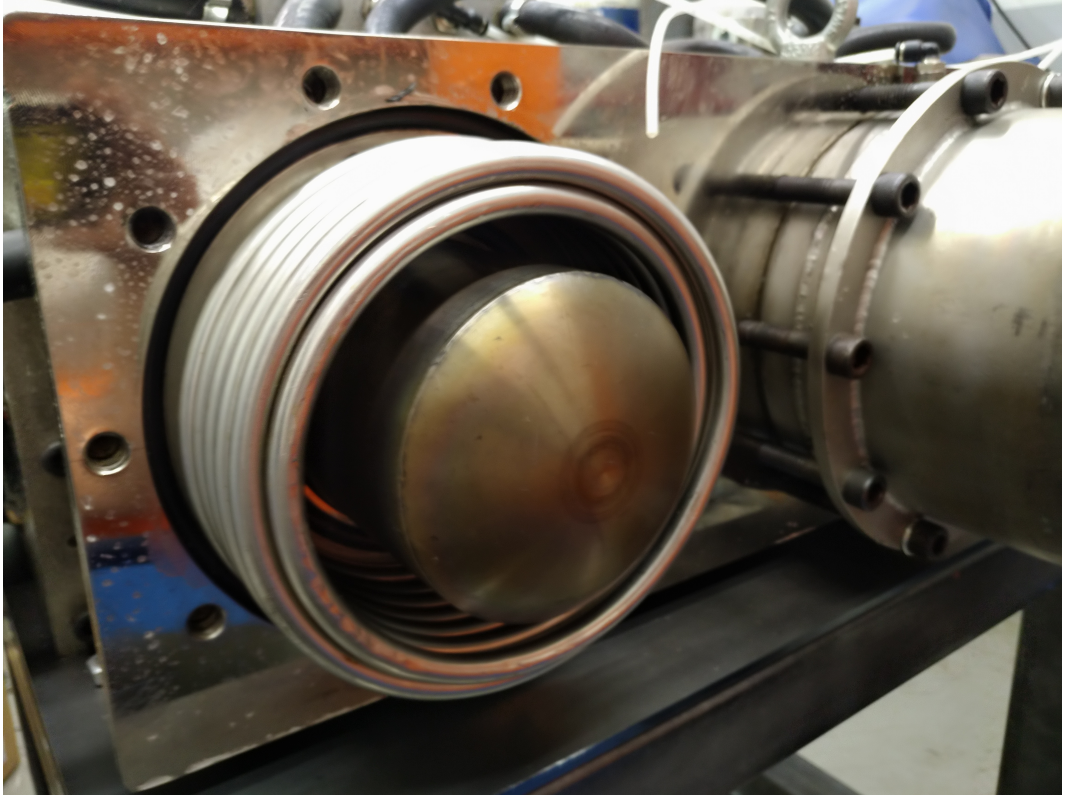


Figure 3.9: The engine cooling coils



Figure 3.10: Outside view of the heater tubes

3.1.4 Engine dimensions

For convenience, the parameters of the engines, such as the geometrical dimensions of various components that are used in the model are shown in table 3.2. The heat exchange surfaces include the aforementioned tubing and additional surfaces, such as annular space wall, which is subject to cooling, or the hot cylinder head, subject to heating. These were lumped together for modelling purposes.

Table 3.2: Engine dimensions

Cooling surface area	0.284	m ²
Heating surface area	0.1303	m ²
Clearance volume, compressor	$3.1644 \cdot 10^{-4}$	m ³
Clearance volume, expander	$3.8958 \cdot 10^{-4}$	m ³
Regenerator porosity	0.9	-
Regenerator wire diameter	0.1	mm
Regenerator mass	0.5	kg
Crank radius	27.5	mm
Crank rod length	157	mm
Piston diameter	108	mm

It is also important that the engine survey necessitates the modifications of certain initial model assumptions, namely in regards to the mass conservation - leakage has to be taken into account, and heat transfer - heat losses through cylinder liners have to be taken into account. In modelling the engine it is assumed, that the cooler temperature is equal to the arithmetical average of cooler inlet and outlet temperature from the coils and the heater temperature as the average of all measurements on the outside of the hot cylinder for the heater. That is, conduction of metal walls is neglected.

3.2 Auxiliary equipment

The engine is not a self contained power unit. An external heating and cooling system had to be implemented. This equipment is not of scientific interest, however for clarity it is important to provide a description. The heating system consists of a combustion chamber with two independent oil burners, one for each engine unit. The objective has been to reach the engine operating temperatures. The burners are Lamborghini ECO 3R models, with a power output between 14.23 to 35.60 kW, designed for light fuel oil. The burners are fitted with forced air fans and pressure

pumps. Power is regulated by selecting fuel nozzles. Nozzles 0.5 in diameter were selected for the experimental runs based on the burner characteristics. Continuous regulation of the power output is possible only through regulating a pump bypass valve within the range of 16.22 to 24.41 kW. The cooling system is a simple closed loop, with water circulation provided by a domestic circulator pump. Two hot water air heaters are used as heat sinks.

3.3 Measurement system

The experimental stand had to accommodate several diverse kinds of measurements. The main objective was to enable the construction of pressure-volume diagrams for different operating conditions. Second, temperatures and coolant flows had to be measured.

In order to perform engine indication, it is imperative to have a fast data acquisition system and sensors able to react to quick changes of the measured parameters. The nominal engine rotational speed is around 450 rpm, which corresponds to the period of a single rotation being 0.13s. A sufficient number of readings has to be taken during a single rotation to reliably draw a $p - V$ diagram. Although various indication systems exist on the market they are dedicated for IC engines. Due to the engine's hermetic construction their implementation would be considerably difficult. Therefore a system had to be built by the author, using off-the-shelf components. It was decided, that a minimum sampling rate of the system is to be 1000 Hz, as it corresponds to taking 130 samples per a nominal rotation.

3.3.1 Volume and shaft angle measurement

Due to the hermetic construction the engine volume had to be measured indirectly using the shaft angle. The piston positions can be then derived from the equations of motion based on the geometric parameters of the mechanism. Though many shaft encoders are available on the market it was decided to adapt the existing motor encoder already built into the PMAC motor used as a generator.

This device, known as the "RMB29AC01SS1" is a sin/cos encoder, meaning that it provides two analogue signals in the form of a sine and cosine wave, where the angle of the sine functions corresponds to the angle of rotation, thus:

$$\varphi_{el} = \arctan \frac{\sin}{\cos} \quad (3.1)$$

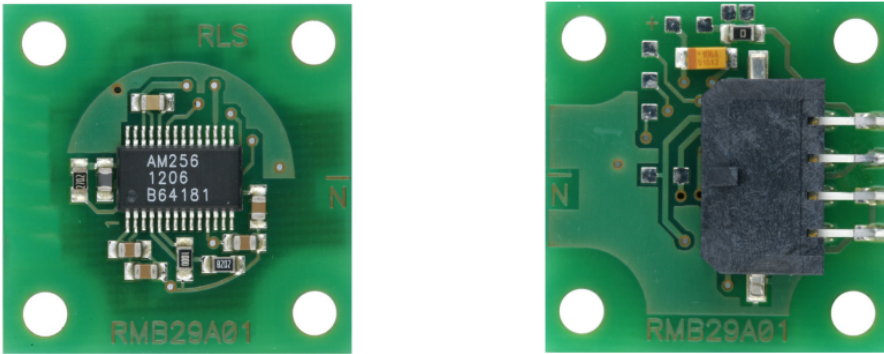


Figure 3.11: The RMB29AC01SS1 sin/cos engine encoder

The device was powered by a 5V line from the SEVCON gen4 motor controller. To enable the operation of the encoder with the controller switched off (as is done when the motor works as a generator) an external power supply has been connected.

In the decoding of signals and their translation to the electric motor (and later Stirling engine) shaft angle, one period of the sine wave corresponds with a single rotation of the electrical machine, which due to the planetary gear corresponds to five Stirling engine shaft rotations. If the starting position of the Stirling shaft is said to be zero degrees, this will correspond to a certain angle of the electrical motor rotation as read from the encoder signal. Though this angle can be noted down, in later measurements the question of which of the five electrical revolutions is the starting one would be open, unless all the experimental work was done as a single, continuous data acquisition process. Due to the impracticality of this, a separate sensor was used as a marker. As its only function is to indicate for which electrical rotation the Stirling engines passes through its "zero" point, it did not have to be of particularly high quality. A simple hall effect sensor was therefore utilized, with its magnet mounted on the engine flywheel.

3.3.2 Pressure measurement

The pressure sensors had to fulfil the following objectives:

- pressure range 0 to 50 bar,
- sampling rate of 1000 Hz or higher,

- response time of 1 ms or lower,
- tolerate high gas temperatures.

Based on these considerations and economic factors DMP 320 pressure transducers manufactured by BD Sensors were chosen, the variant selected being one designed for a 0-60 bar pressure range, producing a standard voltage signal (0 – 10 V). Gas temperatures up to 125°C [1] are tolerated by those devices, therefore the sensors were mounted on the cold cylinder heads. Due to the proximity to the combustion chamber, a separate sensor cooling system has been implemented.



Figure 3.12: The DMP 320 pressure transducer

3.3.3 Data acquisition and processing

A PCIe6353 National Instruments card has been used for data acquisition. This is due to its ability to process analogue signals (48 analogue inputs) with a maximum sampling rate of 1.25 MS/s and the presence of an internal timer. Signals from the encoder and two pressure sensors were connected as analogue inputs in a differential configuration. Acquisition was carried out using the "Data acquisition toolbox" implemented in the MATLAB environment. A dedicated script for data processing

was also implemented. First, data is read and a time window is selected in which a periodic steady state has been reached.

An example time plot of the electric angular velocity is shown in Fig.3.13. As was noted during the first measurements, the angular velocity is varying across the cycle.

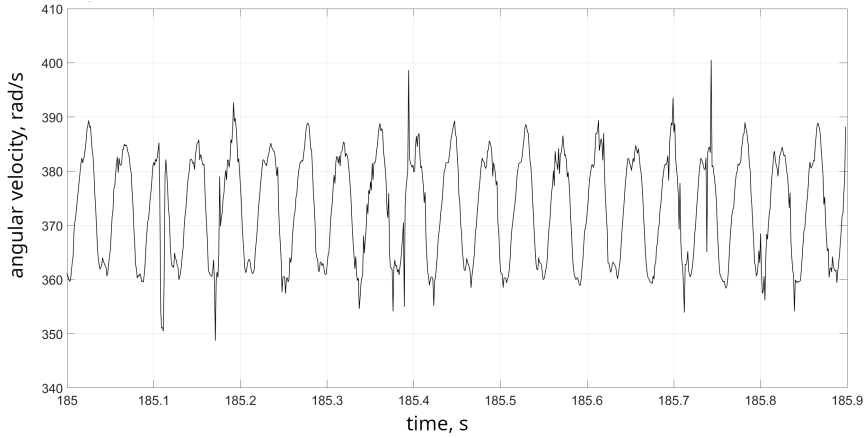


Figure 3.13: Time plot of the angular velocity for example engine measurements

This is to be expected, due to the fact that forces acting on the engine cranks are periodically varying, and also due to the small size of the flywheel. The angular velocities are then divided by 5, corresponding to the gear ratio.

$$\varphi_{i,j} = \varphi_{i,j-1} + \omega_{en,j} \Delta\tau, \quad (3.2)$$

where the j index denotes the time step, and the i index the given cylinder. The volumes can be then calculated based on the equations of motion (eq. 2.2).

Chapter 4

Measurements and model validation

4.1 Sensitivity of the ML3000 engine model to heat transfer coefficients

To show how the engine output depends on the internal heat transfer coefficient, a parametric analysis was carried out. The heat transfer coefficients were varied from 0 to $1000 \frac{\text{W}}{\text{m}^2\text{K}}$. The engine dimensions were those for the Genoastirling ML3000 engine, for a single set of cylinders. The heater temperature was assumed as 980.94 K and the cooler temperature as 295.83 K. The mean buffer pressure was set at 5.44 bar. The engine was assumed to rotate with the rotational speed of 501.4 rpm. It was assumed that the heat transfer coefficient is the same throughout the engine, that is both in the cooler and heater.

The dependence of the engine indicated power on this value is shown in figure 4.1. As one can see, up to reaching the value of circa $200 \frac{\text{W}}{\text{m}^2\text{K}}$ the sensitivity to this parameter is extremely high. After this value the engine power plateaus, though there is still a degree of dependence.

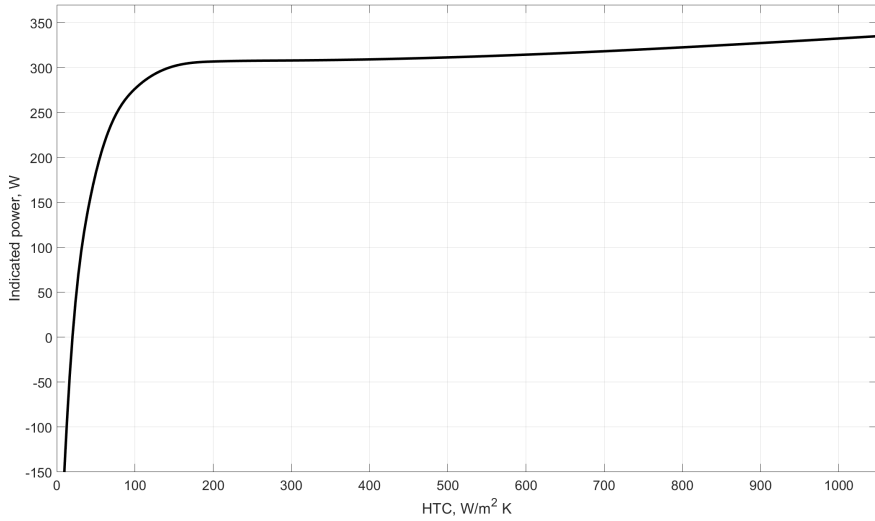


Figure 4.1: An illustration of engine power dependence on internal heat transfer coefficients for the Genoa ML3000 Stirling Engine

To further illustrate the point, indicator diagrams can be shown. This is shown in figure 4.2.

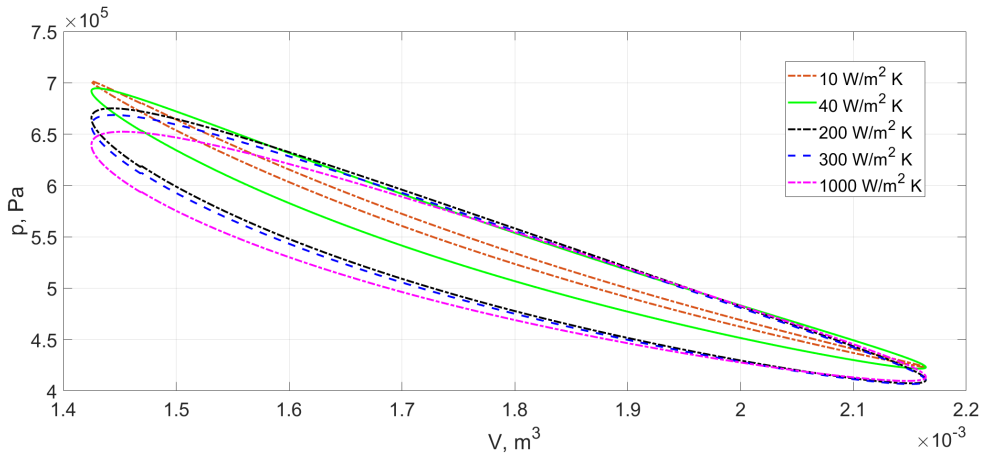


Figure 4.2: ML3000 engine simulated indicator diagrams for selected values of the heat transfer coefficients

As can be seen, the indicator diagram shape depends significantly on the heat

transfer coefficient. Though the maximum and minimum pressure values can change, the model forces the mean pressure to be constant to correspond with the buffer pressure (this is an effect of leakage). The pressure amplitudes stay roughly the same, as they are dependent mostly on the compression ratio.

4.2 Model validation methodology

Based on the aforementioned considerations, it is important that the model validation procedure is carried out several times for different heat transfer correlations used. For validation using experimental measurements, the first step was to process the raw data. This was done according to the method presented in Chapter 5, Section 3. Measurements were carried out with the sampling rate set at 3000 samples per second for crank angle and pressure, and noted down from manual readouts for temperature. Buffer pressures in the engine were varied from 6 to 13 bar, using nitrogen as the fluid. With every pressure change, readouts were only made after the temperatures and rotational speed stabilized themselves, reaching a steady state, with the engine under load. For each working "point" pressure readouts were done. From the readouts, a window of 300 seconds was selected, and indicated power was calculated as an integral of pressure over volume for these rotations. Mean pressure has also been calculated as an arithmetic average of the working space pressure.

Measurements have been carried out for two working fluids, nitrogen, argon. For nitrogen, the buffer space pressure was varied between 5 and 13 bar. For argon the pressure range was narrower and confined to higher values, as in other case the engine would not start. The pressures were between 10 and 14 bar. For the purposes of this particular analysis the measuring was done in 300 second windows, after reaching a steady state. The quality evaluated was the indicated power in the right set of cylinders. As it was found technically difficult to keep any of the engine parameters stable, for the purposes of comparison, it has been elected to calculate the Beale and West numbers for the engine. By their definition, the numbers being relatively constant across a set of measurement implies that they have been done correctly. By their definition, the numbers being relatively constant across a set of measurement implies that they have been done correctly. The Beale number is defined as follows[83]:

$$\text{Be} = \frac{N}{p_m n_s V_{sw}}, \quad (4.1)$$

where N is the engine shaft power, p_m is the mean cycle pressure, and V_{sw} is the swept volume. This number has been ascertained by Beale to have the value of $\text{Be} = 0.15$ for engines evaluated by him. It should generally have a constant value for

a given engine and be independent of rotational speed and pressure. As the engines evaluated worked in a similar temperature range, the influence of temperature can be added, forming the more universal West number:

$$\text{We} = \text{Be} \cdot \frac{T_{in} + T_{out}}{T_{in} - T_{out}}, \quad (4.2)$$

where T_{in} and T_{out} are the heat source and sink temperatures respectively. This number will be used illustratively for the purpose of this evaluation due to significant temperature variations in measurements.

Table 4.1: Measurements for argon, part I

T_{in}, K	898.75	880.10	875.99	872.62	890.57	894.68
T_{out}, K	294.69	295.43	295.36	295.68	295.04	295.19
p, bar	11.59	14.18	14.84	15.30	12.99	12.84
n, rpm	480.12	505.57	516.17	525.69	514.77	510.71
N, W	560.83	666.49	666.94	689.26	678.43	621.93
Be, -	0.0818	0.0755	0.0707	0.0696	0.0824	0.0770
We, -	0.1616	0.1517	0.1425	0.1409	0.1640	0.1527

Table 4.2: Measurements for argon, part II

T_{in}, K	896.98	879.88	875.88	904.19	900.42	884.43
T_{out}, K	294.51	294.90	295.09	293.69	294.28	295.06
p, bar	10.51	10.92	11.22	9.61	10.68	12.13
n, rpm	526.25	578.32	549.73	579.84	526.38	546.94
N, W	587.87	655.65	648.22	600.04	598.05	674.54
Be, -	0.0863	0.0843	0.0853	0.0874	0.0863	0.0825
We, -	0.1706	0.1693	0.1719	0.1715	0.1701	0.1651

Table 4.3: Measurements for nitrogen, part I

T_{in}, K	980.94	975.94	961.26	948.60	944.60	933.52	921.33	918.11
T_{out}, K	295.83	296.23	296.67	297.29	298.37	298.09	299.02	302.07
p, bar	5.44	6.37	7.13	8.09	8.32	9.79	11.28	14.02
n, rpm	501.40	490.82	514.43	526.78	665.22	544.85	553.01	629.61
N, W	340.23	387.80	427.44	543.26	741.62	497.20	663.34	978.69
Be, -	0.1012	0.1007	0.0945	0.1035	0.1087	0.0757	0.0863	0.0900
We, -	0.1887	0.1885	0.1789	0.1980	0.2091	0.1467	0.1693	0.1783

Table 4.4: Measurements for nitrogen, part II

Tin, K	925.75	953.72	953.86	947.33	947.03	955.78	953.74	947.59
Tout, K	300.15	297.15	297.51	297.98	298.14	298.32	299.99	300.83
p, bar	12.42	7.08	6.94	8.58	9.29	8.81	10.31	12.74
n, rpm	593.10	515.73	552.78	534.51	506.46	574.57	623.84	620.60
N, W	824.28	387.32	387.32	609.57	611.96	636.26	746.81	920.02
Be, -	0.0908	0.0861	0.0819	0.1079	0.1056	0.1021	0.0942	0.0944
We, -	0.1780	0.1640	0.1562	0.2070	0.2026	0.1947	0.1807	0.1823

Table 4.5: Measurements for Carbon Dioxide

Tin, K	841.05	887.86	873.00	840.19	842.84	912.88	951.39	994.75
Tout, K	294.92	294.77	296.47	296.59	296.74	294.34	293.85	292.51
p, bar	8.87	8.60	11.67	14.26	13.81	7.35	5.86	3.76
n, rpm	561.04	479.77	513.52	518.29	560.39	553.92	497.44	416.46
N, W	523.84	508.78	646.89	709.00	740.24	534.77	419.96	176.04
Be, -	0.0854	0.1000	0.0876	0.0778	0.0776	0.1067	0.1170	0.0911
We, -	0.1776	0.1995	0.1777	0.1628	0.1620	0.2082	0.2217	0.1671

4.3 Evaluation of heat transfer correlation validity

For the purposes of Stirling Engine modelling, a narrower selection of heat transfer correlations should be made (from within the correlations in Chapter 2). As is evident, some of the later formulas were created to provide improvement upon previous formulas, making them practically obsolete. Second of all, care has to be taken with whether the experimental setup from which the formulas were formulated is similar to the experimental Stirling machine in question. From this point of view however not many options are available. The Genoa ML3000 engine is equipped with tubular heat exchangers and cooling coils. The tubular exchangers would at first glance point towards the Zhao and Cheng [91, 92, 93] and Xiao [88, 89] formulas, especially as these were derived specifically for Stirling Machines. The other correlation directly based on the Stirling Engine results is the one of Toda et al [77], however it refers technically only to the heat losses through cylinder walls and not to the main heat exchange processes. The formula of Kanzaka et al [30] is promising as the only one derived for the heat exchangers in a kinematic Stirling machine - though at much higher pressures than in the machine available to the author. To widen the selection, it was also elected to use the formulas of Woschni - due to its

ubiquitousness, despite it being an IC engine formula, without using the formulas for the combustion phase, also, the formula of Annand and Pinfold [9] to investigate the influence of the time derivative term, the formula of Adair [3], as compressors for which it was derived can be considered similar to Stirling Engines through the lack of combustion and finally the formula of Lekic and Kok [44, 43, 45] in order to investigate the influence of its complex terms. The selected formulas are thus:

- Kanzaka (1992),
- Annand (1980),
- Adair (1972),
- Woschni (1967),
- Toda (1991),
- Zhao (1996),
- Lekic and Kok (2011).

As can be seen, this narrow selection does not feature any formula that would fit the experimental case with any accuracy - indeed to the authors best knowledge, no such correlation is available.

Model calculations were carried out utilizing the temperatures, buffer pressure and rotational speed as input data. The model results are shown on a chart (Fig. 4.3) where the x-axis are the measured values of indicated power and the y-axis is the indicated power as calculated with the losses subtracted. Models should ideally follow the $y = x$ line, shown in red. This can also be shown for nitrogen and argon separately (Fig. 4.4 and 4.5).

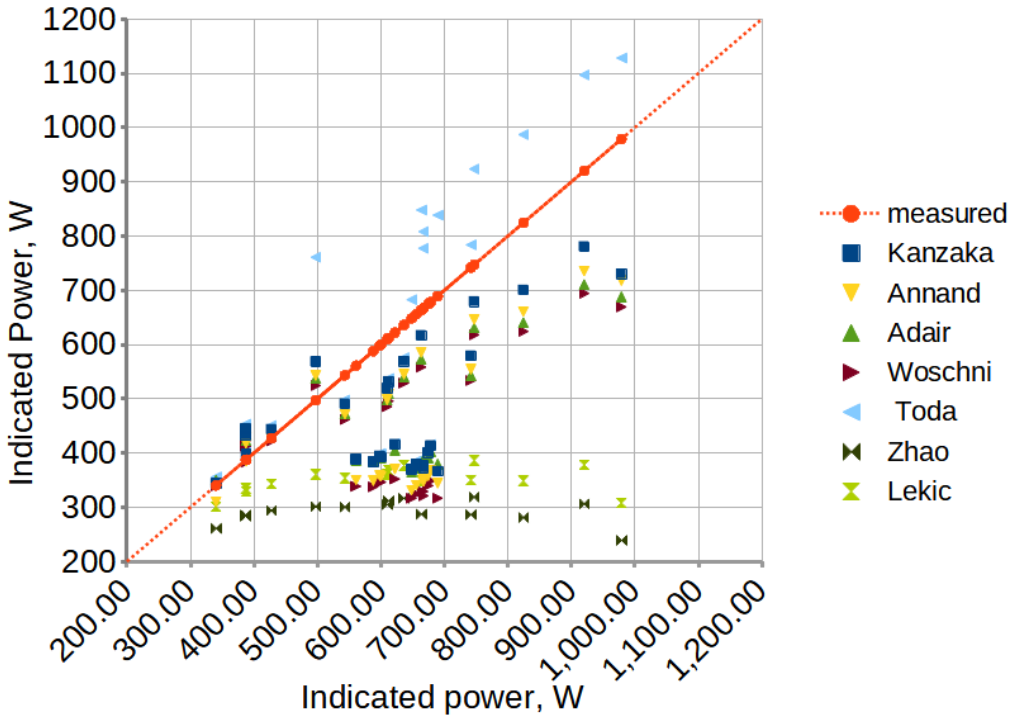


Figure 4.3: Model fit quality with different heat transfer models used

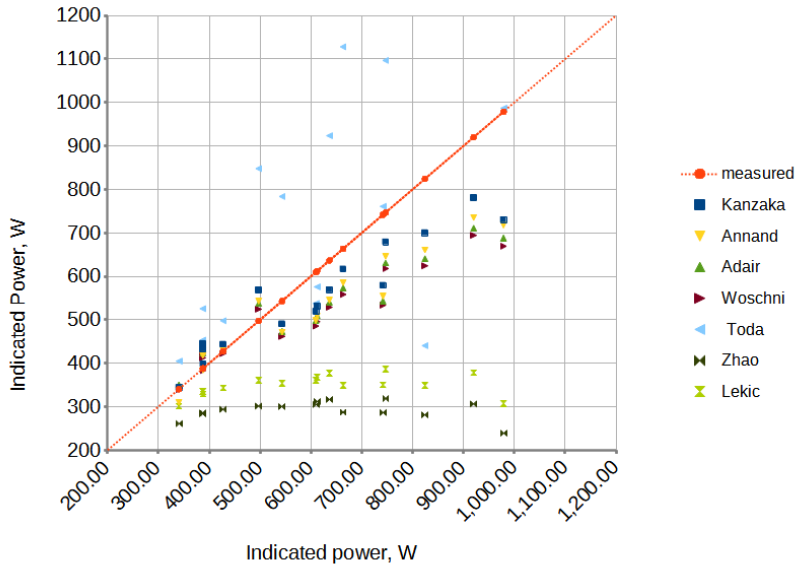


Figure 4.4: Model fit quality for nitrogen

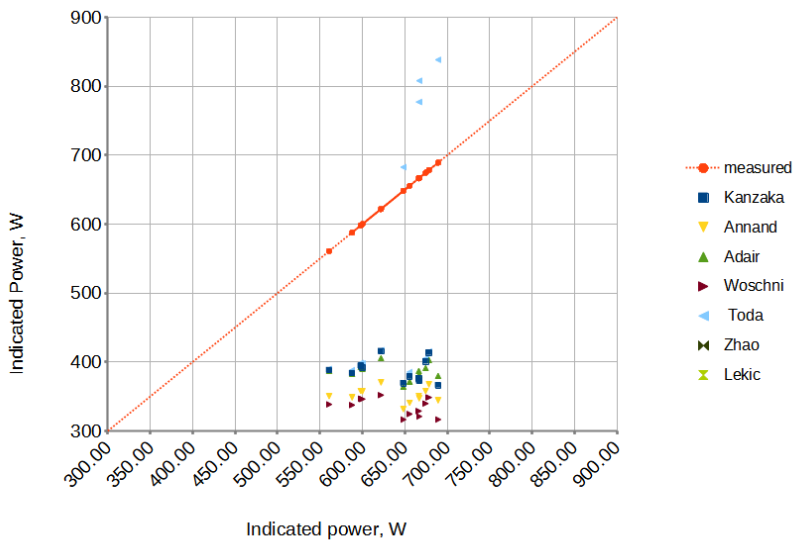


Figure 4.5: Model fit quality for argon

As one can notice from figures 4.5 and 4.4 the quality of fit for all models is

somewhat good for lower power levels and drops significantly for higher levels of power. This is especially visible for argon, where the measurements were all carried out in a high pressure range, where the engine should have a larger power density. As the level of power is mostly correlated with pressure for Stirling engines, noting that other parameters did not vary as significantly, we can hypothesise that the correlations underestimate heat transfer at higher gas pressures. Thus, it can be proposed that they be adjusted. Before this is carried out however, a narrower selection of correlations is sought. For this, it was decided to calculate the overall root mean square error of estimated power, defined as:

$$RMSE = \sqrt{\frac{\sum_1^n (N_{meas,i} - N_{model,i})^2}{n}} \quad (4.3)$$

The values of RMSE are shown in Fig. 4.6.

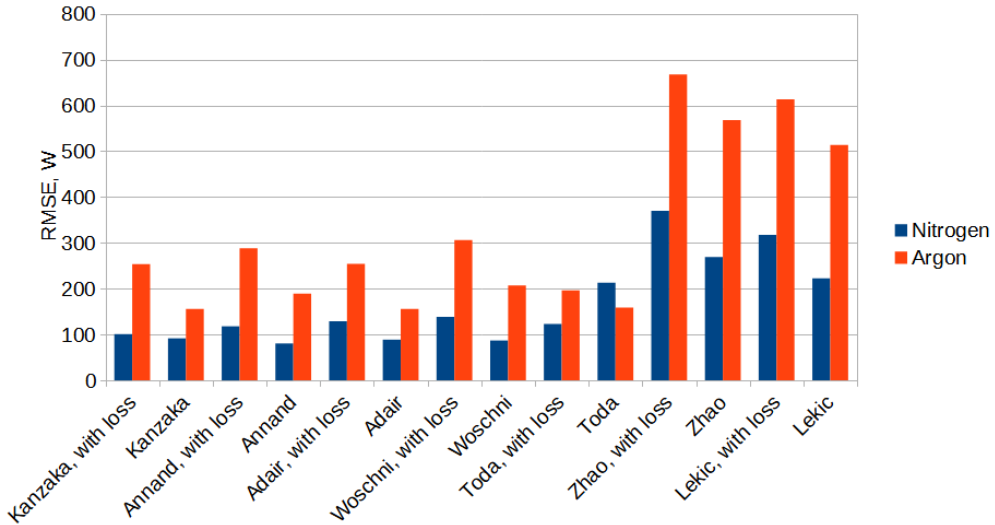


Figure 4.6: Root mean square error of indicated power for different heat transfer models

Interestingly, the model with losses included (this concerns pressure and finite time losses) is not necessarily more accurate.

Table 4.6: RMSE values for different heat transfer models, with and without losses, for nitrogen and argon, values in Watts

	nitrogen	argon
Kanzaka, with loss	100.89	253.94
Kanzaka	91.73	155.74
Annand, with loss	118.02	288.47
Annand	80.55	189.25
Adair, with loss	128.79	254.45
Adair	88.83	155.78
Woschni, with loss	138.66	306.25
Woschni	87.05	207.21
Toda, with loss	123.24	196.25
Toda	212.77	158.93
Zhao, with loss	369.96	667.33
Zhao	269.01	567.95
Lekic, with loss	317.46	612.99
Lekic	222.67	513.88

4.3.1 Investigation of model discrepancies

According to literature [67] the West number is a characteristic parameter of the engine, it should be constant across measurement points. Tables 4.2, 4.3, 4.4 show that in the experiment this is the case. For argon, the standard deviation of the West number is 0.011, for nitrogen 0.017 and shows no visible correlation with any of the working parameters. Contrary to measurement results, where the We number is constant, the values for the model results show variations. Notably, they seem to be underpredicted for points characterized by a higher power output and higher charge pressure. **Based on the this, a hypothesis can be formulated that the discrepancies correlate with pressure.** To verify this, the West number values (model calculated) can be shown as a function of pressure. Also, their covariance with pressure can be calculated.

From figures 4.7 and 4.8 it can be seen, that for the Kanzaka and Annand (1980) models, the West number seems to inversely correlate with pressure. For the Toda model, the opposite is the case. For the set of measurements with argon, the correlations fail, which is expected in line with this, as that set of measurements was carried out in a narrower range of higher pressures. Covariance values calculated from this data are shown in table 4.7. These values are in agreement with the figures. Fur-

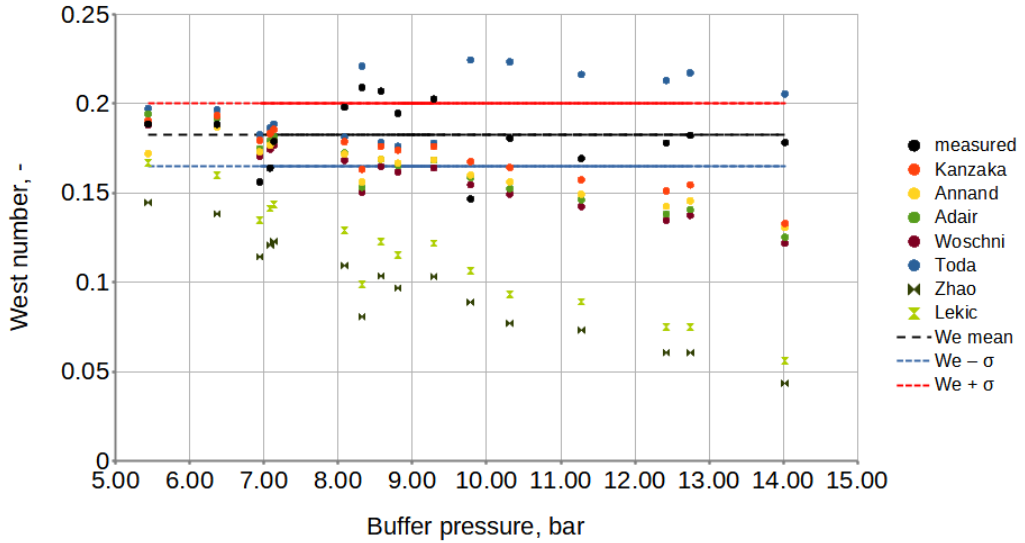


Figure 4.7: West numbers, model calculated and measured, with lines of the measured mean \pm standard deviation, sorted by pressure for nitrogen.

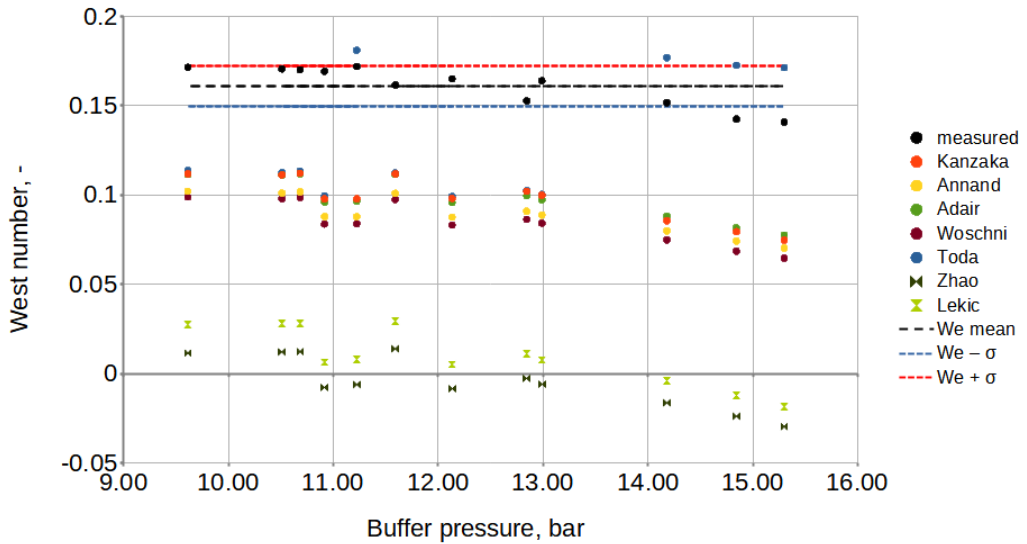


Figure 4.8: West numbers, model calculated and measured, with lines of the measured mean \pm standard deviation, sorted by pressure for argon.

Table 4.7: Covariance values for different heat transfer models, for nitrogen and argon

	nitrogen	argon
measured	-0.00496	-0.01764
Kanzaka	-0.03510	-0.01913
Annand	-0.03224	-0.01607
Adair	-0.04330	-0.01734
Woschni	-0.03929	-0.01748
Toda	0.02109	0.03264
Zhao	-0.06394	-0.02107
Lekic	-0.07036	-0.02363

thermore, it can be seen that the agreement for lower pressure values is quite decent for the Kanzaka and Annand models.

Chapter 5

Measurement based model tuning

5.1 Fine-tuning of correlations

5.1.1 Selection of correction method

Based on the assessment of error values it was elected to carry out the adjustment or validation on the correlations of Kanzaka and Iwabuchi [31], Annand and Pinfold [9] and Toda [77]. The method used, was as follows; first the engine parameters, that is hot and cold heat exchanger temperatures, buffer pressure, and rotational speed, together with the fluid used are made into a data vector \mathbf{X} , likewise the power measurements are formed into a result vector \mathbf{N} . The engine model is treated as a black box function, where for the selected heat transfer models its parameters x_i are adjusted as in a curve fitting problem, so that the RMSE is minimized.

For the adjustment process, the data for nitrogen and argon has been lumped together, and then divided into two separate sets, a validation set and a verification set. The first comprising of 2/3 of the measurement points. Several routes for the adjustment were considered, these being either the varying of the coefficients in the correlations or adding a separate correction factor. Parameter adjustment did not yield meaningful results.

It is proposed that the correction factor should have a form that would compensate for the pressure values, ideally to keep We constant, as is the case in reality. Therefore, the proposed form is:

$$C_f = \left(\frac{\rho(p_i, T_i)}{\rho(p_{ref}, T_i)} \right)^a, \quad (5.1)$$

where the index i refers to instantaneous values, and ref to a reference value of 1 bar. The exponent a is the subject of search.

5.1.2 The adjustment process

The data for both argon and nitrogen has been first separated into two sets, 2/3 as a data set for the calculation (set 1), and 1/3 for verification (set 2). As the Stirling Engine model is not particularly computationally heavy, it was decided that first, for illustrative purposes, and to avoid falling into local minima during subsequent optimization, to calculate the values of the RMSE and also the mean relative error and mean absolute error between the model results and measurement while varying the coefficient a in equation 5.1 as applied to the different correlations. The value was varied between 0 and 1 for the Kanzaka and Annand models and between -1 and 1 for the Toda model (as the Toda model shown the opposite error at higher pressures). To speed up the computations, they were carried out using parallel computing. Also, to further speed up convergence, the data vector for the model included the starting crank angle and starting pressure.

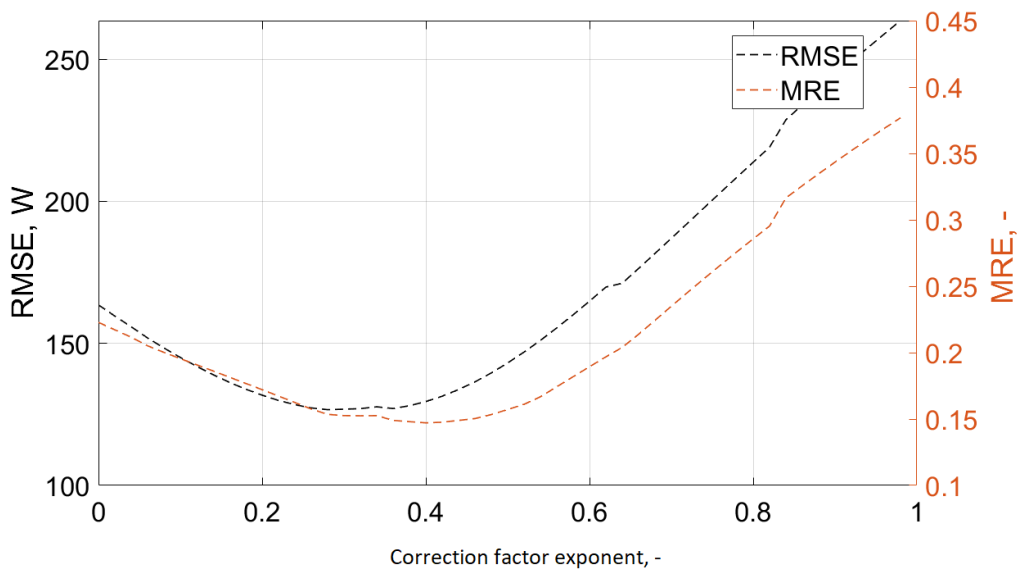


Figure 5.1: Root mean square and mean relative error for the Kanzaka correlation with correction factor, for different values of correction factor exponent

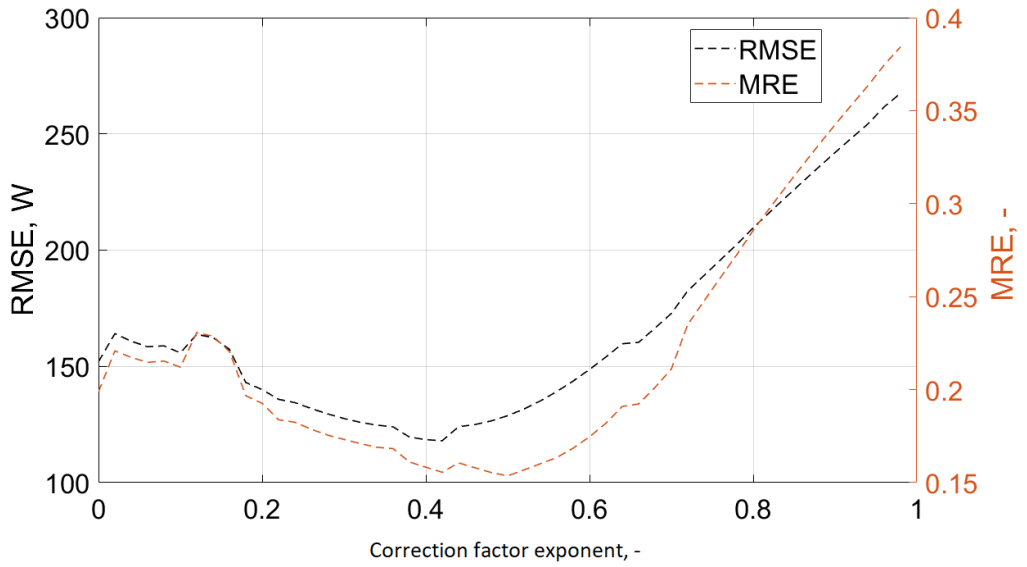


Figure 5.2: Root mean square and mean relative error for the Annand (1980) correlation with correction factor, for different values of correction factor exponent

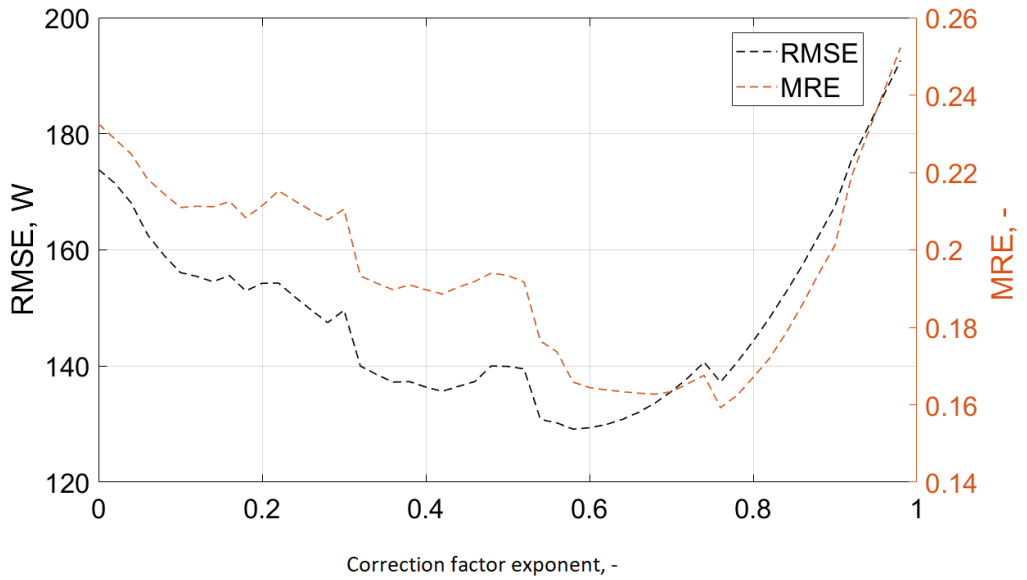


Figure 5.3: Root mean square and mean relative error for the Toda correlation with correction factor, for different values of correction factor exponent, positive range

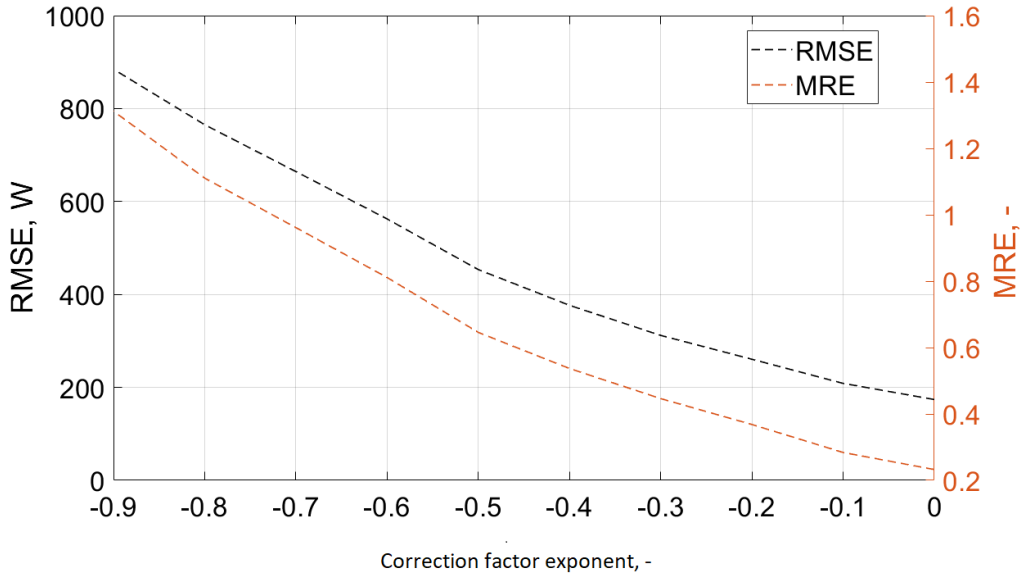


Figure 5.4: Root mean square and mean relative error for the Toda correlation with correction factor, for different values of correction factor exponent, negative range

It can be seen from the charts (5.1 to 5.4) that the use of the correction factor has a small, but noticeable effect for the Kanzaka and Annand models, reducing the RMSE by about a third in the optimum range. The effect with the Toda model is more striking, though the initial hypothesis of the exponent falling in the negative range was not confirmed and the values reached are still higher than for the previous relations.

5.1.3 Adjustment results

The values of the exponent for the correction factor were finally adjusted to the measured data using the Levenberg-Marquardt method.

As a result of this calculation, the values obtained of the exponent a were 0.4013, 0.4214 and 0.586 for the Kanzaka, Annand and Toda correlations respectively. The quality of fit for the set used in calculation and the set used for verification can be seen in figures 5.5 and 5.6.

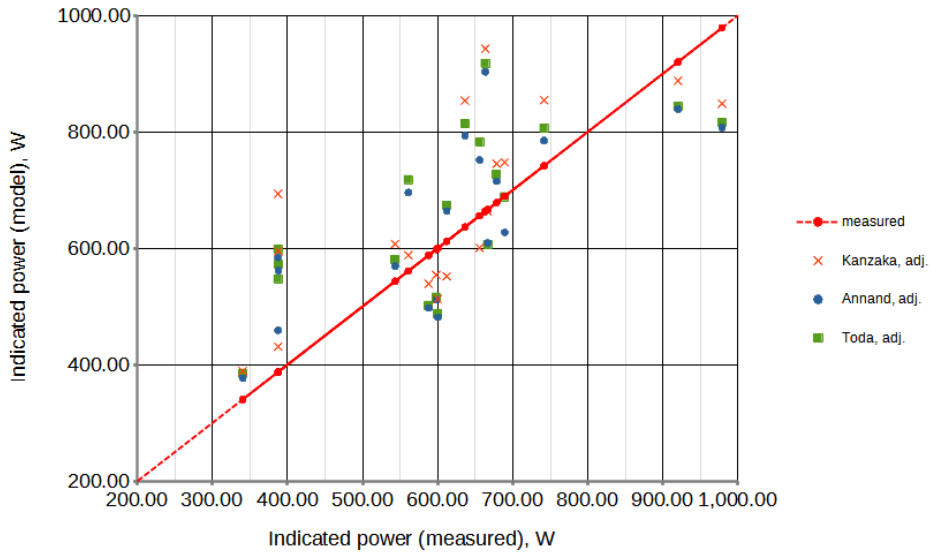


Figure 5.5: Fit quality for adjusted models for validation set (set 1)

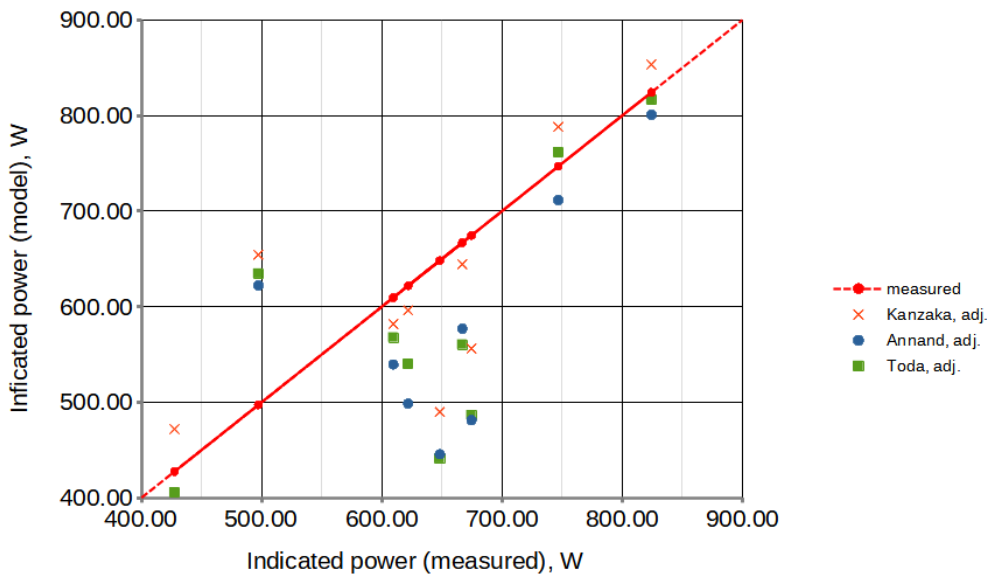


Figure 5.6: Fit quality for adjusted models for verification set (set 2)

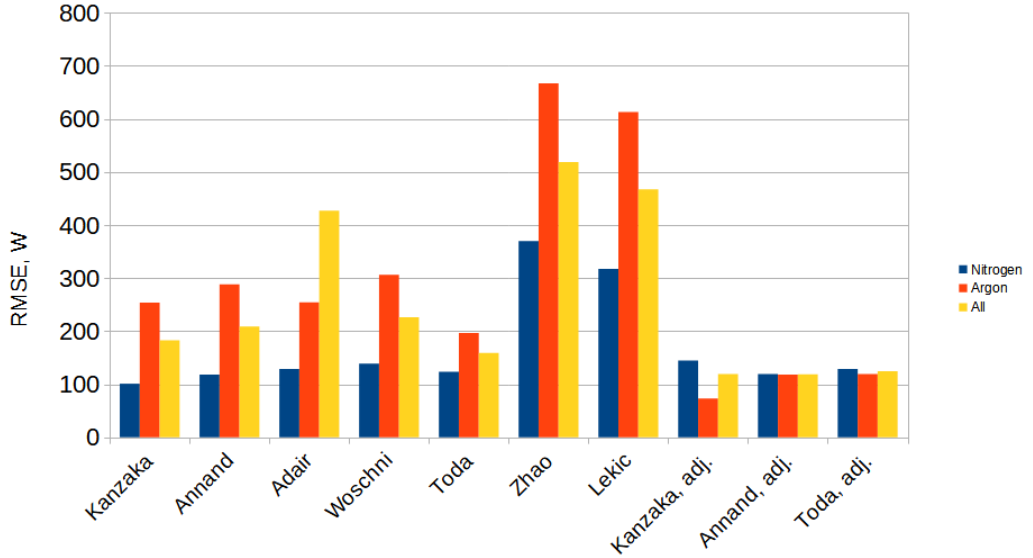


Figure 5.7: Root mean square error of indicated power for different heat transfer models, including the adjusted correlations.

Table 5.1: Root mean square error for selected and adjusted correlations, separated for the verification set and overall

RMSE, W	Unadjusted, verification set	Unadjusted, all data	Adjusted, verification set	Adjusted, all data
Kanzaka	187.262	182.903	88.73	119.277
Annand	215.410	124.571	119.884	118.617
Toda	173.310	189.792	114.361	124.604

The adjusted correlations show a decent quality of fit, both for high and low power measurement points. To further ascertain their quality, the RMSE value was calculated for them as for the unadjusted versions. These results are shown in table ?? and in Fig.5.7.

The formulas tested gave the 0D model a decent quality of fit when compared with experimental results, however this quality was lost at higher pressures. The proposed adjustment based on experimental data decreased the root mean square error in indicated power, shown in table 5.1. Those gains are however not as significant as could have been expected. If one looks at the overall data set, considerable improvement can be seen for the adjusted formulas. A closer look at the data however

reveals a minimal raise in error for nitrogen and significant drop for argon. As the argon measurements were all carried out at higher pressures, this means that the previously noted high pressure range error was compensated, but at some cost to the error in the low pressure ranges. Based on this, it can be deduced that the Kanzaka and Iwabuchi, Annand and Toda formulas with correction factors can be of use coupled with 0D models of Stirling engines, and for machines working at the same ranges of pressure, temperature and rotational speed as the authors experimental rig, and provided the engine has a similar design.

The adjusted Kanzaka formula has the following form:

$$\text{Nu} = 0.21\text{Re}_{\text{sc}}^{0.8}\text{Pr}^{0.4} \left(\frac{T_w}{T_i}\right)^{-0.5} C' \left(\frac{\rho_i}{\rho_{\text{ref},i}}\right)^{0.4013}, \quad (5.2)$$

The Annand and Pinfold formula:

$$\text{Nu} = 0.3\text{Re}^{0.7} + \left(1 + 0.27\frac{D}{V\Delta T}\frac{dT}{dt}\right) \left(\frac{\rho_i}{\rho_{\text{ref},i}}\right)^{0.4214}. \quad (5.3)$$

For the Toda formula: for heating and expansion:

$$\text{Nu} = 0.70\text{Re}^{0.58} \left(\frac{\rho_i}{\rho_{\text{ref},i}}\right)^{0.586}, \quad (5.4)$$

for cooling and compression strokes:

$$\text{Nu} = 0.63\text{Re}^{0.53} \left(\frac{\rho_i}{\rho_{\text{ref},i}}\right)^{0.586}, \quad (5.5)$$

where ρ_i is the fluid density in the given engine volume at a given instance, and $\rho_{\text{ref},i}$ is the fluid density at 1 bar pressure and at the instantaneous temperature.

5.2 Influence of correlation selection on local, instantaneous heat transfer

5.2.1 Comparison of pressure-angle signals for selected measurements

Using the three chosen correlations (Toda, Annand and Kanzaka et al.) a study of influence of heat transfer models on the shape of $p-V$ diagrams have been carried out. As the correction factors were derived for power measurement, it is of interest to see whether this adjustment method has any discernable influence on the validity of the model for predicting not just the power output but the shape of the cycle

itself. Indicator diagrams were drawn on the basis of measurement data and model calculations. They were compared visually, with special emphasis on comparing based and adjusted models, but also several quantities were evaluated to quantify the comparison, this being:

- the overall Root Mean Square Error between the calculated and measured points,
- phase difference between the crank-angle pressure data sets,
- the relative error of pressure amplitude.

These values were considered, as the cycle pressure is in essence a periodic signal. The data used comes from the measurement points shown in table 5.2.

Table 5.2: Measurements for individual comparison

	I	II	III	IV	V	VI
T_{in}, K	898.75	894.68	875.88	980.94	961.26	925.75
T_{out}, K	294.69	295.19	295.09	295.83	296.67	300.15
p, bar	11.59	12.84	11.22	5.44	7.13	12.42
n, rpm	480.12	510.71	549.73	501.40	514.43	593.10
fluid	argon	argon	argon	nitrogen	nitrogen	nitrogen
N, W	560.83	621.93	648.22	340.23	427.44	824.28
Be, -	0.0818	0.0770	0.0853	0.1012	0.0945	0.0908
We, -	0.1616	0.1527	0.1719	0.1887	0.1789	0.1780

For the purposes of visual comparison, the $p - V$ diagrams, both modeled and calculated are shown for the six measurement points and three correlations with and without adjustment. This can also serve as a general, visual validation of the model.

Measurement point I:

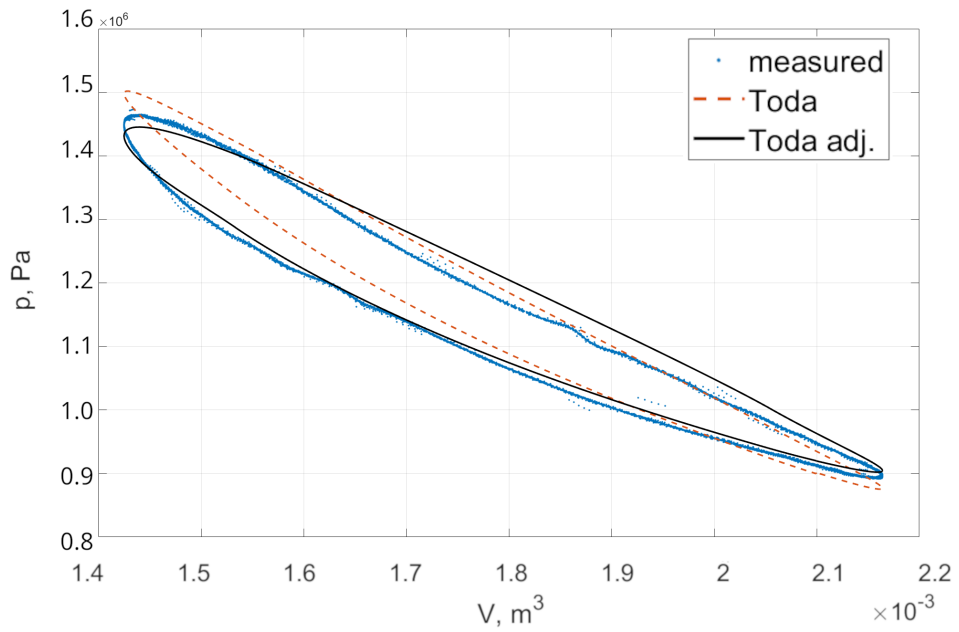


Figure 5.8: Comparison between the $p - V$ diagrams for measurement point I, with the base and adjusted Toda model calculations

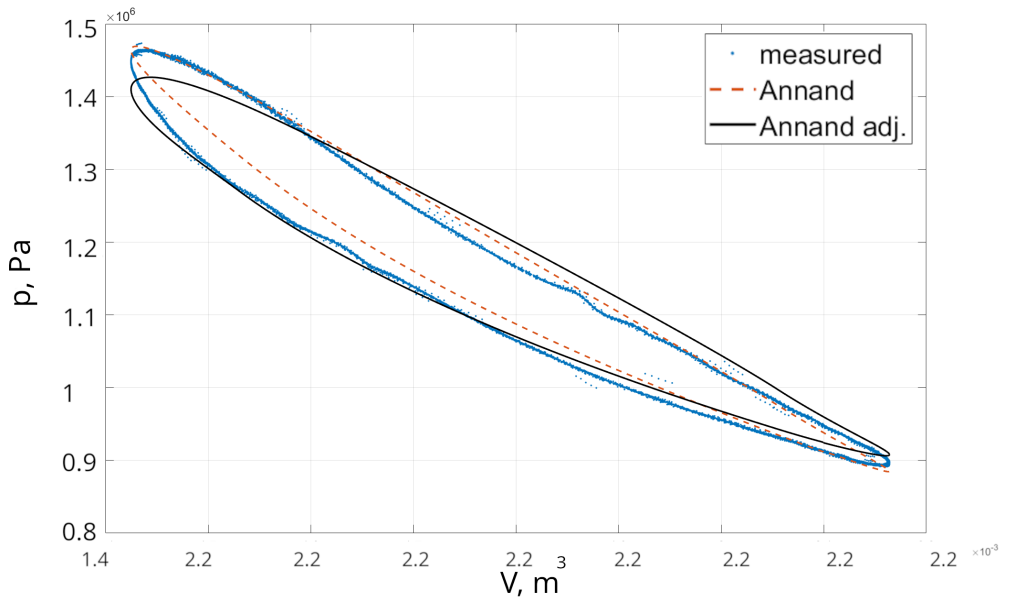


Figure 5.9: Comparison between the $p - V$ diagrams for measurement point I, with the base and adjusted Annand model calculations

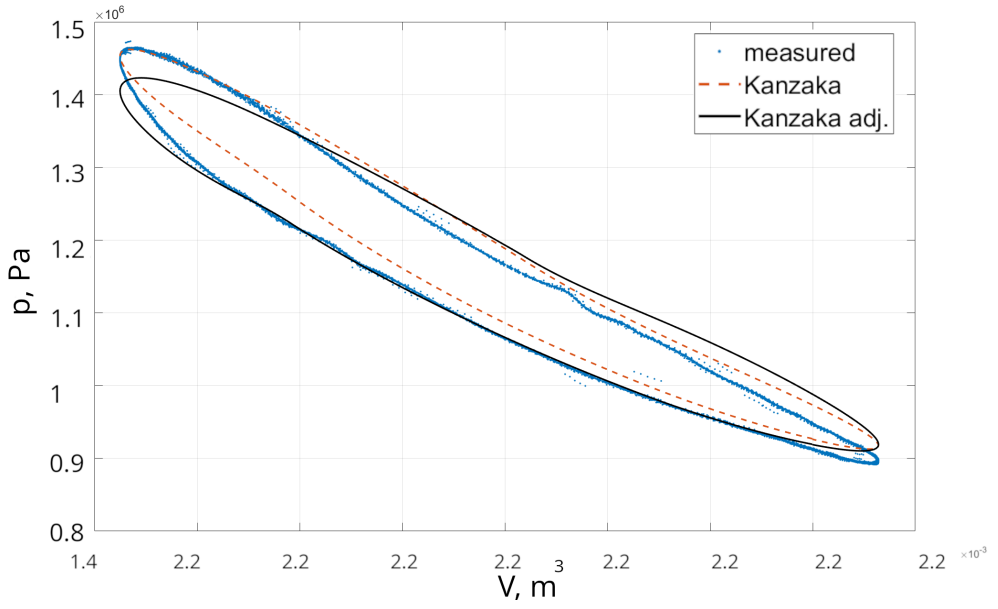


Figure 5.10: Comparison between the $p - V$ diagrams for measurement point I, with the base and adjusted Kanzaka model calculations

Measurement point II:

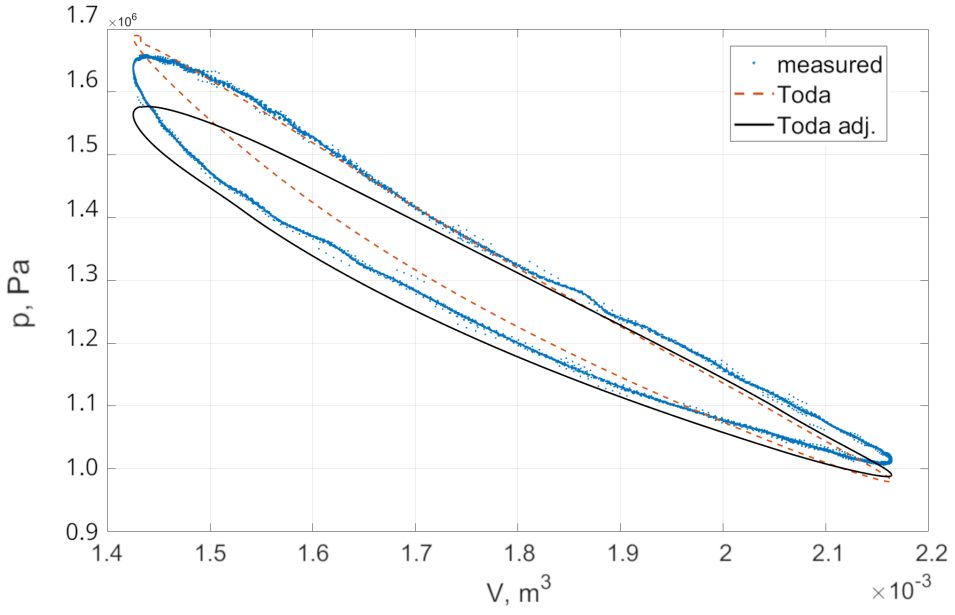


Figure 5.11: Comparison between the $p-V$ diagrams for measurement point II, with the base and adjusted Toda model calculations

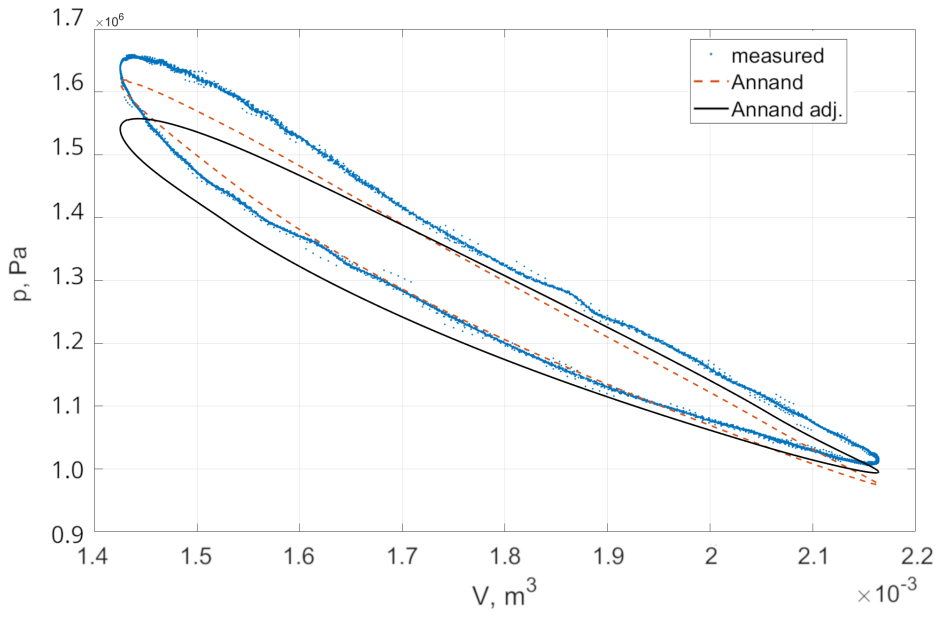


Figure 5.12: Comparison between the $p-V$ diagrams for measurement point II, with the base and adjusted Annand model calculations

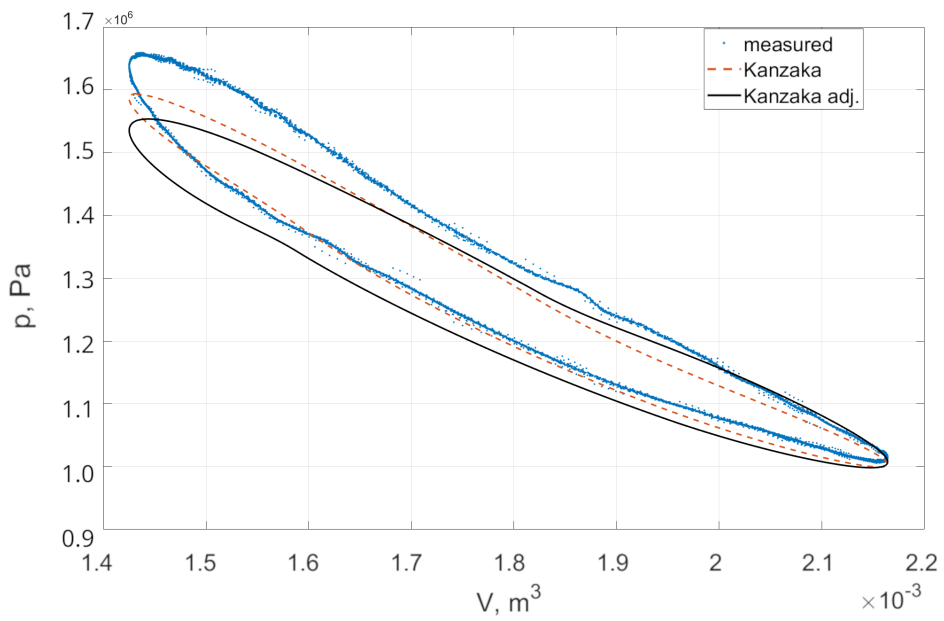


Figure 5.13: Comparison between the $p-V$ diagrams for measurement point II, with the base and adjusted Kanzaka model calculations

Measurement point III:

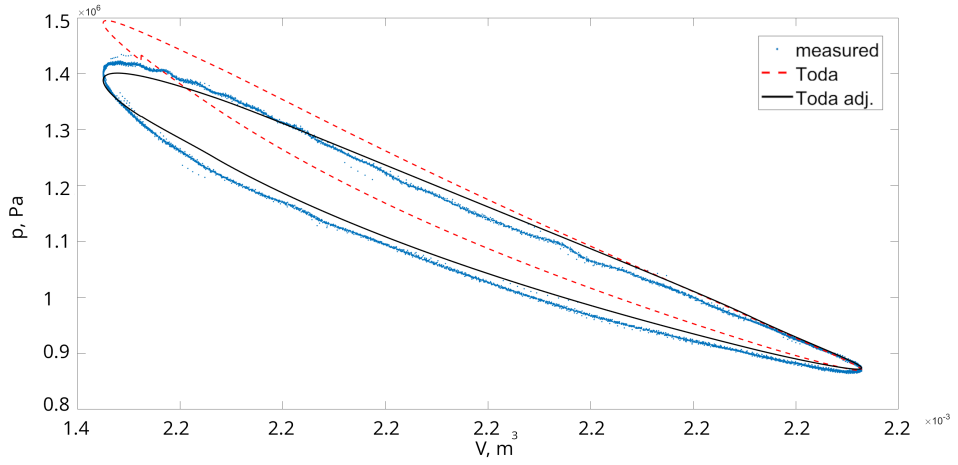


Figure 5.14: Comparison between the $p - V$ diagrams for measurement point III, with the base and adjusted Toda model calculations

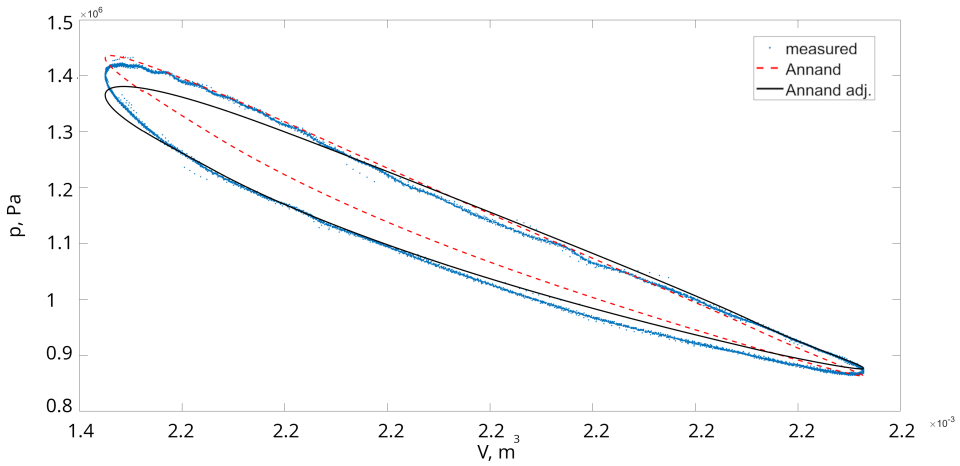


Figure 5.15: Comparison between the $p - V$ diagrams for measurement point III, with the base and adjusted Annand model calculations

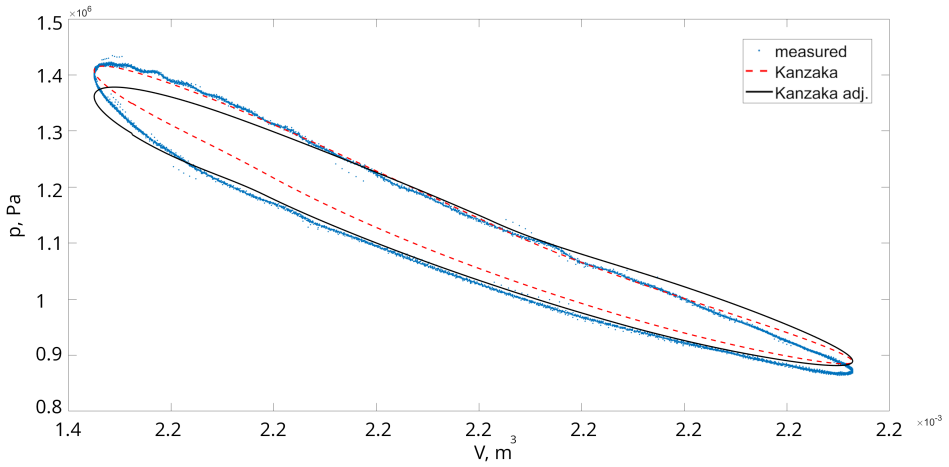


Figure 5.16: Comparison between the $p - V$ diagrams for measurement point III, with the base and adjusted Kanzaka model calculations

Measurement point IV:

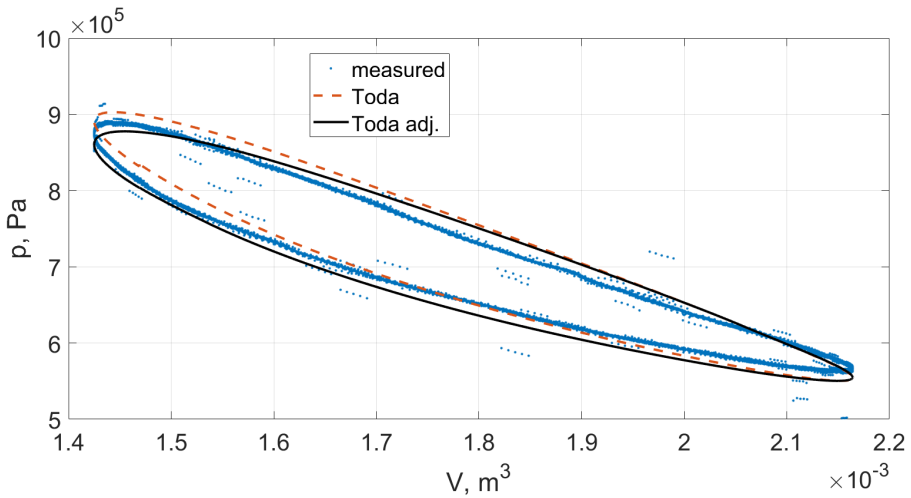


Figure 5.17: Comparison between the $p - V$ diagrams for measurement point IV, with the base and adjusted Toda model calculations

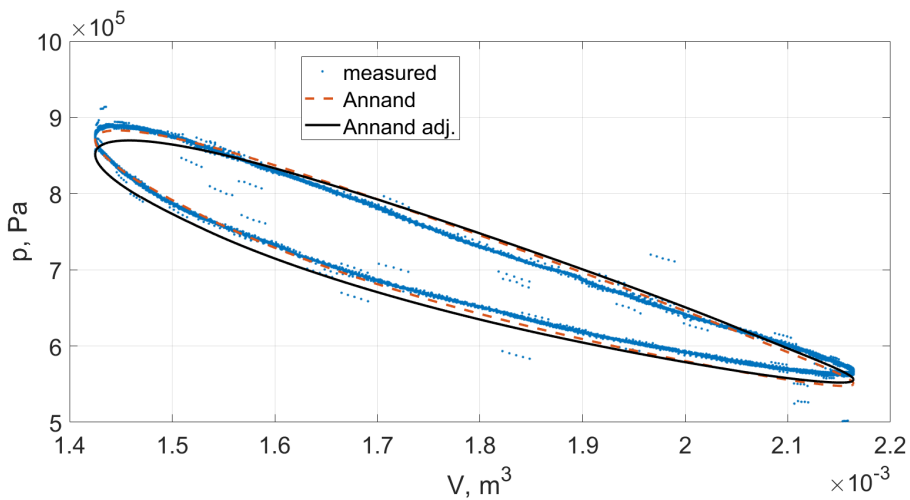


Figure 5.18: Comparison between the $p - V$ diagrams for measurement point IV, with the base and adjusted Annand model calculations

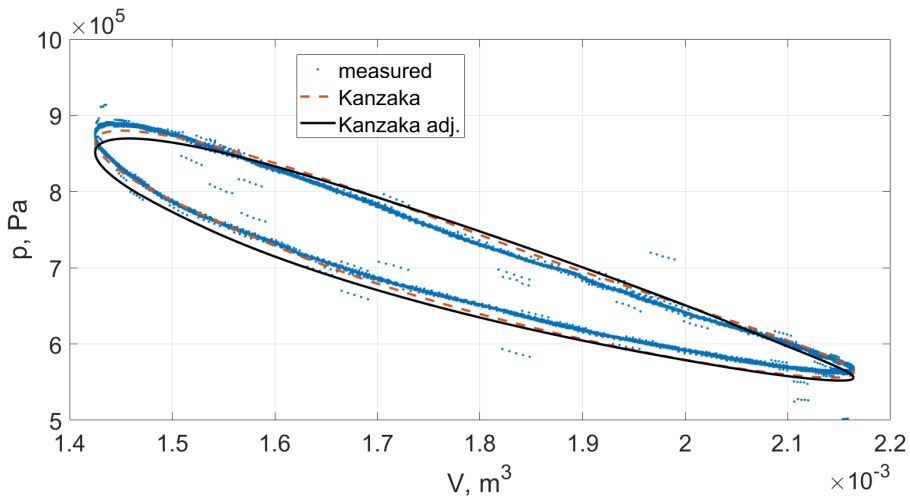


Figure 5.19: Comparison between the $p - V$ diagrams for measurement point IV, with the base and adjusted Kanzaka model calculations

Measurement point V:

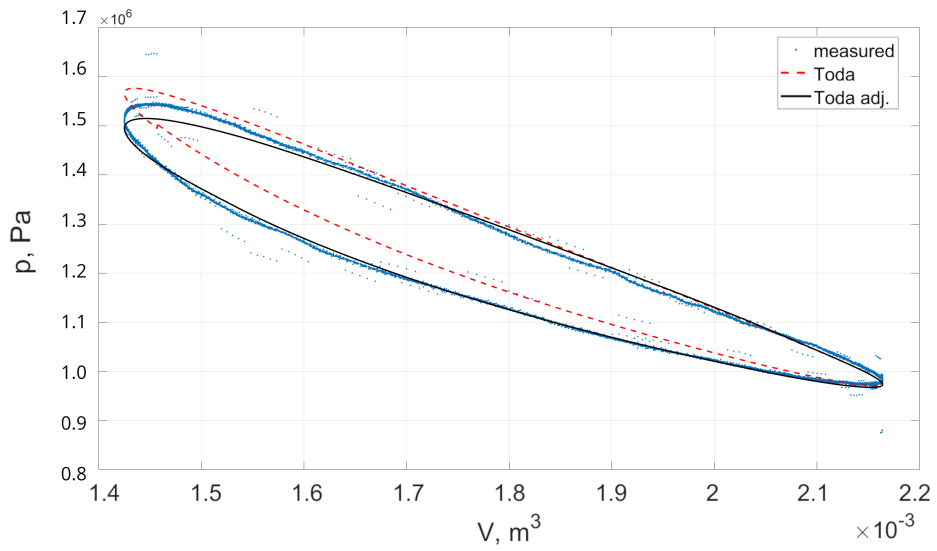


Figure 5.20: Comparison between the $p-V$ diagrams for measurement point V, with the base and adjusted Toda model calculations

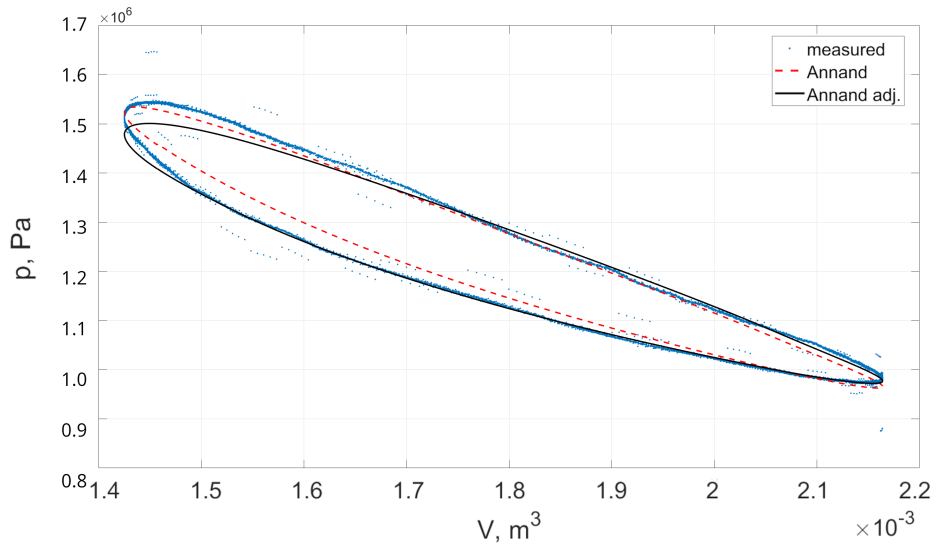


Figure 5.21: Comparison between the $p-V$ diagrams for measurement point V, with the base and adjusted Annand model calculations

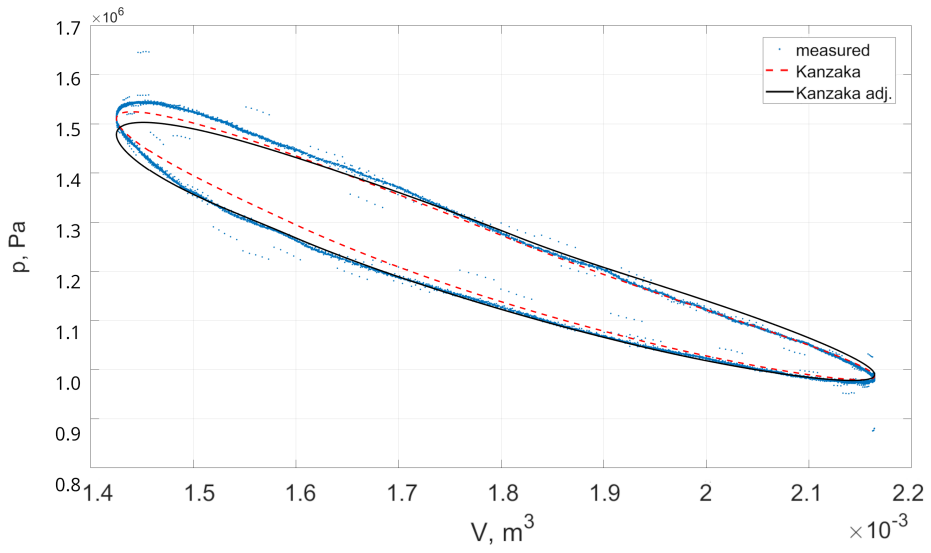


Figure 5.22: Comparison between the $p-V$ diagrams for measurement point V, with the base and adjusted Kanzaka model calculations

Measurement point VI:

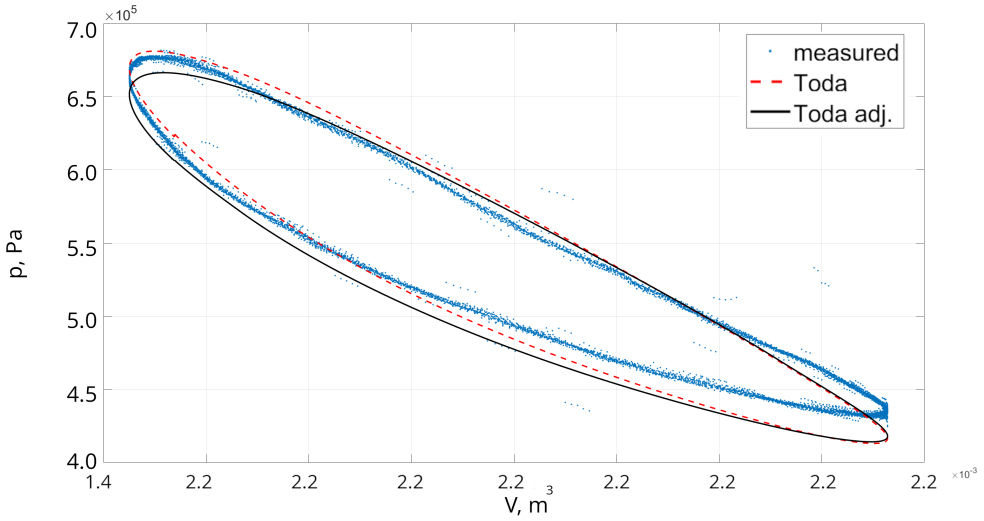


Figure 5.23: Comparison between the $p - V$ diagrams for measurement point VI, with the base and adjusted Toda model calculations

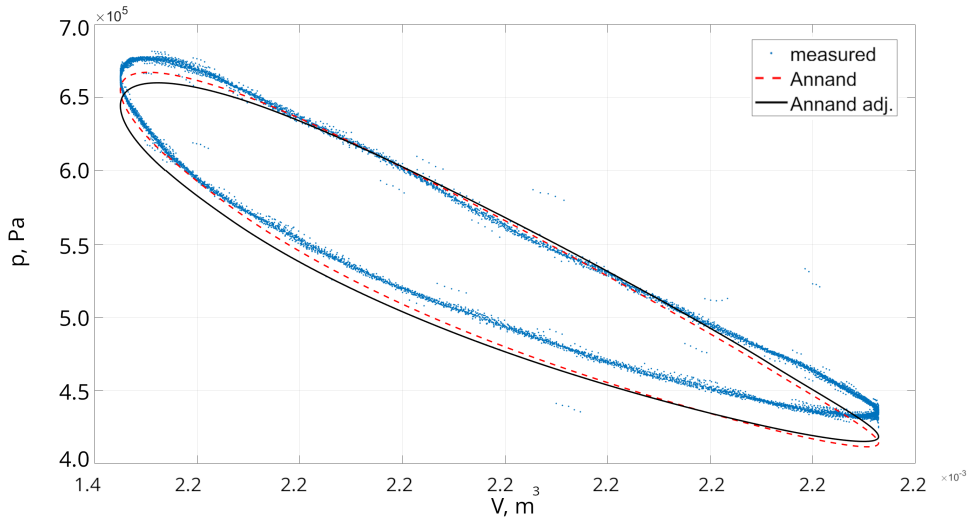


Figure 5.24: Comparison between the $p - V$ diagrams for measurement point VI, with the base and adjusted Annand model calculations

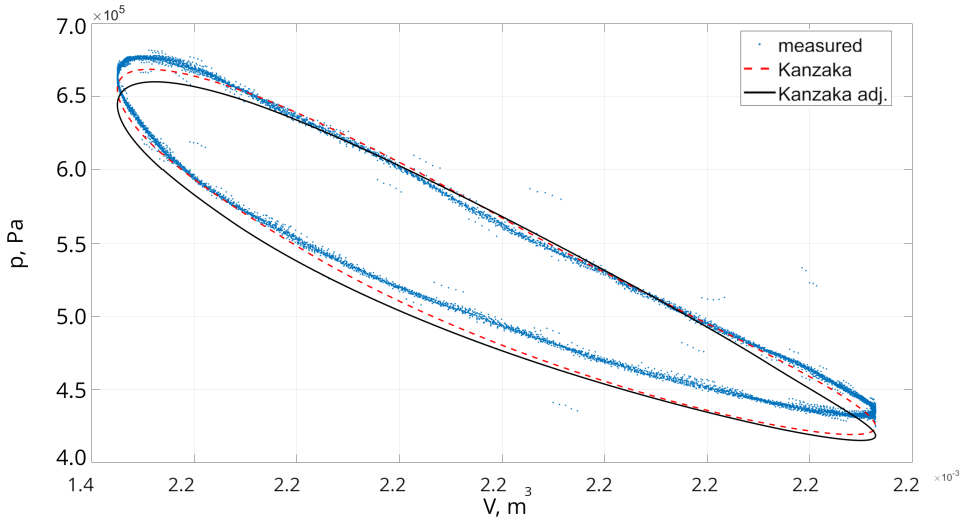


Figure 5.25: Comparison between the $p - V$ diagrams for measurement point VI, with the base and adjusted Kanzaka model calculations

The pressure signal, taken as a function of angle, is a periodic one. Due to this, for additional comparative purposes, we can compare the model and measurement outputs in the form of vector plots, drawn from the buffer pressure as their starting point, with length defined by signal amplitude and the phase defined in relation to the measured signal. This form can serve as a convenient visual comparison - full agreement between the measurement and model would imply that the vectors fully align and are equal in length. An example signal, illustrating this property is seen in Fig.5.26. The vector plots are shown in figures 5.27, 5.28, 5.29, 5.30, 5.31, 5.32.

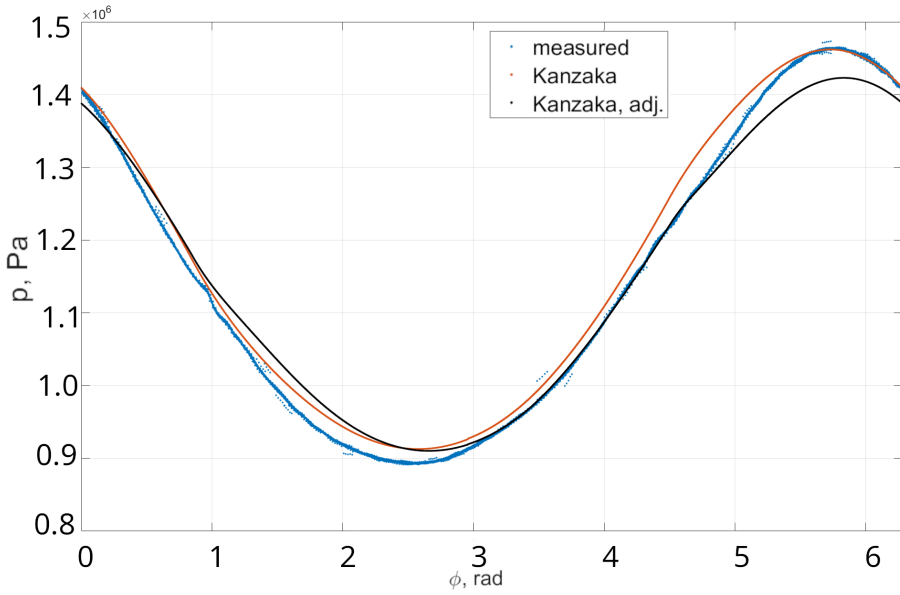


Figure 5.26: Illustration of the pressure as a signal approach, for measurement I.

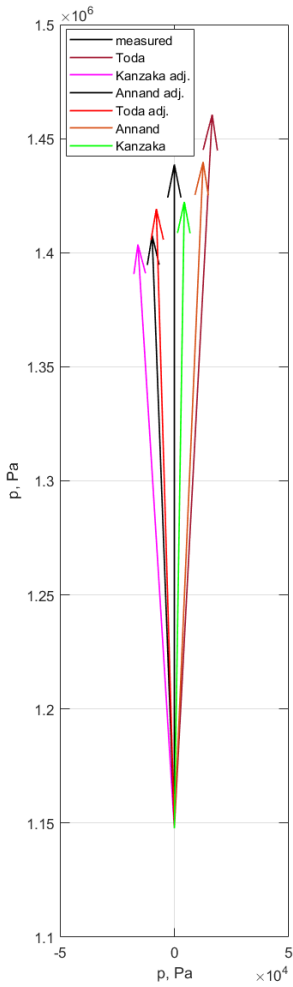


Figure 5.27: Pressure vector plot for measurement point I

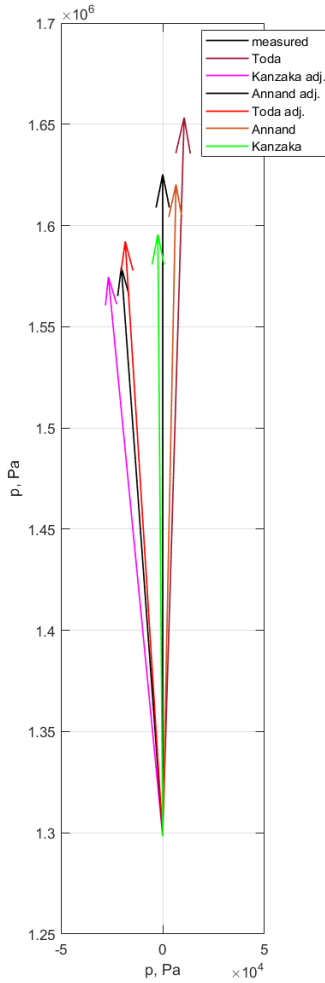


Figure 5.28: Pressure vector plot for measurement point II

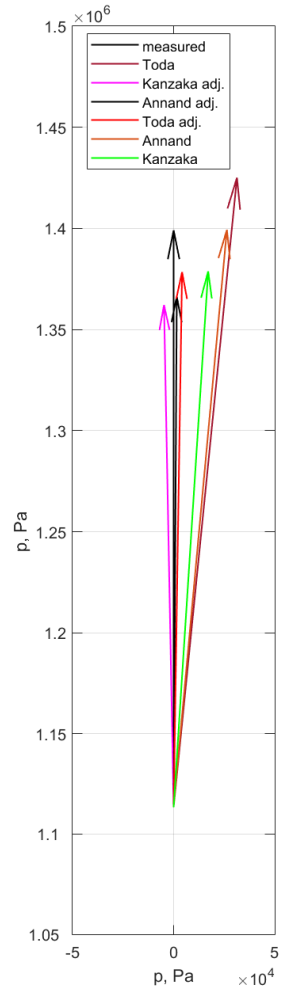


Figure 5.29: Pressure vector plot for measurement point III

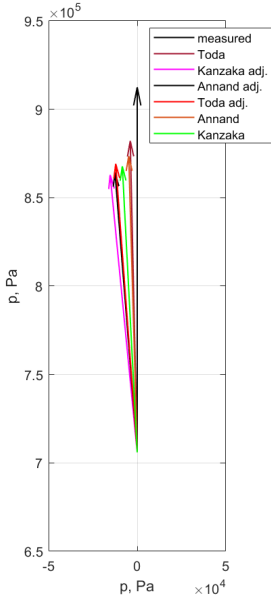


Figure 5.30: Pressure vector plot for measurement point IV

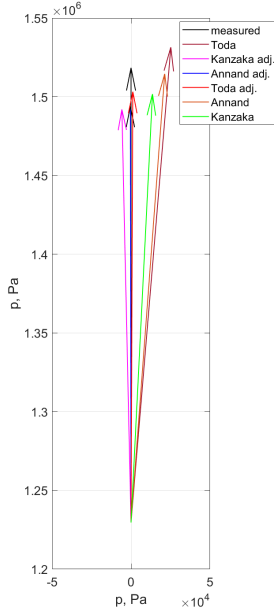


Figure 5.31: Pressure vector plot for measurement point V

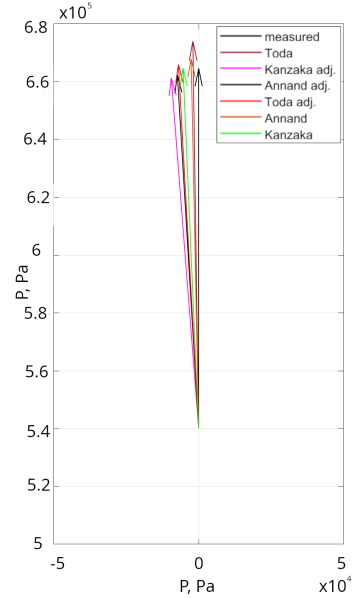


Figure 5.32: Pressure vector plot for measurement point VI

Furthermore, to avoid relying only on visual comparisons, the values of the phase error are shown in table 5.3. A relative amplitude error (relative to the measured amplitude) was also calculated, and this is shown in table 5.4. Root mean square error values, expressed in bar, are shown shown in table 5.5.

Table 5.3: Phase differences between model and selected measurements, for the pressure signal

phase difference, rad measurement:	models:					
	Toda	Kanzaka adj.	Annand adj	Toda adj	Annand	Kanzaka
I	0.053	-0.062	-0.037	-0.029	0.043	0.016
II	0.030	-0.096	-0.072	-0.063	0.020	-0.008
III	0.100	-0.019	0.006	0.016	0.092	0.064
IV	-0.022	-0.097	-0.079	-0.074	-0.029	-0.052
V	0.083	-0.022	-0.002	0.004	0.075	0.050
VI	-0.015	-0.078	-0.060	-0.056	-0.020	-0.043

Table 5.4: Relative pressure amplitude error for selected measurement points

Amplitude error (relative)	models:					
measurement:	Toda	Kanzaka adj,	Annand adj	Toda adj	Annand	Kanzaka
I	0.077	0.119	0.106	0.067	0.005	0.056
II	0.086	0.151	0.138	0.099	0.015	0.091
III	0.097	0.129	0.115	0.072	0.005	0.069
IV	0.147	0.236	0.231	0.208	0.188	0.216
V	0.049	0.091	0.085	0.053	0.011	0.057
VI	0.076	0.024	0.017	0.012	0.027	0.002

Table 5.5: Root mean square error of the pressure signal in bar

RMSE, bar	models:					
measurement:	Toda	Kanzaka adj,	Annand adj	Toda adj	Annand	Kanzaka
I	0.325	0.252	0.203	0.171	0.194	0.215
II	0.293	0.561	0.534	0.429	0.256	0.310
III	0.593	0.210	0.175	0.136	0.297	0.224
IV	0.152	0.145	0.149	0.131	0.107	0.096
V	0.364	0.197	0.194	0.144	0.205	0.168
VI	0.117	0.128	0.146	0.128	0.130	0.096

Based on these metrics, we can conclude, that at least for the six random measurement points selected the correction factor has negative effect on the reconstruction quality as far as the shape of the pressure signal is concerned. In other words, there is a negative effect, often an increase of RMSE values between the measured and modelled pressure signals. This however only applies to situations where the model user actively seeks the shape of the $p - V$ diagram rather than the more useful external engine metrics. Furthermore, this loss of fidelity is not significant as the visual comparison shows. Only in the Toda correlation is a significant drop of RMSE visible, however on average the error does not go below the base value calculated for the Kanzaka correlation.

Interestingly, even though the phase differences between the models and measurements vary, the overallall *direction* of model phase angles stays relatively constant. This unfortunately points to there being random errors in the phase measurement system of the lab stand.

5.2.2 Investigation of possible further adjustment

The possibility of further adjustments was investigated based on the $p - V$ diagrams of 14 selected measurement points, belonging to the former validation set. The number of points was reduced for the sake of computational cost, bearing in

mind, that the new selection should entail measurements representative of the full range of buffer pressures. The values considered for adjustment were firstly the correction factor exponents for the selected correlations, but also the Reynolds number exponents. The root mean square error, previously defined, was used as a metric, calculated for all the 14 measurements for different exponent values.

Before attempting any optimization, much like with the previous process, it was elected to first illustrate the influence of the value on the RMSE in charts. The influence of the correction factor exponent on the Kanzaka and Annand correlations is shown in figures 5.33 and 5.34. It can be seen, that for the Kanzaka formula, the correction factor has a minor negative effect on the error in regards to diagram shape. The Annand correlation demonstrates an existence of some optimum, close to the previously found value, though likely lower. The charts show a certain level of oscillations, likely due to model errors. As the Toda correlation shows improvement in the shape related errors with the correction factor application, no analysis was carried out.

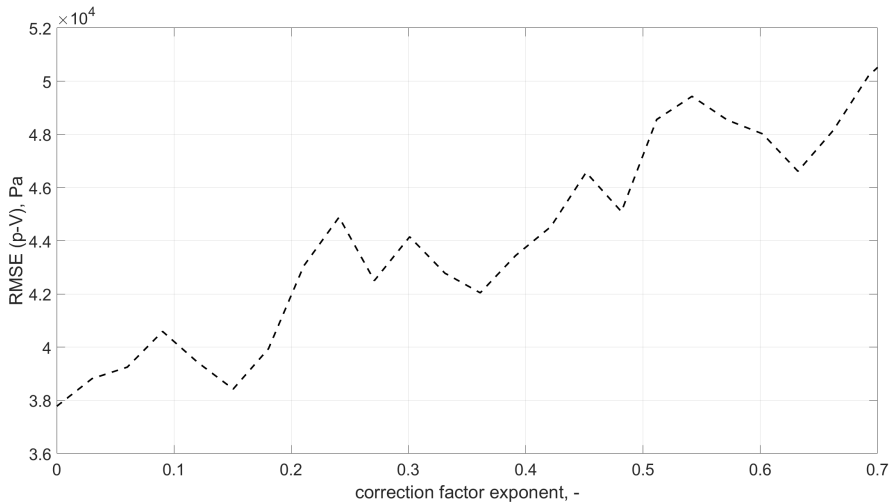


Figure 5.33: RMSE for the selected measurements for varying correction factor exponents, Kanzaka correlation

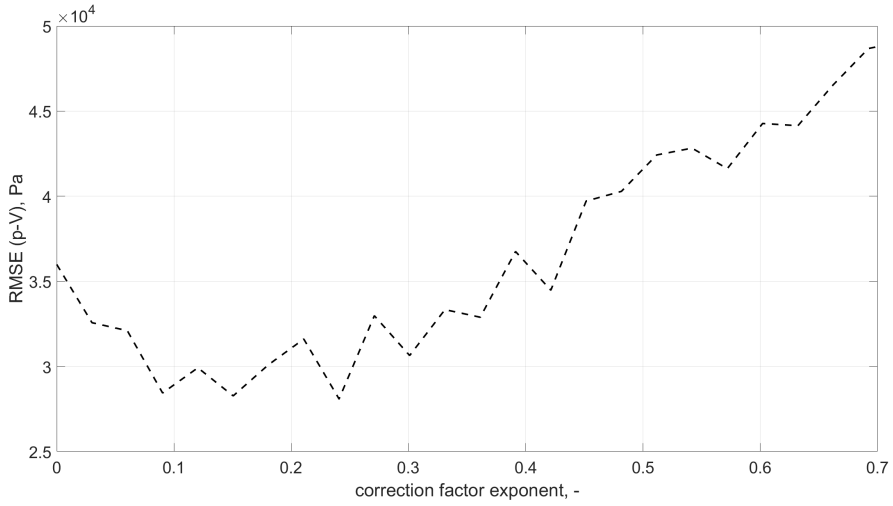


Figure 5.34: RMSE for the selected measurements for varying correction factor exponents, Annand correlation

The investigation of the Reynolds factor exponents shows that the optima are close to the original values. As such, no possibility of improvement is seen in this regard. This is shown in figures 5.35 and 5.36 .

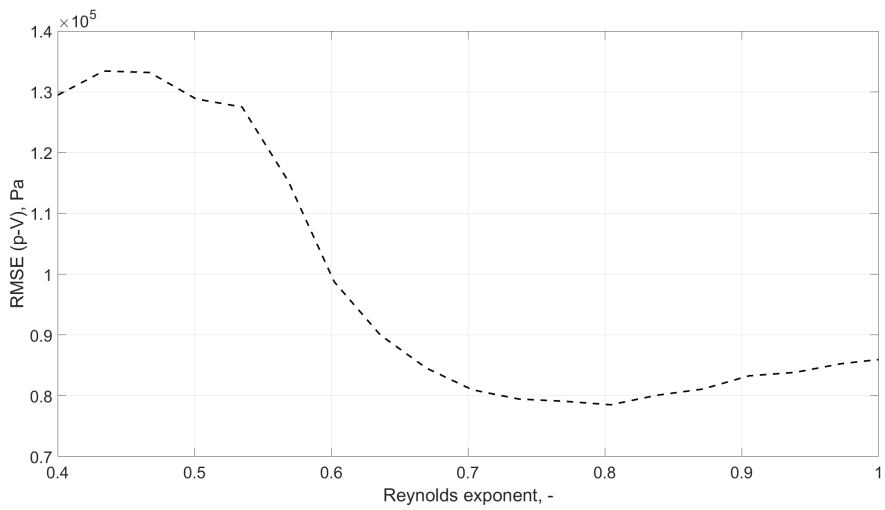


Figure 5.35: RMSE for the selected measurements for varying Reynolds exponents, Kanzaka correlation

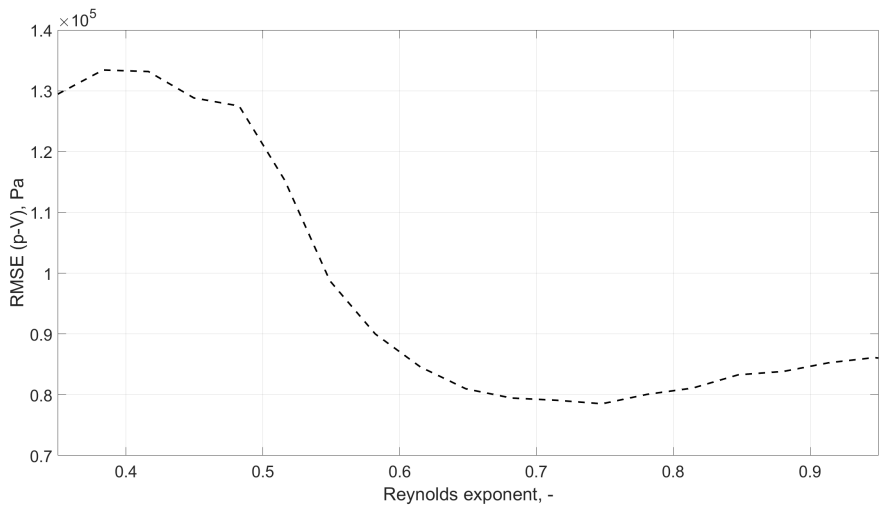


Figure 5.36: RMSE for the selected measurements for varying Reynolds exponents, Annand correlation

Chapter 6

Summary and conclusions

In the course of the presented research, investigation has been carried out into the question whether Stirling engine modelling by simplified, second order methods can be improved in terms of accuracy by employing a more in depth focus on heat transfer formulas, that previously done in other work. The review of literature has shown that this issue is indeed often "hand-waived" or outright neglected. On the other hand, it was also found that correlations befitting the problems are scarce. A thorough review of formulas concerning heat transfer in piston-cylinder systems has been performed and summarized for use in this work and other possible future use.

In order to analyse the problem in question, a model of Stirling cycle engines, known as the differential, real-gas model. The model has been created by employing the assumptions and methods previously coined by other researchers, though the assumption of using a real gas as the working fluid is novel. This model has been validated before employment by comparison to CFD data, and experimental data kindly shared by other researchers, that being the data for the Cleanergy engine from the Zilina University of Technology.

Improvement of the model by implementing a more complex model of the regenerator was considered. As shown in Fig.2.14, the small gains in regenerator effectiveness with the high value range have a tremendous influence on engine efficiency. Due to this, it is imperative that those values are accurately estimated when modelling engines, or in the design phase. It should also be noted, that a model should provide the ability to test many variants in a relatively short time. CFD models, as the one mentioned in the paper provide high accuracy, however the calculation is counted in days, even using a powerful, computational cluster. The differential model, while showing good agreement with the CFD, allowed to make the calculations on a much less powerful PC computer within two hundred seconds or less. Therefore it is much more suited for parametric analysis and design optimization.

In the course of parametric analysis using both models it was shown, that the heat capacity of the material has small influence on regenerator performance within the range of heat capacities of commonly used materials. However, the porosity of the material has a tremendous influence due to affecting both the heat transfer area, convective heat transfer coefficients and the solid mass of the regenerator.

The rotational speed of the engine, being inversely proportional to the time duration of a full working cycle of the regenerator is likewise important. The effectiveness of the regenerator shows itself to be higher at lower engine speeds. Which further confirms that Stirling Engines cannot optimally run at high rotational speed, due to both this fact and the reduction of the time periods for heating and cooling of the gas within the heat exchangers.

In later course of the work, a research stand has also been constructed based on the Genoastirling ML3000 engine. This enabled to perform engine indication and carry out a validation of the engine model with different heat transfer correlations employed.

Using the created model, it was shown that using the engine data there is quite a significant dependence of the engine power output on heat transfer coefficient values. This further corroborated the thesis that it is this parameter that demands further investigation. Based on the measurement results, and the literature review conducted, the selection of heat transfer correlations was narrowed.

Analysis in regard to the heat transfer correlation validity has been carried out using the experimental data. It has been found that the correlations of Kanzaka and Iwabuchi [30], Annand and Pinfold [9] and Toda [77] lead to the most accurate results. Furthermore, it was found that an inclusion of a pressure based correction factor can improve the result accuracy in regards to the power output characteristics. The hypothesis which lead to this finding has been formulated based on the West number as applied to the model results and measurements, which is understood to be a novel approach.

For engines of similar designs as the employed Genoastirling engine, it is recommended to use the Kanzaka, Annand and Toda correlations for this purpose, with the proposed correction factors.

The adjusted Kanzaka formula has the following form:

$$\text{Nu} = 0.21\text{Re}_{\text{sc}}^{0.8}\text{Pr}^{0.4} \left(\frac{T_w}{T_i}\right)^{-0.5} C' \left(\frac{\rho_i}{\rho_{\text{ref},i}}\right)^{0.4013}, \quad (6.1)$$

The Annand and Pinfold formula:

$$\text{Nu} = 0.3\text{Re}^{0.7} + \left(1 + 0.27 \frac{D}{V\Delta T} \frac{dT}{dt}\right) \left(\frac{\rho_i}{\rho_{\text{ref},i}}\right)^{0.4214}, \quad (6.2)$$

And the Toda formula:

$$\text{Nu} = 0.70\text{Re}^{0.58} \left(\frac{\rho_i}{\rho_{ref,i}} \right)^{0.586}. \quad (6.3)$$

For cooling and compression strokes:

$$\text{Nu} = 0.63\text{Re}^{0.53} \left(\frac{\rho_i}{\rho_{ref,i}} \right)^{0.586}, \quad (6.4)$$

where ρ_i is the fluid density in the given engine volume at a given instance, and $\rho_{ref,i}$ is the fluid density at 1 bar pressure and at the instantaneous temperature.

An investigation has been carried out into the model quality in terms of shape of the pressure-volume diagram. This has shown a decent representation compared to the measurements with the root mean square error values

Overall, it can be concluded, that Stirling engine modelling can be accurately performed by the use of relatively simple differential models, provided that the heat transfer is modelled properly. This is understood to confirm the initial thesis proposed at the work set out.

Bibliography

- [1] Dmp 320 data sheet, <https://www.bdsensors.de>.
- [2] J. Staliński. A. Perepeczko. *Okrętowe kotły i silniki parowe*. Wydawnictwo Morskie, Gdansk, 1971.
- [3] RP Adair, EB Qvale, and J_ T Pearson. Instantaneous heat transfer to the cylinder wall in reciprocating compressors. 1972.
- [4] Roland Aigner, Herbert Steinrück, and L Savic. Modelling fluid dynamics, heat transfer and valve dynamics in a reciprocating compressor. In *Proc. of the 5th Conference of the EFRC*, 2007.
- [5] Fatih Aksoy, Hamit Solmaz, Halit Karabulut, C Cinar, YO Ozgoren, and Seyfi Polat. A thermodynamic approach to compare the performance of rhombic-drive and crank-drive mechanisms for a beta-type stirling engine. *Applied Thermal Engineering*, 93:359–367, 2016.
- [6] Organ Allan. *Thermodynamics and Gas Dynamics of the Stirling Cycle Machine*. CUP, 1992.
- [7] Stig Kildegård Andersen, Henrik Carlsen, and Per Grove Thomsen. Preliminary results from simulations of temperature oscillations in stirling engine regenerator matrices. *Energy*, 31(10-11):1371–1383, 2006.
- [8] WJD Annand and TH Ma. Second paper: instantaneous heat transfer rates to the cylinder head surface of a small compression-ignition engine. *Proceedings of the Institution of Mechanical Engineers*, 185(1):976–987, 1970.
- [9] WJD Annand and D Pinfold. Heat transfer in the cylinder of a motored reciprocating engine. Technical report, 1980.

- [10] BS Bačić and GD Dragutinović. Asymmetric-unbalanced counterflow thermal regenerator problem: solution by the galerkin method and meaning of dimensionless parameters. *International journal of heat and mass transfer*, 34(2):483–498, 1991.
- [11] Ian H. Bell, Jorrit Wronski, Sylvain Quoilin, and Vincent Lemort. Pure and pseudo-pure fluid thermophysical property evaluation and the open-source thermophysical property library coolprop. *Industrial & Engineering Chemistry Research*, 53(6):2498–2508, 2014.
- [12] David Bendersky. A special thermocouple for measuring transient temperatures. *Mechanical Engineering*, 117, 1953.
- [13] Gary Borman and Kazuo Nishiwaki. Internal-combustion engine heat transfer. *Progress in energy and combustion science*, 13(1):1–46, 1987.
- [14] Zbigniew Buliński, Adam Kabaj, Tomasz Krysiński, Ireneusz Szczygieł, Wojciech Stanek, Bartłomiej Rutczyk, Lucyna Czarnowska, and Paweł Gładysz. A computational fluid dynamics analysis of the influence of the regenerator on the performance of the cold stirling engine at different working conditions. *Energy Conversion and Management*, 195:125–138, 2019.
- [15] Zbigniew Buliński, Ireneusz Szczygieł, Adam Kabaj, Tomasz Krysiński, Paweł Gładysz, Lucyna Czarnowska, and Wojciech Stanek. Performance analysis of the small-scale α -type stirling engine using computational fluid dynamics tools. *Journal of Energy Resources Technology*, 140(3):032001, 2018.
- [16] Zbigniew Buliński, Ireneusz Szczygieł, Tomasz Krysiński, Wojciech Stanek, Lucyna Czarnowska, Paweł Gładysz, and Adam Kabaj. Finite time thermodynamic analysis of small alpha-type stirling engine in non-ideal polytropic conditions for recovery of lng cryogenic exergy. *Energy*, 141:2559–2571, 2017.
- [17] David R Buttsworth, Robert Stevens, and C Richard Stone. Eroding ribbon thermocouples: impulse response and transient heat flux analysis. *Measurement Science and Technology*, 16(7):1487, 2005.
- [18] HS Carslaw and JC Jaeger. Conduction of heat in solids. *Clarendon, Oxford*, 1959.
- [19] Fernanda P Disconzi, Cesar J Deschamps, and Evandro LL Pereira. Development of an in-cylinder heat transfer correlation for reciprocating compressors. 2012.

- [20] G Eichelberg. Some new investigations on old combustion engine problems. *Engineering*, 148:547–550, 1939.
- [21] Karl Elser. *Der instationäre Wärmeübergang in Dieselmotoren: theoretische und experimentelle Untersuchungen*. Leemann, 1954.
- [22] Fabian Fagotti and Alvaro T Prata. A new correlation for instantaneous heat transfer between gas and cylinder in reciprocating compressors. 1998.
- [23] Fabian Fagotti, ML Todescat, RTS Ferreira, and AT Prata. Heat transfer modeling in a reciprocating compressor. 1994.
- [24] Jan A Gatowski, Mark K Smith, and Alex C Alkidas. An experimental investigation of surface thermometry and heat flux. *Experimental Thermal and Fluid Science*, 2(3):280–292, 1989.
- [25] D Gedeon and J G. Wood. Oscillating-flow regenerator test rig: Hardware and theory with derived correlations for screens and felts. 03 1996.
- [26] Osama H Ghazal. Simulation of natural gas combustion process using pressure based solver. *European Scientific Journal*, 12(12), 2016.
- [27] Clifford M Hargreaves. The phillips stirling engine. 1991.
- [28] Naeim Abdou Henein. Instantaneous heat transfer rates and coefficients between the gas and combustion chamber of a diesel engine. Technical report, 1965.
- [29] Günter F Hohenberg. Advanced approaches for heat transfer calculations. Technical report, 1979.
- [30] Mitsuo Kanzaka and Makio Iwabuchi. Study on heat transfer of heat exchangers in the stirling engine: heat transfer in a heated tube under the periodically reversing flow condition. *JSME international journal. Ser. 2, Fluids engineering, heat transfer, power, combustion, thermophysical properties*, 35(4):641–646, 1992.
- [31] Mitsuo Kanzaka and Makio Iwabuchi. Study on heat transfer of heat exchangers in the stirling engine: performance of heat exchangers in the test stirling engine. *JSME international journal. Ser. 2, Fluids engineering, heat transfer, power, combustion, thermophysical properties*, 35(4):647–652, 1992.
- [32] S Kasthuriengan, G Srinivasa, GS Karthik, DS Nadig, U Behera, and KA Shafi. Experimental and theoretical studies of a two-stage pulse tube cryocooler operating down to 3 k. *International Journal of Heat and Mass Transfer*, 52(3-4):986–995, 2009.

- [33] William Morrow Kays and Alexander Louis London. Compact heat exchangers. 1984.
- [34] Reto Kind. *Messung des instationären Wärmeüberganges in einem Zweitakt-Dieselmotor hoher Drehzahl*. PhD thesis, ETH Zurich, 1962.
- [35] BE Knight. Paper 6: The problem of predicting heat transfer in diesel engines. In *Proceedings of the Institution of Mechanical Engineers, Conference Proceedings*, volume 179, pages 99–115. SAGE Publications Sage UK: London, England, 1964.
- [36] AA Kornhauser and JL Smith Jr. Application of a complex nusselt number to heat transfer during compression and expansion. 1994.
- [37] Alan Abram Kornhauser. *Gas-wall heat transfer during compression and expansion*. PhD thesis, Massachusetts Institute of Technology, 1989.
- [38] Pei Moo Ku. Factors affecting heat transfer in the internal-combustion engine. 1940.
- [39] M Kuosa, K Saari, A Kankkunen, and T-M Tveit. Oscillating flow in a stirling engine heat exchanger. *Applied Thermal Engineering*, 45:15–23, 2012.
- [40] B Lawton. Effect of compression and expansion on instantaneous heat transfer in reciprocating internal combustion engines. *Proceedings of the Institution of Mechanical Engineers, Part A: Power and Process Engineering*, 201(3):175–186, 1987.
- [41] KP Lee. A simplistic model of cyclic heat transfer phenomena in closed spaces. In *iecc*, volume 2, pages 720–723, 1983.
- [42] T. LeFeuvre, P. S. Myers, and O. A. Uyehara. Experimental instantaneous heat fluxes in a diesel engine and their correlation. *SAE Transactions*, 78:1717–1738, 1969.
- [43] U Lekic and Jacobus BW Kok. Heat transfer and fluid flows in gas springs. *The Open Thermodynamics Journal*, 4(1), 2010.
- [44] U Lekić and JBW Kok. Heat flows in piston compressors. *5th EURO THERM*, 2008.
- [45] Uroš Lekić, S Sprin, et al. Fluid flow and heat transfer in a helium gas spring. 2011.

- [46] Ruihu Liu and Zicheng Zhou. Heat transfer between gas and cylinder wall of refrigerating reciprocating compressor. 1984.
- [47] DW Loveridge. Robert stirling—preacher and inventor. *Transactions of the Newcomen Society*, 50(1):1–10, 1978.
- [48] SGK Lundholm and BO Moodysson. The design and development of a 40 kw stirling engine-the power system. IMech E, 1982.
- [49] Nadia Martaj and Pierre Rochelle. 1d modelling of an alpha type stirling engine. *International Journal for Simulation and Multidisciplinary Design Optimization*, 5, 02 2014.
- [50] William R Martini. *Stirling engine design manual*. US Department of Energy, Office of Conservation and Solar Applications . . . , Cleveland, 1978.
- [51] H Moss. *Heat transfer in internal combustion engines*. HM Stationery Office, 1927.
- [52] W nusselt. Der wärmeübergang in der verbrennungskraftmaschinen. *VDI-Forschungsheft*, (264):47–54, 1923.
- [53] W Nusselt. Der warmeubergang zwischen arbeitmedium und zylinderwand in kolbenmaschinen. *Forachungsarb. Geb. Ing*, 1928.
- [54] Stanisław Ocheduszko. *Teoria maszyn cieplnych*, volume 3. Państwowe Wydawn. Techniczne, 1953.
- [55] Tatsu Oguri. On the coefficient of heat transfer between gases and cylinder walls of the spark-ignition engine. *Bulletin of JSME*, 3(11):363–369, 1960.
- [56] Allan J Organ. *Stirling cycle engines: Inner workings and design*. John Wiley and Sons, Chichester, 2013.
- [57] Vern D Overbye, James E Bennethum, OA Uyehara, and PS Myers. Unsteady heat transfer in engines. *SAE Transactions*, 69:461–494, 1961.
- [58] WH Percival. Historical review of stirling engine development in the united tates from 1960 to 1970. 1974.
- [59] Stoian Petrescu, M Costea, C Harman, and T Florea. Application of the direct method to irreversible stirling cycles with finite speed. *International Journal of Energy Research*, 26(7):589–609, 2002.

- [60] Walter Pflaum. Der wärmeübergang bei dieselmotoren mit und ohne aufladung. *MTZ*, 22:70, 1961.
- [61] H Pfriem. Periodic heat transfer at small pressure fluctuations. 1943.
- [62] A Pischinger. Zur frage der wärmebelastung in dieselmotoren. *MTZ*, 16:181, 1955.
- [63] Bartłomiej Rutczyk and Ireneusz Szczygiel. Development of internal heat transfer correlations for the cylinders of reciprocating machines. *Energy*, 230:120795, 2021.
- [64] Bartłomiej Rutczyk, Ireneusz Szczygiel, and Zbigniew Buliński. A zero-dimensional, real gas model of an α stirling engine. *Energy Conversion and Management*, 199:111995, 2019.
- [65] G Schmidt. The theory of lehmann’s calorimetric machine. *Zeitschrift Des Vereines Deutscher Ingenieure*, 15(1):98–112, 1871.
- [66] James R Senft. *Mechanical efficiency of heat engines*. Cambridge University Press, 2007.
- [67] JR Senft. A simple derivation of the generalized beale number. In *IECEC’82; proceedings of the seventeenth intersociety energy conversion engineering conference*, volume 4, pages 1652–1655, 1982.
- [68] Ramesh K Shah and Dusan P Sekulic. *Fundamentals of heat exchanger design*. John Wiley & Sons, 2003.
- [69] John Henry Shipinski. Relationships between rates-of-injection and rates-of-heat release in deisel engines. 1968.
- [70] K Sihling and G Woschni. Experimental investigation of the instantaneous heat transfer in the cylinder of a high speed diesel engine. Technical report, 1979.
- [71] Ireneusz Szczygiel and Zbigniew Bulinski. Overview of the liquid natural gas (lng) regasification technologies with the special focus on the prof. szargut’s impact. *Energy*, 165:999–1008, 2018.
- [72] Ireneusz Szczygiel, Wojciech Stanek, and Jan Szargut. Application of the stirling engine driven with cryogenic exergy of lng (liquefied natural gas) for the production of electricity. 105, 09 2015.

- [73] Roy C Tew, Kent Jefferies, and David Miao. *A Stirling engine computer model for performance calculations*, volume 78884. Department of Energy, Office of Conservation and Solar Applications . . . , 1978.
- [74] Thermodynamics, Fluid Mechanics Group, and WJD Annand. Heat transfer in the cylinders of reciprocating internal combustion engines. *Proceedings of the Institution of Mechanical Engineers*, 177(1):973–996, 1963.
- [75] Lanny G Thieme and Roy C Tew Jr. Baseline performance of the gpu 3 stirling engine. 1978.
- [76] Kuppan Thulukkanam. *Heat exchanger design handbook*. CRC press, 2013.
- [77] F Toda and Shoichi Iwamoto. Heat transfer on a small stirling engine. *Marine Engng Soc Japan Bull*, 19(1):49–60, 1991.
- [78] J Tuhovcak, J Hejcik, and M Jicha. Comparison of heat transfer models for reciprocating compressor. *Applied Thermal Engineering*, 103:607–615, 2016.
- [79] Israel Urieli and David M Berchowitz. *Stirling cycle engine analysis*. A. Hilger, Bristol, 1984.
- [80] Graham Walker and James R Senft. Free-piston stirling engines. In *Free piston stirling engines*, pages 23–99. Springer, 1985.
- [81] C Wang. Numerical analysis of 4 k pulse tube coolers: Part i. numerical simulation. *Cryogenics*, 37(4):207–213, 1997.
- [82] Kai Wang, Swapnil Dubey, Fook Hoong Choo, and Fei Duan. A transient one-dimensional numerical model for kinetic stirling engine. *Applied energy*, 183:775–790, 2016.
- [83] CD West. Theoretical basis for the beale number. In *Proc., Intersoc. Energy Convers. Eng. Conf.:(United States)*, volume 2. Westware Co, Oliver Springs, Tenn, USA, 1981.
- [84] ND Whitehouse. Heat transfer in compression-ignition engines: First paper: Heat transfer in a quiescent chamber diesel engine. *Proceedings of the Institution of Mechanical Engineers*, 185(1):963–975, 1970.
- [85] A John Willmott. The development of thermal regenerator theory: 1931-the present. *Journal-Institute of Energy*, pages 54–54, 1993.

- [86] Gerhard Woschni. Computer programs to determine the relationship between pressure flow, heat release, and thermal load in diesel engines. *SAE Transactions*, pages 550–559, 1966.
- [87] Gerhard Woschni. A universally applicable equation for the instantaneous heat transfer coefficient in the internal combustion engine. Technical report, 1967.
- [88] Gang Xiao, Conghui Chen, Bingwei Shi, Kefa Cen, and Mingjiang Ni. Experimental study on heat transfer of oscillating flow of a tubular stirling engine heater. *International Journal of Heat and Mass Transfer*, 71:1–7, 2014.
- [89] Gang Xiao, Yiqing Huang, Shulin Wang, Hao Peng, Mingjiang Ni, Zhihua Gan, Zhongyang Luo, and Kefa Cen. An approach to combine the second-order and third-order analysis methods for optimization of a stirling engine. *Energy Conversion and Management*, 165:447 – 458, 2018.
- [90] Youmans Y.L and Youmans W.J. Domestic motors. *Popular Science Monthly*, 18:334, 1880.
- [91] Tianshou Zhao and Ping Cheng. A numerical solution of laminar forced convection in a heated pipe subjected to a reciprocating flow. *International Journal of Heat and Mass Transfer*, 38(16):3011–3022, 1995.
- [92] TS Zhao and Ping Cheng. Oscillatory heat transfer in a pipe subjected to a laminar reciprocating flow. *J. Heat Transfer*, (118(3)):592–597, 1996.
- [93] TS Zhao and Ping Cheng. Oscillatory heat transfer in a pipe subjected to a laminar reciprocating flow. *Journal of heat transfer*, 118(3):592–597, 1996.
- [94] Nguen Van Ziong and Aleksandr Vitalevich Belogub. Raschjot processa teplootdachi v dizelnom dvigatele tipa d-100 s ispolzovaniem izvestnyh a-formul. *Dvigateli vnutrennego sgoranija*, (2), 2018.
- [95] Stefan Żmudzki. *Silniki Stirlinga*. WNT, Warszawa, 1993.

List of Figures

1.1	An illustration of engine power dependence on internal heat transfer coefficients for the Genoa ML3000 Stirling Engine	8
1.2	Stirling engine original 1816 patent drawing	9
1.3	The β type Stirling engine	10
1.4	The γ type Stirling engine	11
1.5	The α type Stirling engine	12
1.6	A Rider engine in cross-section [90]	12
1.7	A Rider engine found by the author in the collection of the National Agricultural museum in Szreniawa.	12
1.8	A $T - s$ and $p - V$ diagram for the ideal Stirling cycle	13
1.9	Schematic and temperature distribution in the control volumes of the Schmidt isothermal model. 1 - compressor/cooler, 2 - regenerator, 3 - expander/heater. T_c - cooler temperature, T_h - heater temperature .	16
1.10	Schematic and temperature distribution in the control volumes of the adiabatic model. 1 - compressor, 2 - cooler, 3 - regenerator, 4 - heater, 5 - expander. T_c - cooler temperature, T_h - heater temperature . . .	17
1.11	Schematic and temperature distribution in the control volumes of the "SIMPLE" model. 1 - compressor, 2 - cooler, 3 - regenerator, 4 - heater, 5 - expander. T_c - cooler temperature, T_h - heater temperature	18
1.12	Schematic and temperature distribution in the control volumes of the polytropic model. 1 - compressor/cooler, 2 - regenerator, 3 - expander/heater. T_c - cooler temperature, T_h - heater temperature . .	19
2.1	System boundaries of the model	23
2.2	A simplified flowchart for the algorithm used with the real gas model	53
2.3	Simple regenerator model [79]	54
2.4	Mass flows between the cylinder and the regenerator as a function of crank angle	56
2.5	A schematic representation of the regenerator model	60
2.6	Regenerator effectiveness for an example engine as a function of porosity.	62

2.7	Regenerator effectiveness for an example engine as a function of matrix heat capacity.	63
2.8	Regenerator effectiveness for an example engine as a function of the engine cycle duration.	64
2.9	Influence of the unequality parameter ψ on regenerator effectiveness according to the differential and Hausen models.	65
2.10	A schematic drawing of the evaluated engine	66
2.11	Stirling engine T-s diagram, as evaluated by CFD techniques by Bulinski et al [16].	67
2.12	Stirling engine T-s diagram as evaluated with the 0D model.	67
2.13	Cryogenic engine efficiency characteristics as plotted from the author's model overlaid by cryogenic engine characteristics as plotted from the CFD model by Bulinski et al	68
2.14	The evaluated engine's efficiency as a function of the regenerator effectiveness	69
2.15	Temperatures of gas flowing outside of the regenerator across time for the proposed model and a CFD simulation, for the porosity of 0.7	70
2.16	Temperatures of gas flowing outside of the regenerator across time for the proposed model and a CFD simulation, for the porosity of 0.8	70
2.17	Temperatures of gas flowing outside of the regenerator across time for the proposed model and a CFD simulation, for the porosity of 0.9	71
2.18	Cleanergy C9C, cross-section. 1 - hot piston, with cap, 2 - hot heat exchanger, 3 - regenerator, 4 - cooling tube bank, 5 - cold piston, 6 - crank mechanism	73
2.19	C9C engine power, different heat transfer models within the polytropic model, Adiabatic model and measurements included for comparison	74
2.20	C9C engine electrical efficiency, different heat transfer models within the polytropic model, Adiabatic model and measurements included for comparison	75
3.1	A cross-Section of the Genoastirling ML3000 engine	77
3.2	ML3000 engine crankshaft	78
3.3	A view of the connecting rod	79
3.4	Drawing of the eccentric with major dimensions	79
3.5	Drawing of the connecting rod with major dimensions	80
3.6	A crossSection of the engine working spaces	81
3.7	Side view of the piston. Sealing groves visible in detail B.	82

3.8	One of the cylinder pairs in crossSection. A - compression cylinder, B - gas opening, C - annular space, D - heat exchanger assembly, E - cooling coils, F - regenerator space, G - heater tubes, H - expansion cylinder, I - heater tube fillaments, J - Heylandt crown, K - hot cap, L - expansion cylinder liner, M - expander piston, N - compressor piston, O - compression cylinder liner, P - engine body	84
3.9	The engine cooling coils	85
3.10	Outside view of the heater tubes	86
3.11	The RMB29AC01SS1 sin/cos engine encoder	89
3.12	The DMP 320 pressure transducer	90
3.13	Time plot of the angular velocity for example engine measurements	91
4.1	An illustration of engine power dependence on internal heat transfer coefficients for the Genoa ML3000 Stirling Engine	93
4.2	ML3000 engine simulated indicator diagrams for selected values of the heat transfer coefficients	93
4.3	Model fit quality with different heat transfer models used	98
4.4	Model fit quality for nitrogen	99
4.5	Model fit quality for argon	99
4.6	Root mean square error of indicated power for different heat transfer models	100
4.7	West numbers, model calculated and measured, with lines of the measured mean +/- standard deviation, sorted by pressure for nitrogen.	102
4.8	West numbers, model calculated and measured, with lines of the measured mean +/- standard deviation, sorted by pressure for argon.	102
5.1	Root mean square and mean relative error for the Kanzaka correlation with correction factor, for different values of correction factor exponent	105
5.2	Root mean square and mean relative error for the Annand (1980) correlation with correction factor, for different values of correction factor exponent	106
5.3	Root mean square and mean relative error for the Toda correlation with correction factor, for different values of correction factor exponent, positive range	107
5.4	Root mean square and mean relative error for the Toda correlation with correction factor, for different values of correction factor exponent, negative range	108
5.5	Fit quality for adjusted models for validation set (set 1)	109
5.6	Fit quality for adjusted models for verification set (set 2)	109

5.7	Root mean square error of indicated power for different heat transfer models, including the adjusted correlations.	110
5.8	Comparison between the $p - V$ diagrams for measurement point I, with the base and adjusted Toda model calculations	113
5.9	Comparison between the $p - V$ diagrams for measurement point I, with the base and adjusted Annand model calculations	114
5.10	Comparison between the $p - V$ diagrams for measurement point I, with the base and adjusted Kanzaka model calculations	115
5.11	Comparison between the $p - V$ diagrams for measurement point II, with the base and adjusted Toda model calculations	116
5.12	Comparison between the $p - V$ diagrams for measurement point II, with the base and adjusted Annand model calculations	117
5.13	Comparison between the $p - V$ diagrams for measurement point II, with the base and adjusted Kanzaka model calculations	118
5.14	Comparison between the $p - V$ diagrams for measurement point III, with the base and adjusted Toda model calculations	119
5.15	Comparison between the $p - V$ diagrams for measurement point III, with the base and adjusted Annand model calculations	119
5.16	Comparison between the $p - V$ diagrams for measurement point III, with the base and adjusted Kanzaka model calculations	120
5.17	Comparison between the $p - V$ diagrams for measurement point IV, with the base and adjusted Toda model calculations	120
5.18	Comparison between the $p - V$ diagrams for measurement point IV, with the base and adjusted Annand model calculations	121
5.19	Comparison between the $p - V$ diagrams for measurement point IV, with the base and adjusted Kanzaka model calculations	121
5.20	Comparison between the $p - V$ diagrams for measurement point V, with the base and adjusted Toda model calculations	122
5.21	Comparison between the $p - V$ diagrams for measurement point V, with the base and adjusted Annand model calculations	123
5.22	Comparison between the $p - V$ diagrams for measurement point V, with the base and adjusted Kanzaka model calculations	124
5.23	Comparison between the $p - V$ diagrams for measurement point VI, with the base and adjusted Toda model calculations	125
5.24	Comparison between the $p - V$ diagrams for measurement point VI, with the base and adjusted Annand model calculations	125
5.25	Comparison between the $p - V$ diagrams for measurement point VI, with the base and adjusted Kanzaka model calculations	126
5.26	Illustration of the pressure as a signal approach, for measurement I.	127

5.27	Pressure vector plot for measurement point I	128
5.28	Pressure vector plot for measurement point II	128
5.29	Pressure vector plot for measurement point III	128
5.30	Pressure vector plot for measurement point IV	129
5.31	Pressure vector plot for measurement point V	129
5.32	Pressure vector plot for measurement point VI	129
5.33	RMSE for the selected measurements for varying correction factor exponents, Kanzaka correlation	131
5.34	RMSE for the selected measurements for varying correction factor exponents, Annand correlation	132
5.35	RMSE for the selected measurements for varying Reynolds exponents, Kanzaka correlation	133
5.36	RMSE for the selected measurements for varying Reynolds exponents, Annand correlation	133

List of Tables

2.1	Regenerator base parameters	61
2.2	Engine parameters	66
2.3	C9C engine parameters	72
2.4	C9C measurements, data obtained by the courtesy of "UNIZA"	74
3.1	Engine nominal parameters	77
3.2	Engine dimensions	87
4.1	Measurements for argon, part I	95
4.2	Measurements for argon, part II	95
4.3	Measurements for nitrogen, part I	95
4.4	Measurements for nitrogen, part II	96
4.5	Measurements for Carbon Dioxide	96
4.6	RMSE values for different heat transfer models, with and without losses, for nitrogen and argon, values in Watts	101
4.7	Covariance values for different heat transfer models, for nitrogen and argon	103
5.1	Root mean square error for selected and adjusted correlations, separated for the verification set and overall	110
5.2	Measurements for individual comparison	112
5.3	Phase differences between model and selected measurements, for the pressure signal	129
5.4	Relative pressure amplitude error for selected measurement points	130
5.5	Root mean square error of the pressure signal in bar	130